Max Planck Institut für Kolloid und Grenzflächenforschung
Abt. Grenzflächen

Integration of Freestanding Polyelectrolyte Multilayer Membranes in Larger Scale Structures

Dissertation
zur Erlangung des akademischen Grades
"doctor rerum naturalium"
(Dr. rer. nat.)
in der Wissenschaftsdisziplin "Physikalische Chemie"

eingereicht an der
Mathematisch-Naturwissenschaftlichen Fakultät
der Universität Potsdam

von
Marc Nolte
aus Münster

Potsdam, den 23.1.2006

Vorsitzender: Prof. Dr. Bechmann

Gutachter: Prof. Dr. Möhwald, Prof. Dr. v. Klitzing, Prof. Tsukruk
Beisitzer: Prof. Dr Beuermann, Prof. Dr. v. Klitzing, Prof. Dr. Möhwald, Prof. Dr Saalfrank, Priv. Doz. Riegler

Tag der mündlichen Prüfung: 10.5.2005

Abstract

Ultrathin, semi-permeable membranes are not only essential in natural systems (membranes of cells or organelles) but they are also important for applications (separation, filtering) in miniaturized devices.

Membranes, integrated as diffusion barriers or filters in micron scale devices need to fulfill equivalent requirements as the natural systems, in particular mechanical stability and functionality (e.g. permeability), while being only tens of nm in thickness to allow fast diffusion times. Promising candidates for such membranes are polyelectrolyte multilayers, which were found to be mechanically stable, and variable in functionality.

In this thesis two concepts to integrate such membranes in larger scale structures were developed. The first is based on the directed adhesion of polyelectrolyte hollow microcapsules. As a result, arrays of capsules were created. These can be useful for combinatorial chemistry or sensing. This concept was expanded to couple encapsulated living cells to the surface.

The second concept is the transfer of flat freestanding multilayer membranes to structured surfaces. We have developed a method that allows us to couple mm^2 areas of defect free film with thicknesses down to 50 nm to structured surfaces and to avoid crumpling of the membrane. We could again use this technique to produce arrays of micron size. The freestanding membrane is a diffusion barrier for high molecular weight molecules, while small molecules can pass through the membrane and thus allows us to sense solution properties. We have shown also that osmotic pressures lead to membrane deflection. That could be described quantitatively.

Table of Contents

1 Motivation

Membranes are known as essential building blocks in nature, and are highly specialized with respect to their function. They separate cells, allow cells the possibility to obtain information about their environment and provide mechanical strength to cells. Inside cells, membranes provide a barrier around organelles. Membranes thus allow organelles to function by concentrating functional elements in the membrane itself or in a confined volume. For technical applications membranes also play an important role such as in diffusion barriers or filters. Because the field of microfluidics has attracted considerable attention in the past decade, the development of membranes also for miniaturized devices has been a focal point of interest. As in natural systems, these membranes must be ultrathin as processes in cells or micro-devices are diffusion limited, and diffusion is a function of the membrane thickness. Other parameters such as selective permeability (for ions, uncharged molecules or macromolecules) and mechanical stability are important as well. A promising candidate for building versatile membrane systems are polyelectrolytes, assembled using the layer-by-layer technique to form membranes. Supported polyelectrolyte multilayer membranes are already widely used as functional coatings with defined thickness (adjustable in the nm regime), tunable permeability, and versatile mechanical properties [1]. An interesting aspect, with respect to integrating multilayer membranes in micro-devices, is the fact that membrane interactions with each other or the substrate are dominated by the properties of the last adsorbed layer. Therefore, strong adhesion or repulsion can be triggered easily. The integration of ultrathin freestanding membranes in larger scale structures however is a key step to making effective use of membranes in microfluidics. Two different approaches to integrating freestanding membranes within larger scale structures will be presented in this thesis.

The first approach is the directed adhesion of polyelectrolyte capsules and is presented in the first chapter of the results. Polyelectrolyte capsules can be formed by coating a dissolvable core using the layer-by-layer technique. The properties of the resulting polyelectrolyte capsules have already been intensively studied in the bulk. This includes techniques to load capsules and release encapsulated matter and studies on changing their permeability and adhesive and mechanical properties. Reviews of these “smart” capsule systems can be found in references [2,3]. The coupling of polyelectrolyte capsules to defined positions on a substrate is therefore

interesting for the development of methods in combinatorial chemistry. Here, capsules could be used as micron sized reaction containers linked to specific substrate positions. In addition, this self-assembly technique used to make capsules could be applied in sensor applications where an indicator material could be stored inside the capsule containers. The key advantage of the presented approach is that the production of the capsules, the surface coating, and the coupling of the two are based on self-assembly. The methods used avoid both costly techniques requiring either vacuum equipment or clean room facilities. Both containers and surface coatings can be made from a variety of materials including biocompatible components [4] that make the system highly versatile.

The adhesion of single encapsulated living cells could also be directed, by the same approach. This application offers the possibility of single cell based biosensors. For a broader review on this topic, we refer the reader to the review article of Bousse [5]. An additional noteworthy application is the potential use in drug discovery [6].

Flat freestanding membranes, which are the topic of the second part of the results, are complementary to the capsule system. In contrast to the capsule system, the ultrathin membrane is not stabilized by its spherical shape. The missing stabilization raises the problem of crumpling caused by in-plane stresses. Therefore, a novel transfer method that avoids in-plane stresses has been developed during this thesis. By applying this transfer technique, huge areas of a topographical structured substrate were covered by the film without defects. As a result, an array of micron sized cavities was produced. The membrane covering cavity array has been employed in two different studies. In the first study, the polyelectrolyte membrane separated the micron sized cavities from the bulk solution. If they were filled with macromolecular probes, such membrane arrays can locally sense solution properties. These arrays could also find application in combinatorial chemistry, where the cavities could serve as reaction containers. For the latter application, it will be advantageous for the arrays to be fabricated by soft lithography, which is widely used in microfluidics and that allows for multiple structure designs [7,8]. In addition, freestanding membranes can be used as highly sensitive pressure sensors [9]. Membranes which are produced as described above would allow to sensitive measurements of osmotic pressures of small sample volumes by detecting the deflection of the membrane with high accuracy, small measuring time, and high lateral resolution. Lastly, a membrane array allows for fundamental studies on the

membrane system. Because of the simpler geometry compared to the capsule system, not only an E-Modulus but also the stress strain relation could be recorded with this system.

2 Scientific Background

The scientific background of the work presented in this thesis will be the subject of the following chapter. First, the behavior of polyelectrolytes in solution will discussed, with a special emphasis on their effect on a solution's osmotic pressure. Next, properties of polyelectrolyte-complexes will be conferred: These properties are used to describe the behavior of polyelectrolyte multilayers, which will be reviewed in the third and fourth part in detail. Here structure and preparation of multilayers and their physical properties, in particular the interactions of polyelectrolyte coated surfaces will be distinguished. Finally methods to produce freestanding multilayers will be described.

2.1 Polyelectrolytes in Solution

Polyelectrolytes are charged polymers. A positively or negatively charged polyelectrolyte is called a polycation (polybase) or a polyanion (polyacid), respectively. If positive and negative charges are on the same chain, the polyelectrolyte is called a polyampholyte (e.g. proteins). The degree of charge depends on the particular polyelectrolyte and ranges from a small fraction to 100% of the monomer units. Polyelectrolytes are soluble in water, although their backbone is often hydrophobic. Their solubility is related to the gain in entropy when counterions are released in water. The behavior of polyelectrolytes in solution is rather complex, because polyelectrolyte behavior is a convolution of polymer and electrolyte behavior. Therefore, the important effects of polymers in solution will be discussed followed by the relevant properties of electrolyte solutions. From these two systems the behavior of a polyelectrolyte solution is concluded.

Polymers are usually treated using the Freely-Jointed-Chain-Model (FJC) or the Freely-Rotating-Chain-Model (FRC): In the FJC Model, a polymer consists of N+1 monomer units, which are connected by N bonds defined by bound vectors $\mathbf{r}_j$ (j=1,…N). Here the length of the bonds is denoted as $|\mathbf{r}_j|=a$ and usually named the Kuhn length. This length is related to the monomer size, but does not equal the monomer size itself because of chain stiffening. The FRC takes the detailed microscopic chain structure (in particular the bond angle) into account and gives the relation between the monomer size and the Kuhn length.

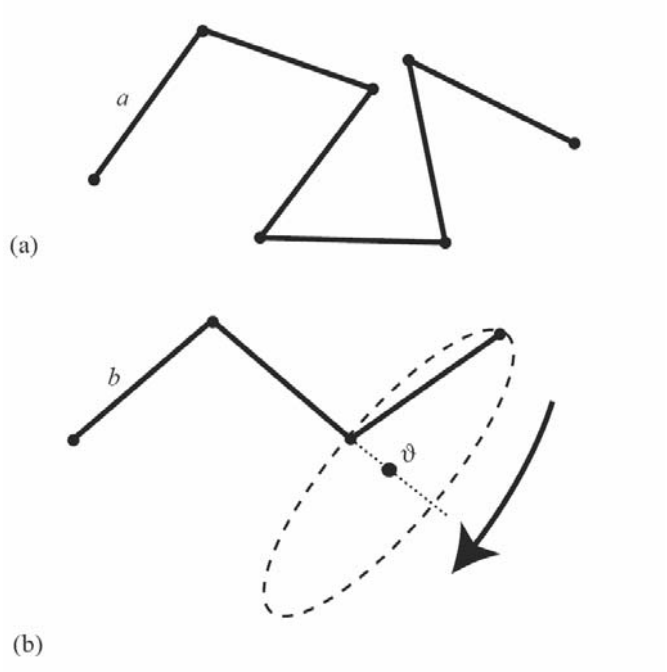

Figure 2-1 : (a) Freely-Jointed-Chain-Model (FJC). *N* bonds of a length *a* are bound together to form a flexible chain. The bond angle is a free parameter. (b) Freely Rotating-Chain-Model (FRC). The bond angle is fixed at 70°, but freely rotating [10].

The advantage of these simple models is the ease in which parameters such as the contour length ($L=N\cdot a$), the end-to-end distance, and the end-to-end radius can be calculated.

The end-to-end radius R is generally for $N >> 1$ given as

2-1 $$R \cong \frac{aN^{\nu}}{\sqrt{6}}.$$

The exponent ν is a function of the polymer/solvent interactions. For an ideal polymer chain in which the monomer/solvent interactions cancel, $\nu=½$ and R is called the unperturbed radius of gyration (R_G). These conditions (in particular the temperature) are called the Θ-conditions and the respective solvent is named a Θ-solvent. When the interactions between the solvent and the monomer are more favorable than the monomer-monomer interactions, the solvent is called a good solvent. The polymer coil swells in this case and $\nu\approx3/5$. Here, the end-to-end radius is called the Flory radius (R_F). At the other extreme a bad (or poor) solvent leads to a collapse of the coil ($\nu=1/3$) or precipitation in the extreme case.

These theories only describe the behavior of completely flexible polymer chains for which the rotation of the bonds is not hindered. If there is a hindrance due to bulky

side-chains (or charges as it will be discussed later), an orientational correlation between near but not adjacent bonds emerges. This correlation results in an increased stiffness of the chain that plays an important role for the local structure of polymers. The length over which this correlation takes place is called the persistence length (l_0).

The electrolyte behavior of polyelectrolytes is reflected by the Coulomb interaction of the charges located along the polymer chain. Therefore, the charges can be used to categorize polyelectrolytes: For strong polyelectrolytes, the degree of charge does not depend on the pH of the aqueous solution. If its charge changes with pH, the polyelectrolyte is called a weak polyelectrolyte. In this case, the degree of charge depends on the protonation-degree of the polymer ($a(A^-)/a(AH)$) and is a function of pH and can be described by the Henderson Hasselbach equation:

2-2 $$pK_a = -\log\left(\frac{a(H^+)_{aq}\cdot a(A^-)_{aq}}{a(AH)_{aq}}\right) = pH + \log\left(\frac{a(AH)}{a(A^-)}\right).$$

Due to non-cooperative interactions between neighboring groups, the effective pK_a of an unprotonated group next to a protonated group is higher than for its non-charged neighbors. This range of pK_a's broadens the equivalence point. Therefore no distinct pK_a but an apparent pK_a (pK_{app}) is defined.

The conformation of the polyelectrolyte is strongly affected by the charges along its chain. The effect of the charge can be described using characteristic lengths like the Bjerrum length, the distance between two charges and the Debye-screening length for solutions that contain additional salt.

The Bjerrum length, usually denoted as l_B, equals the distance at which the Coulombic interactions between two unit charges (e) in a dielectric medium (with a dielectric constant of ε) is equal to thermal energy (k_BT) and is defined as

2-3 $$l_B = \frac{e^2}{4\pi\cdot\varepsilon\cdot k_BT}.$$

In water at room temperature one finds l_B = 0.7 nm.

On a typical strong synthetic polyelectrolyte chain, the charge density (τ, the inverse of the distance between two charges) along the polymer chain is 4 nm^{-1}, corresponding to one charge per monomer. The energy loss due to like charges at distances smaller than the Bjerrum length is compensated by counterion

condensation (Manning Condensation). Counterion condensation leads to a reduced effective charge density of τ=1.4 nm^{-1} for a strong polyelectrolyte chain with a monovalent counterion. This effect can be described quantitatively by

2-4 $$l_B \cdot \tau \cdot z = 1$$

with *z* being the valency of the counterion.

In polyelectrolyte solutions that contain salt (which is the case for biological or industrial systems), the electrostatic interactions are screened by the added ions. This effect can be described in the limit of ideal dilute solutions with the Debye Hückel theory. The characteristic length scale is the so called screening or Debye length (κ^{-1}) where the initial potential between two charges has fallen to 1/*e*.

2-5 $$\kappa^{-1} = \sqrt{1/(8 \cdot I \cdot l_B \cdot N_A \cdot \pi)}$$

With the ionic strength (I) defined as

2-6 $$I = \frac{1}{2}\sum_i z_i^2 c_i \ .$$

while *z* is the valence of the ion and *c* the concentration of ions in solution. The screening effect by additional ions results in conformational changes of the polymer chain. Figure 2-2 shows this effect. The persistence length of the uncharged backbone was kept constant in the Monte-Carlo simulations. The addition of charges to the backbone leads to an electrostatic contribution to the persistence length:

2-7 $$l_{0(tot)} = l_{0(polym)} + l_{0(el)}$$

2-8 $$l_{0(el)} = \frac{l_B \tau^2}{4\kappa^2 f^2} \quad \text{with:} \quad f = 1 \forall \tau^{-1} > l_b \vee f = l_b \tau \ \forall \ \tau^{-1} < l_b \,,$$

This contribution is more pronounced for long screening lengths (corresponding to low salt concentrations), as it is shown in Figure 2-2 c. Here the persistence length corresponds to the contour length, the polymer is stretched. For higher salt concentrations the polymer coils, and the polyelectrolyte can be described like an uncharged polymer (Figure 2-2 a).

Figure 2-2 : Monte-Carlo Simulations of the influence of different salt concentrations on the polyelectrolyte conformation. The bare persistence length was kept constant while the Debye screening length was chosen to give an electrostatic contribution to the persistence length which is on the order of the monomer size (a), (b) several monomers, (c) the contour length of the polymer [10].

It is noteworthy that the Debye-(screening)-length of a 0.5 M saline solution (which is typical for a multilayer buildup) is about 0.4 nm. This is less than the charge spacing along the chain, taking counterion condensation into account. This means electrostatic contributions to the persistence length can be neglected for salt concentration higher than 0.1M, where κ^{-1} is around 1 nm. A more detailed overview on polyelectrolytes in solution is presented in [10,11].

Osmotic pressures of polyelectrolytes in solution

Osmosis was first observed when a semi-permeable membrane divides two chambers with different solute concentrations. The solvent will pass through the membrane when a concentration gradient is present or until the hydrostatic pressure compensates the so-called osmotic pressure. Thermodynamically the osmotic pressure arises because the chemical potential of two components in equilibrium must be equal.

2-9 $$\mu_A^*(p) = \mu_A(x_A, p+\Pi) = \mu_A^*(p) + RT\ln x_A + \int_p^{p+\Pi} V_M dp$$

Here μ^* is the standard chemical potential of the pure solvent (A), x_A is the mole fraction of A, V_M is the molar volume of the pure solvent and p and Π are pressure and osmotic pressure respectively.

For very diluted solutions, the van't Hoff equation can be calculated from equation 2-9:

2-10 $$\Pi = c(B)RT\,,$$

with *c(B)* being the concentration of the solute. The virial expansion of Π in terms of *c(B)* can be used to determine the molecular mass of macromolecules, as it is related to *c(B)* [g/l], and the number of polymer chains in solution.

The osmotic pressure of polyelectrolyte solutions is more complicated. In the simplest case, the case of excess salt the polyelectrolyte solution can be treated like polymer solution and the molecular weight of polyelectrolytes can be determined.

Salt free solutions can be treated using the assumption that the electrostatic energy of each monomer unit is on the order of $k_B T$. The osmotic pressure of the polyions thus scale with the free energy per unit volume and is on the order of

2-11 $$\frac{\Pi}{RT} \propto c$$

where *c* is the monomer concentration of the polyelectrolyte. This means Π scales with the counterion concentration [12] and thus depends on the monomer concentration of the polyelctrolyte. The proportionality constant is called the osmotic coefficient (ϕ). It describes the fraction of counterions generating the osmotic pressure and is usually around 0.4 for different polymer systems [13,14].

2.2 Polyelectrolyte Complexes

Polyelectrolyte complexes (PECs) are formed when a polyelectrolyte is added to a solution, which already contains the oppositely charged polyelectrolyte. PECs are of interest for this thesis because these complexes help to understand the behavior of polyelectrolyte multilayers. Of special interest are the structure of the complex and the possible reversibility of the complex formation. In multilayers these properties correspond to the layer growth and stability, respectively.

The driving force of complex formation is entropy gain, that is achieved by the release of counterions originally located in the vicinity of the polymer coils (see scheme in Figure 2-3). Usually the complexes have a 1:1 stoichiometry, where the neutralized core is stabilized by the excess component. However, other factors like hydrophobic interactions or hydrogen bonding also may contribute [15]. The rate determining step is the diffusion of the polymers in the solution. This results in “frozen” non-equilibrium complexes for low salt concentrations. The addition of salts can have various effects: At higher salt concentrations, some polyelectrolyte systems show a slow equilibration to their equilibrium structure. The same is true for polyion exchange reactions (see Figure 2-3). The rate of the rearrangement strongly

depends on the salt concentration and the type of salt used. Temperature has a similar effect as an added salt (glass transition [16]).

For high salt concentrations dissolution of polyelectrolyte complexes was observed [15]. Also pH changes can lead to dissolution of the complex. Complexes of highly charged and/or high molecular weight polyelectrolytes tend to aggregate and flocculate at high salt concentrations. The high cooperativity in these complexes increase their stability, while the screening of the stabilizing outer charges causes precipitation [17].

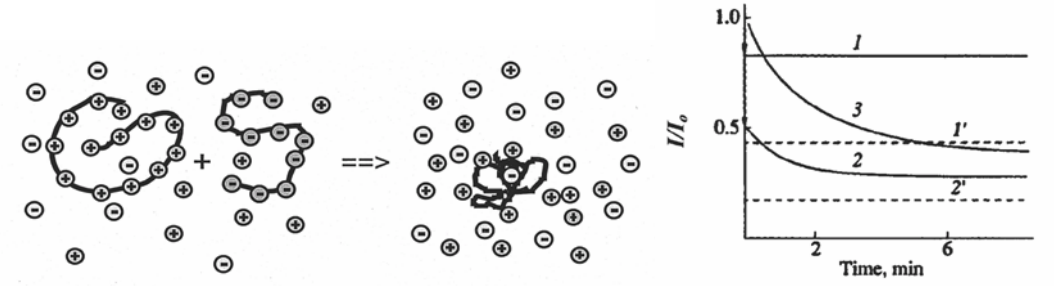

Figure 2-3 : Scheme: Entropy gain due to the release of counterions is the driving force of complex formation [18]. Graph: Typical kinetic curves of polyion coupling and exchange reactions, measured by fluorescence quenching of pyrenyl tags on the polymethylacrylate by the complexion polyvinylpyredine. Curve 1 is without added salt, curve 2 is with a salt concentration of 0.03 mol/l, curve 3 represents a polyion exchange reaction (unlabeled PMA is replaced by labeled PMA) The curves 1' and 2' are the equilibriums limits for 1 and 2 respectively [19].

In addition the structure of the complex depends on the nature of the polyelectrolyte used. The two extreme cases are the model of a ladder structure with fixed ionic cross-links and a more chaotic scrambled-egg structure with statistical charge compensation [19-21].

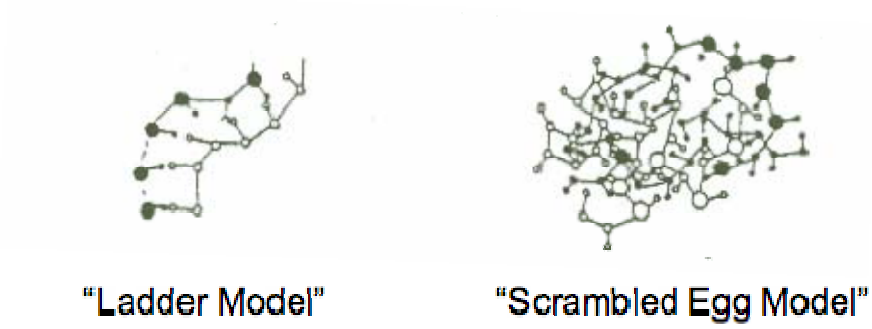

Figure 2-4: The two limiting structures of the complex precipitate [20].

2.3 Structure of Polyelectrolyte Multilayers

The "layer-by-layer" Technique

Multilayers can be prepared as first introduced by Decher in the early 1990's [22,23]. The standard way of forming polyelectrolyte multilayers, is by alternate dipping of the substrate in aqueous solutions of oppositely charged polyelectrolytes [22] This method is presented in Figure 2-5 and is the main preparation technique used in this thesis.

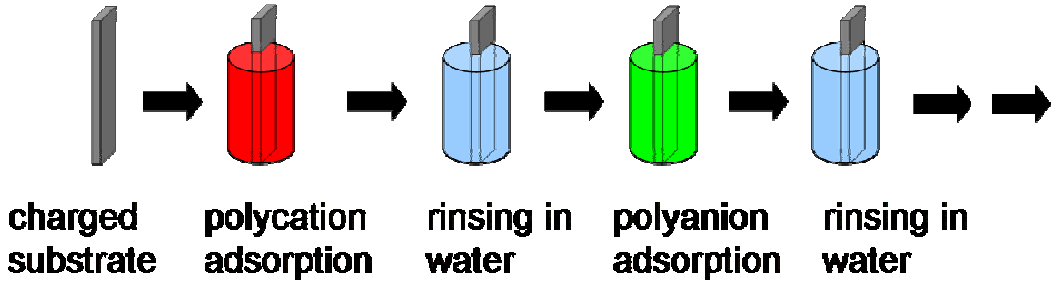

Figure 2-5 : The standard procedure for forming polyelectrolyte multilayers is dipping alternatingly in aqueous solutions of oppositely charged polyelectrolytes with washing steps in between.

The layer build-up can be detected in various ways. The most widely used techniques are UV-Vis Spectroscopy and X-ray reflectivity [22], quartz crystal microbalance (QCM), surface plasmon resonance [24], Ellipsometry [25], and neutron reflectometry [26]. (See reference [27] for a recent overview of experimental methods). Other possibilities for multilayer formation (which have advantages for certain applications) were also reported: Multilayers can be produced by spraying [28,29], which was reported to be faster than the dipping process and more flexible in the choice of substrate since no immersion is needed [30]. Because the spraying approach was used in the latest experiment, more details about this technique will be given in the experimental section. Build-up of multilayers by spin coating was reported by Chiarelli and co-workers [31] and also results in significant reduction of the preparation time.

The main interest in polyelectrolyte multilayer membranes and what makes them attractive for material science stems from the versatility of multilayer building blocks. Examples of materials that can be integrated are synthetic polyelectrolytes like poly-(styrenesulfonate) (PSS) and poly-(allylaminehydrochloride) (PAH) [32,33], natural polyelectrolytes [34-37], proteins [38,39] and DNA [40], inorganic particles (like clay or carbon nanotubes [41]) and metallo-supramolecular-polyelectrolytes [42].

The resulting multilayers can thus have interesting optical, electronic, lubrication, adhesive, antibacterial, bio-sensing or chemical-sensing properties (see reference [4] for an overview).

Structure of Multilayers

Polyelectrolyte-multilayers are interesting from a physical-chemistry point of view due to the complex principles of layer growth [10,27,43]. Although the adsorption of the multilayers is done layer by layer (for an exception see [29]), the structure of the multilayer is not lamellar. The structure can rather be described by a strong interdigitation of neighboring layers (see Figure 2-6). This was shown using X-ray reflectivity measurements (absence of Bragg peaks) and neutron reflectometry where only every second layer was deuterated. However, e.g. with clay particles or nanotubes, a lamellar layer-by-layer structure can be achieved, because of the morphology of the adsorbed particles [44].

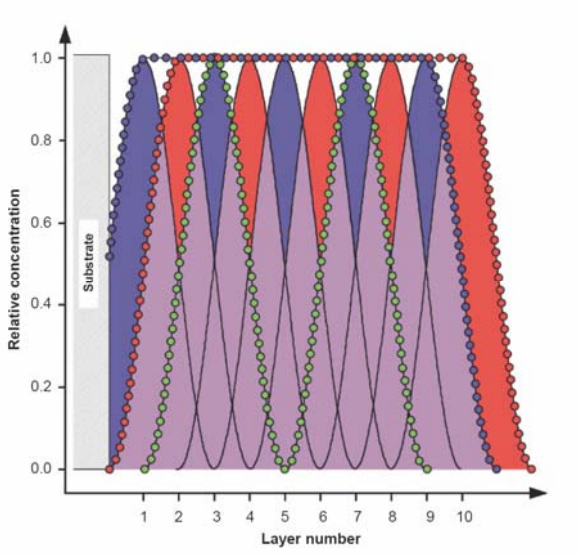

Figure 2-6 : Structure of a polyelectrolyte multilayer made from PAH and PSS, extracted from X-ray and neutron reflectivity curves [45].

For distances well above a single layer pair: e.g. by labeling several bilayers within an unlabeled film or by using different sets of polymers (composite materials) a lamellar structure can be achieved. For multilayers built from weak polyelectrolytes, a strong mobility of the polyelectrolyte chains was observed that eliminates the lamellar structure of the composite material [46]. The mobility of strong polyelectrolytes is smaller than the detection limit. Addition of salt increases the mobility of the chains. This increase of mobility with salt concentration was observed by measuring self

diffusion within the multilayer by means of fluorescence recovery after photobleaching and neutron reflectivity [47,48].

The multilayer assembly itself has an internal structure. Three regions can be distinguished. The area close to the substrate is called the precursor zone. Here substrate effects are relevant. This region is followed by the inner zone that has the properties of a dense surface unaffected multilayer. The surface zone is where the charges of the polyelectrolyte are not completely compensated by the last layer. Here the polyelectrolyte is very sparse and contains a high concentration of counterions [49,50].

Depending on the polymers and adsorption conditions, an exponential or linear growth of the layer thickness with the number of the deposited layers is observed [22,51,52]. Typically, several factors like polymer charge density [53], molecular mass and secondary interactions of the polyelectrolytes [54-56] have an impact on the growth mode. For the linear growth conditions, the layer thickness is typically several nm per bilayers [22] and can be fine-tuned by electrolyte concentration for charged systems [4]. The exponential growth regime correlates with a high mobility of the chains [57]. This allows a movement of a labeled polymer through the entire film. Usually, this type of multilayer systems are not mechanically stable enough for the construction techniques discussed later. However, some of these exponential growths systems dissolve under certain conditions. This effect is important for the production of freestanding films and can easily be understood by looking at the behavior of PEC.

The knowledge about the structure of polyelectrolytes in complexes and films leads to several interesting applications, where the structure of the multilayer is directly related to its function. Some examples are the embedding of functional molecules (in particular but not only proteins) to build sensing films [58] or achieving cytophilic or cytophobic surfaces [59-64]. Also superhydrophilic and superhydrophobic films were studied recently.

An interesting aspect of one of the studies performed by Rubner et al. is the use of the dewetting behavior of a weak polyelectrolyte film. By bringing the film close to its dissolution conditions, the film obtained a micro-roughness (Figure 2-7 left). After the addition and fluorination of Si-nanoparticles (nano-roughness Figure 2-7 middle) this leads to a super hydrophobic surface (Figure 2-7) [65].

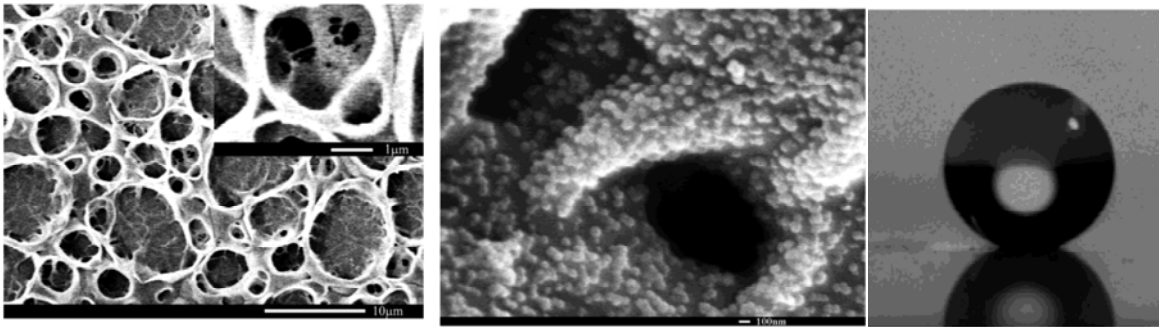

Figure 2-7 : *left :* SEM of Honeycomb structure made by partial dewetting of a PAA/PAH film. *middle :* SEM of a similar sample after treatment with Si-nanoparticles and fluorination, *right :* water droplet on this super-hydrophobic surface. (Adapted from [65])

2.4 Physical Properties of Polyelectrolyte Multilayers

Important physical properties of polyelectrolyte multilayers with respect to the work presented in this thesis are the permeability of the layers, their mechanical properties and the interaction between polyelectrolyte coated surfaces.

Permeability

Systematic investigations on the permeability of polyelectrolyte multilayers were mainly performed on multilayer shells (a study for a supported film is presented in [50]). Here it is easily possible to apply fluorescence recovery after photobleaching (FRAP) for molecules of different molecular weights [66-69]. The diffusion coefficients calculated in these publications for fluorescein vary from faster than 10^{-14} to 10^{-18} m^2/s. The very fast diffusion coefficients obtained by measuring FRAP on multilayer shells are due to hole formation during the core dissolution process [67], while the lower diffusion coefficients are the result of the capsule wall resealing [66,67,70]. Selective permeability of ions [71-76] and uncharged molecules [66,68-70,77,78] has been demonstrated as well for supported membranes or microcapsules.

For the permeability of high molecular weight compounds through multilayer capsule walls [66,67,69,78], a molecular weight cutoff between 4000 and 70000 g/mol for uncharged molecules has been found [67]. By changing the pH, salt concentration, the solvent, or by adsorbing additional layers after core dissolution, the permeability for high molecular weight molecules can be adjusted [67,68,70]. This offers the possibility of using these membranes as containers with defined permeability properties, like those needed in this thesis. [See chapters Selective Adhesion of Multilayer Capsules, Microcompartments as Model Sensors and Pressure Sensors]

Mechanical Properties of Polyelectrolyte Multilayers

Several independent methods to obtain the E-Modulus are presented in the literature. The E-Modulus reported in these studies is in the range of several hundreds of MPa to a GPa, depending on the polyelectrolyte-system and the environment. Dried membranes are very hard. Immersing in water raising the temperatures [79] and increasing the salt concentrations [80] softens the membrane. Gao et. al [81] presented a method based on osmotically driven deformations. Using colloidal probe AFM the E-Modulus can be obtained easily [82,83] and under different conditions such as ionic strength (including specific salt effects) [80], temperature [79], or different layer components [84]. Also the wrinkling period of a stiff thin coating on an elastic support has been reported to give information on the E-Modulus of polyelectrolyte-multilayer-films [85]. Although the system investigated in this particular study, was not a polyelectrolyte-multilayer, a detailed study of Rubner et al. has shown that the technique is applicable for multilayer systems built up on PDMS as an elastic support [86]. For the studies performed in this thesis (see chapters on “Multilayer Membrane Transfer” and “Pressure Sensors”) a medium stiffness is required as a compromise between stability and sensitivity. Therefore PAH/PSS membranes were used. The elasticity of these membranes was reported to be around 400 MPa [80,86].

Interactions of coated polyelectrolyte surfaces

The interaction between polyelectrolyte surfaces is not only important for the directed adhesion but also for the patterning of surfaces or the transfer of a freestanding membrane as presented in the results section. The interactions between polyelectrolyte coated surfaces were systematically investigated using colloidal probe AFM [87,88]. It was found that like charged surfaces repel one another while oppositely charged surfaces strongly adhere together. The coupling of polyelectrolyte shells to homogenous surfaces via electrostatic interactions was studied by Elsner and co-workers [89] and found the same result. Additionally this study showed the adhesion areas can be tuned by changing the wall thickness of the capsules. This dependence can be explained by the balance of adhesion and mechanical deformation energies in this system. Figure 2-8 shows the strong dependency of adhesion area size on wall thickness, which allows for accurate tuning of the adhesion process. Notably, adhering capsules can stand high shear stresses without

membrane failure or detachment [90,91], which is important for the investigations performed in this thesis.

For the printing of polyelectrolytes [92], multilayer transfer printing [93], and the transfer of multilayer membranes [94] polyelectrolyte/polyelectrolyte interactions are important as well because the polyelectrolyte (or membrane) must break old to form new interactions. For example different types of interactions with different strengths can be utilized. Hydrophobic and electrostatic interactions are employed in the case of the multilayer transfer printing, and the reversal of attractive interactions by dissolving parts of the membrane is used during the transfer of multilayer membranes.

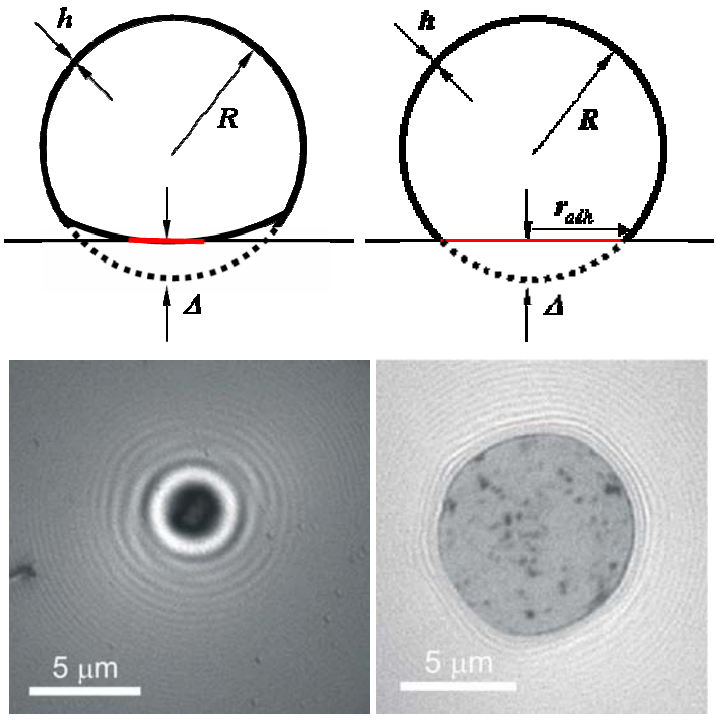

Figure 2-8: Scheme of weak and strong capsule adhesion (top). Corresponding Reflection Interference Contrast Microscopy Images of two polyelectrolyte-shells with a radius of 10 µm and a wall thickness of 7 (left) and 4 (right) bilayers PAH, PSS. The change of the adhesion area (grey) is dramatic from barely detectable to almost collapsing (buckling transition). (Adapted from [89])

2.5 Freestanding Polyelectrolyte Multilayer Films

Flat Multilayer-Membrane sheets

The formation of freestanding polyelectrolyte-multilayer-sheets uses dissolvable substrates or “sacrificial layers” between the substrate and the films. Several types of sacrificial layers which are dissolvable under different conditions (e.g. salt

concentration, pH) were initially reported by Dubas et al. [95]. The dissolution of the substrate is also a way to obtain freestanding membranes [9,41,96-99]. Mallwitz and Laschewsky [100] introduced a substrate free approach for membrane formation. While most examples of freestanding membranes are mesoscopic in 2 dimensions, Strook and co-workers showed that laterally confined multilayer “flakes” can be produced using structured surfaces for multilayer growth [101,102]. Mechanical tests of dried nanoparticle enforced freestanding polyelectrolyte membranes have been performed recently [9,103,104]. The embedded gold nanoparticles can be used as functional elements within the freestanding membrane [103,105-108]. The missing step needed to make use of flat freestanding membranes in water as semipermeable barriers, the binding to a structured pattern over large areas, is presented in this thesis.

Polyelectrolyte Multilayer Shells

Polyelectrolyte-multilayer shells are a special case of freestanding multilayer membranes. These shells are formed by coating a colloidal particle with a polyelectrolyte-multilayer and subsequent dissolution of the particle under conditions that do not destroy the multilayer [109].

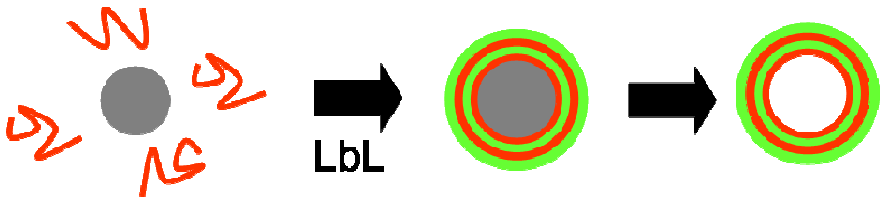

Figure 2-9 : Scheme of the capsule preparation process.

Core particles, which were successfully used, are colloids made from weakly crosslinked melamine-formaldehyde, polystyrene, silica, calcium carbonate crystals or cells (see [3] for an overview). The microcapsules produced in this way have sizes ranging from 25 nm [110] up to 20 µm [82], since their shape is fixed by the template particles used. Thus the capsules will be highly monodisperse. Wall thickness and interactions are controlled just as well as for solid supported multilayers. These properties are very important for the discussion of the results obtained in this thesis.
Another important property of microcapsules is their switchable permeability, which was used in several encapsulation studies [111,112]. Encapsulation adds another level of functionality to polyelectrolyte membranes. A subject of this thesis is the

encapsulation of polymers in compartments with flat freestanding polyelectrolyte membranes as lid. Other alternatives for entrapping large molecular weight molecules are co-crystallization with the core [61,113] and precipitation on the core prior to dissolution. In an additional method, the “ship in a bottle” technique, polymerization is performed inside the shell and the formed polymers are thus captured polymers [114]. The monomers are able to pass through the membrane but when polymerized they are trapped. Using these encapsulation techniques, several “smart” capsule-systems were prepared (for a more general review see references [3,115]), that show the improved functionality of polyelectrolyte-membranes. Encapsulated proteins keep their activity under conditions where unprotected proteins become inactive [112]. Biosensing applications of such systems have already been described [116]. The activity of the encapsulated enzyme can be controlled by low molecular weight inhibitors, while high molecular weight inhibitors are not able to pass the membrane and therefore do not show an effect [117]. As it will be presented in the first parts of the results, the defined coupling of this smart capsule system to surfaces however opens perspectives in the field of microfluidics and “lab-on-a-chip” approaches. A review with that emphasizes the encapsulation process, its implications for drug delivery applications and permeability of capsules can be found in [113]. A more general review on freestanding polyelectrolyte multilayer as functional and construction elements can be found in [118].

3 Methods

In this chapter the basics of the used methods, are briefly explained. The focus will be on practical working knowledge and aspects, particularly relevant for the later discussion. If review literature or text-books are available, then a selection will be given at the end of each chapter and classified as introductory or advanced literature. Techniques less relevant for the results and their discussion will be described only briefly at the end.

3.1 Microscopy

Microscopy is one of the most important optical analytical techniques in science. Because a plenty introductory literature is available, basic working principles and quantities like magnification and resolution will be first briefly introduced. Later special microscopy techniques such as the interferometry based reflection interference contrast microscopy, fluorescence microscopy, and confocal laser scanning microscopy (CLSM) will be explained[α].

Light Microscopy – Basics

The schematic setup of a light microscope in transmission mode is shown in Figure 3-1. Reflection geometry, where the incoming and reflected both pass through the objective, is also widely used. In particular reflection geometry is used for fluorescence- or reflection interference microscopy. The setup for transmission and reflection is similar. The light coming from the illumination source, usually a halogen lamp, passes through a collector and than a condenser. The collector focuses the light to the aperture diaphragm plane. The opening of the aperture diaphragm can be varied to allow for adjust the radiation intensity on the object. The condenser focuses the light source to infinity and thus prevents a convolution of illumination source and object. The field diaphragm is located at the rear focal plane of the condenser. Because it is projected on the image plane, the field diaphragm can be used to adjust the focus. This allows to adjust the illumination area in the object plane, and to

---

[α] Very instructive introductions including animations, galleries and databases can be found on the following websites: *http://micro.magnet.fsu.edu* and *http://microscopyu.com*.

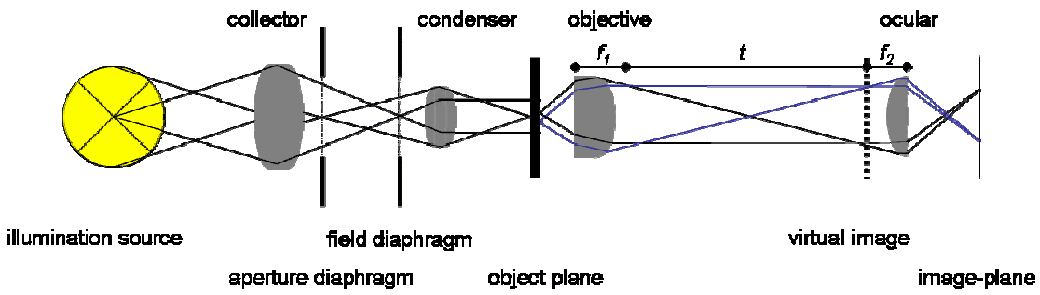

Figure 3-1: Scheme of a light microscope in transmission mode. The collector collects the light from the source; it is focused on the object by the condenser. The objective collects the light from the object and produces a virtual image, which is again magnified by the ocular on the camera or the eye.

prevent the specimen from heating. This illumination system is named “Köhler-Illumination” [119].

The light, coming from the specimen is then collected by the objective. The contrast mechanisms used vary. The most common is bright field contrast, caused by differences in scattering and or adsorption (reflection in reflection geometry). Other mechanism, like phase contrast and dark-field microscopy were not used in this thesis [120].

The objective produces a magnified image, which is again magnified by the ocular on the camera or the eye. The magnification of the microscope Γ_M is the product of the magnification of the objective β_{obj} and the ocular Γ_{ok}.

3-1 $$\Gamma_M = \beta_{obj}\Gamma_{ok}$$

The other important parameter of a microscope is the resolution, which is mainly defined by the objective (along with the type of specimen and the illumination). The resolution is defined as the minimal distance at which two points can be distinguished (d_{min}). For the microscopy scheme as introduced here, the maximum resolution is diffraction limited and given by the ratio of the wavelength of the light (λ) to the numerical aperture (*N.A.*) (Rayleigh limit). The proportionality constant is depending on the illumination and is for example 0.61 for self illuminating point-shaped objects.

3-2 $$d_{\min} \propto \frac{\lambda}{N.A.}$$

The numerical aperture is calculated from the index of refraction of the medium between the objective and the object (in reflection mode the cover slip, respectively) and half of the objective opening angle *($\alpha_{1/2}$)*.

3-3 $$N.A. = n_M \sin \alpha_{1/2}$$

The maximum aperture, which (in theory) can be achieved, is obtained via a high refractive index of the adjacent medium. This leads to the resolution of oil immersion objectives being even higher than for water immersed objectives.
Introductory literature: [119,121]
Advanced literature: [120]

Reflection Interference Contrast Microscopy

In light microscopy, contrast is not only be generated by the amplitude of the light. Using the phase of the light for contrast, objects with the same absorbance (scattering) can be seen, if they cause a change in the phase of the light. The best-known technique in this case is phase contrast, which will not be further discussed.
Phase images cannot be directly observed, but can be made visible using interference. If two light beams, which are coherent, are split and merged again, then the resulting amplitude depends on the difference in distance the beams traveled.
In Figure 3-2, this is shown for the two limiting cases. If the path difference is *$2n\lambda/2$*, the interference is constructive, resulting in a higher amplitude, if *$(2n+1)\lambda/2$,* the wave vanishes and no signal is observed.

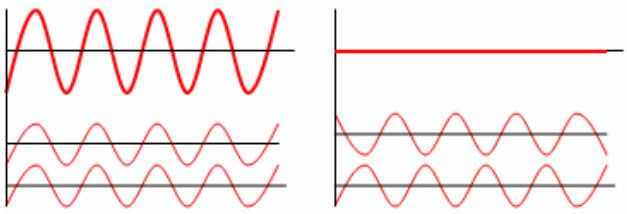

Figure 3-2 : constructive (left) and destructive interference (right)

To observe interference patterns the light must be coherent and monochromatic. Deviations from these conditions result in a blurring of the interference patterns.
The difference in path length may also be due to the reflection of the light on different interfaces caused by the change of the index of refraction at these interfaces. This can be used to determine membrane thicknesses and adhesion areas or to reconstruct the shape of an object close to an interface. Reflection interference

contrast microscopy (RICM) [122] is used to access these properties using a microscope setup presented in Figure 3-3.

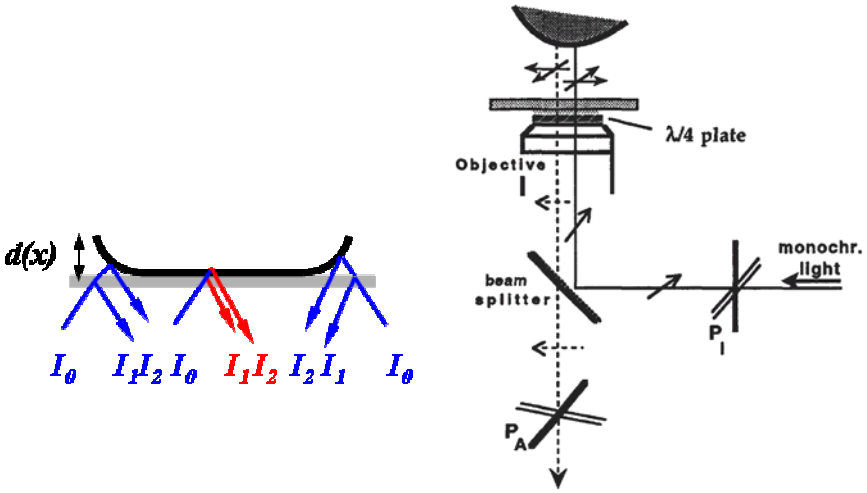

Figure 3-3 : *Left:* Ray diagram of a RICM setup. I_0 are the incoming beams, I_1, I_2 are the reflected beams [84]. *Right:* Setup of an antiflex RICM [122] .

As shown in the left scheme of Figure 3-3, the distance between the two extrema of the interferogram is related to a height difference *Δh* by:

3-4 $$\Delta h = \frac{\lambda}{4n_L} \cdot \frac{1}{\delta_{fa}} \cdot \frac{1}{\delta_{nl}(\theta)}$$

The wavelength of the beam is λ and the index of refraction of the medium is named n_L. The two correction factors δ_{fa} and $\delta_{nl}(\Theta)$ depend on the kind of illumination, the composition of the system, and the geometry of the reflecting interfaces [123].

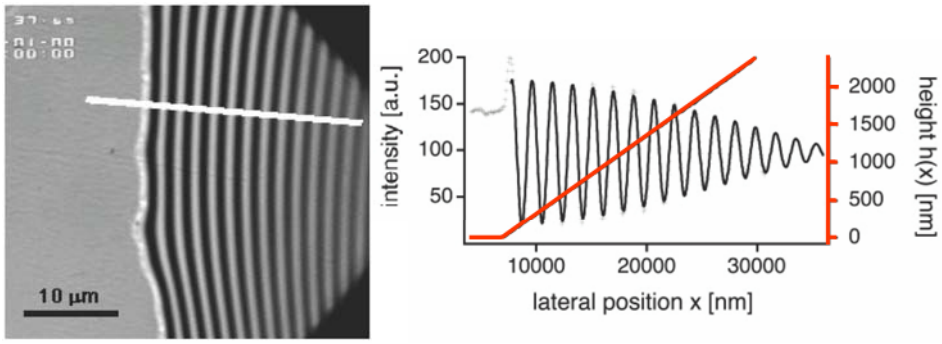

Figure 3-4: *Left:* Interferogram of a small liquid droplet with a finite contact angle. *Right:* A cross section along the white line (black) and the reconstruction of the height profile (red) [123].

From the interference patterns *h(x)* can be determined. The problem, however, is the direct correlation between height and the appearing interference pattern, because the

height-intensity function (not shown) is a function of λ, which changes periodically (with the argument of a cosine). A direct correlation can be made if two sets of monochromatic light, which then can be correlated giving quantitative values are used [124]. High orders of *n* can be neglected, due to the limited coherence of the light from the Hg-source used in this thesis. It is noteworthy that the fringe pattern can only be evaluated if it lies in the object plane, which is also the plane, in which the field diaphragm is in focus.

A more serious problem however is the influence of stray light and internal reflections, which significantly blurs out the interference pattern. The antiflex setup was developed to solve this issue. The polarization of the linear polarized incoming beam is rotated by 90° by $\lambda/4$ plate close to the sample (see Figure 3-3). The polarization of internal reflections is not rotated (while straight light is not polarized at all). With a second polarizer reflexes can then be well separated [122].

Fluorescence Microscopy

In fluorescence microscopy, the fluorescence of the object is the origin of the contrast. Usually a dye, which is fluorescently active, is bound covalently to the object or added to the solution being adsorbed by the object. To excite the chromophore, an electron is lifted from the S_0 to the S_1 level by light; energy is radiated as light when the electron falls back to the ground state. The red shift between excitation and emission has its origin in different vibrational and rotational levels (Franck-Condon-Principle), see also Figure 3-5 a. Bleaching occurs when the excited electron causes a reaction, which destroys the chromophore.

A scheme of a fluorescence microscope is shown in Figure 3-5 b. The main differences from a bright field microscope are the filters used for the excitation and emission wavelength, and the strong illumination source (a Hg-vapor-, Xe-lamp or a laser). The Hg-vapor lamp is used mainly because its spectrum has some high intensity peaks that correspond to the excitation energy of widely used chromophores such as rhodamine B or fluorescein.

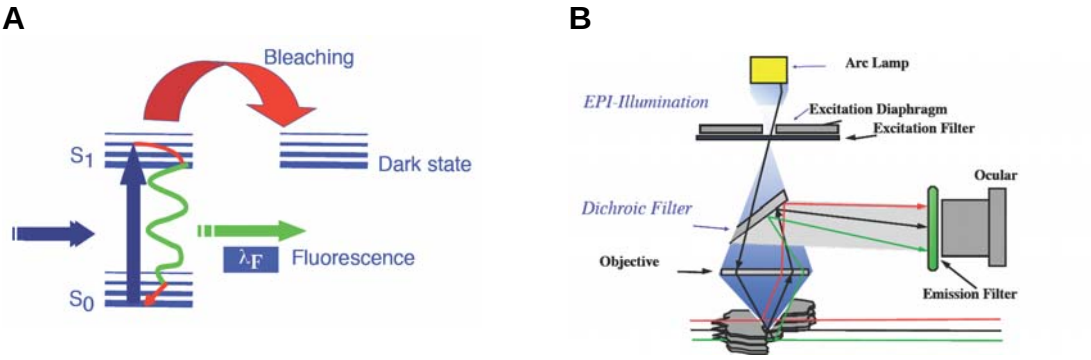

Figure 3-5 : *A:* scheme of the energy states of a fluorescent chromophore. *B:* setup of a fluorescence microscope [125].

Confocal Laser Scanning Microscopy

Confocal Laser Scanning Microscopy (CLSM) has become a versatile tool for 3 dimensional microscopic imaging. The recording of 3-D datasets is possible because the photomultiplier can record light only from the focal plane.

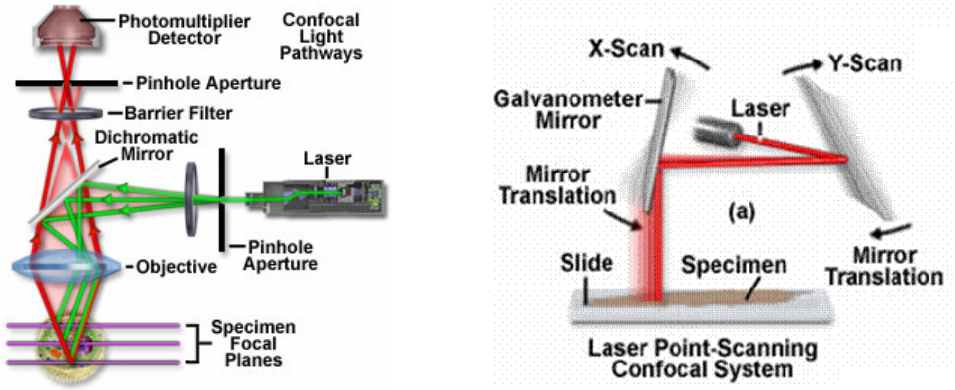

Figure 3-6 : *Left:* scheme of a confocal microscope showing the confocal light pathways [126]. Right: Scheme of the scanning system in confocal microscopes. The illumination spot is moved by two galvanometer mirrors [127].

The laser light, which is used for the excitation of the fluorophores, is passed through a pinhole to become a point-light source and is then focused on the specimen. The exited volume is so small that scanning the sample is required. To achieve a reasonable scanning speed without having large accelerations on the sample, galvanometer mirrors are used to move the beam across the sample (see Figure 3-6). The advantage of the scanning is that only a small volume fraction of the object is excited allowing neighboring objects to be excited separately and thus being separately resolved. The emitted light again passes through a pinhole. The pinhole blocks the light coming from all other planes except the focal plane. Therefore

background blurring is sufficiently suppressed and the contrast is increased. By moving the object relative to the objective, it is possible to record a 3-D image stack. This, however, does not necessarily give the expected results. Having media with two different indices of refraction on each side of the cover-slip (n_1,n_2 in Figure 3-7), an additional refraction takes place. The focal plane (f_o, green line in Figure 3-7) is therefore shifted with respect to the focal plane without the additional reflection (f_{th}, dotted line in Figure 3-7).

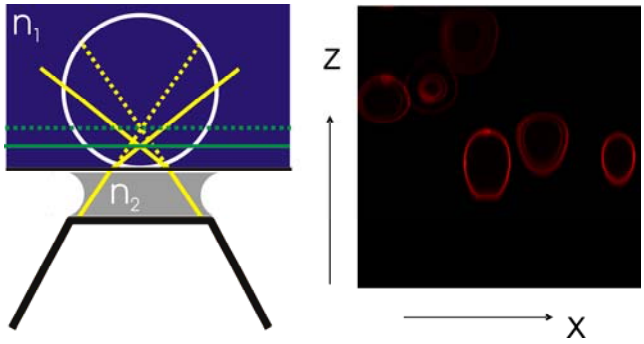

Figure 3-7: Distortion of x-z confocal images: Left schematic representation, shows that differences in the refractive indices of e.g. oil (n_1) and water (n_2), the theoretical focal plane (dotted lines) is shifted (solid lines). Right: Confocal micrograph of apparently distorted spherical polyelectrolyte capsules.

This effect is even more pronounced if f_{th} is deeper in the second medium [128]. The computer processing of the data, however, displays the signal coming from f_o at the height of f_{th} which results in a distortion in z direction. This effect can only be overcome using media with the same refractive index as solvent and immersion oil.
Introductory literature: [126,129]
Advanced literature: [130-132]

3.2 Scanning Force Microscopy

Imaging

The scanning force microscope (SFM) or atomic force microscope (AFM) was invented in the mid 1980's by Binning et al. [133]. The principle of the microscope is related to its elder brother, the scanning tunneling microscope (STM) [134].
A stage is moved by piezos in the x-y direction and thus allows for scanning of the sample. A sharp tip is used as a probe. The size of the tip limits the resolution. While for the STM the size of the tip is on the order of a single atom, this is not the case for the AFM. (The usual radius of curvature of an AFM tip is 10 nm.) The image of small

features is therefore always a convolution of the tip's shape and the sample structure.

The biggest difference between AFM and STM however, is the use of the deflection of the cantilever as a feedback parameter in AFM (while it is a tunneling current in STM). This deflection is kept constant by a piezo that moves in the z-direction (Contact Mode). The deflection of the cantilever is detected by adjusting a laser diode to the very top of the cantilever and recording the reflected light by a photodiode. This principle is also shown in Figure 3-8. The feedback parameter for AFM leads to several advantages over the STM. Namely it is possible to scan a sample under ambient conditions (also in solvents) and the sample does not need to be conductive. A big disadvantage of the described principle are the strong shear forces that appear and that may destroy in particular soft (polymeric) samples.

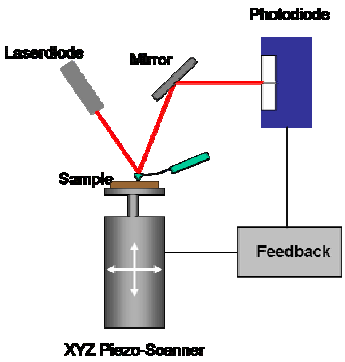

Figure 3-8: Schematic representation of the atomic force microscope; explanation see text.

The shear forces made the development of an alternative feedback mechanism necessary. In the so-called Tapping Mode™ the setup stays principally the same [135]. In addition, a vibration of the cantilever is excited by an additional piezo at its resonance frequency. Shear forces are avoided because the lateral movement is slow when compared to the (vertical) vibration of the cantilever. Thus, situations where the cantilever is laterally moved while in contact are not possible.

A harmonic oscillator can describe the system. The exciting force F_{ext} is a function of the cantilever's frequency ω with amplitude A.

3-5 $$F_{ext} = A_{ext} \sin(\omega t)$$

The resonance frequency ω_R is a function of the cantilever's mass m and its spring constant k.

3-6 $$\omega_R = \sqrt{\frac{k}{m}}$$

When the cantilever comes close to the surface, its oscillation is influenced by interactions with the surface as shown in Figure 3-9. The spring constant of the cantilever changes to an apparent spring constant. The latter can be described as the sum of a linear approximation of the surface long-range attraction and the cantilever spring constant.

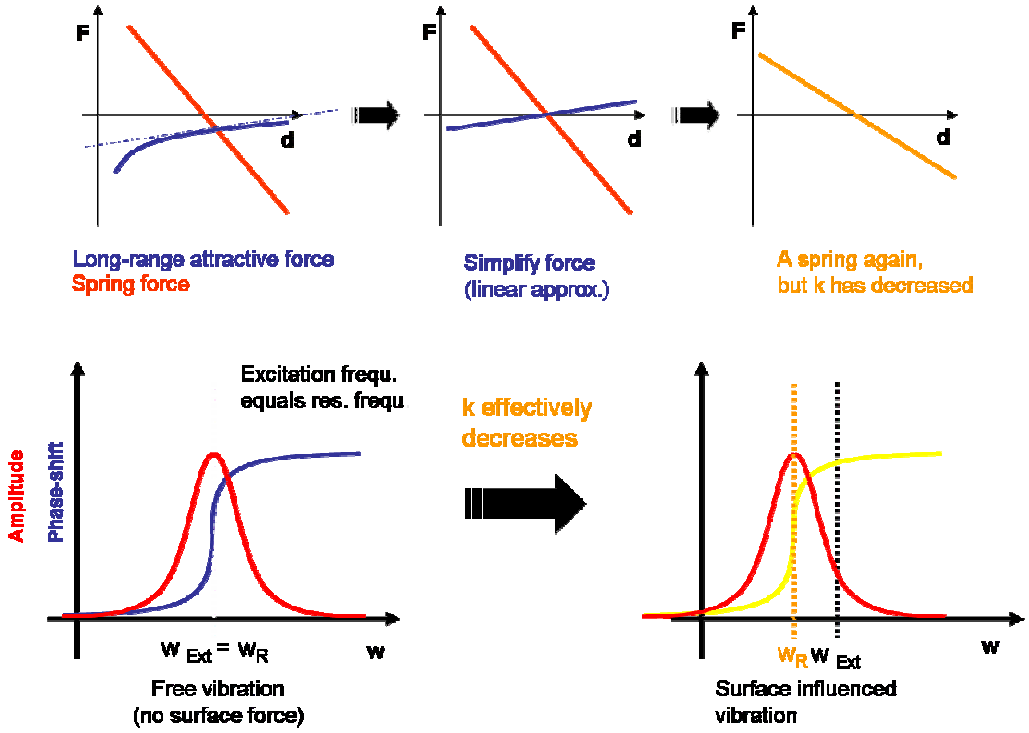

Figure 3-9: *Top:* The change of the apparent spring constant close to a surface. *Bottom:* Influence of the change of apparent spring constant to the amplitude and phase signal in AFM imaging. Here the case of attractive force gradient is depicted. Repulsive force gradients are possible as well and would result in a shift to higher apparent spring constant.

Near a surface the cantilever is no longer perfectly in resonance with the excited oscillation frequency (set for an isolated cantilever) and therefore the amplitude of the resonance drops. Therefore the surface topography can be imaged without damaging the sample by shear forces, when working with constant amplitude as feedback parameter.

Attractive and repulsive interactions with the surface will result in the same drop of the amplitude and therefore cannot be distinguished. Distinguishing between these interactions can be achieved because of the phase shift between the oscillating piezo

and the vibrating tip is 90° at the resonance frequency. Close to the surface a pronounced change in the phase can be observed due to the shift of the resonance frequency. This function is not symmetric with respect to attractive or repulsive interactions with the surface and the interactions can be distinguished. The dissipation of vibrational energy by the surface leads to additional changes in the phase signal that gives additional information [136,137].
Introductory literature: [138,139]

3.3 Other Methods

Ellipsometry

An ellipsometric experiment is an optical reflection experiment that measures the changes in the state of polarization upon reflection from a film covered surface. These changes can be expressed by the so-called ellipsometric angles Δ and Ψ. These angles are related to the reflection coefficients of the light polarized parallel (r_p) and perpendicular (r_s) to the plane of incidence by the basic equation of ellipsometry.

3-7 $$\tan\Psi e^{-i\Delta} = \frac{r_p}{r_s}$$

The reflection coefficients can be calculated using of Fresnel theory. In favorable cases, the film thickness and the refractive index can be obtained.
Here this technique was used as an independent way to determine the thickness of polyelectrolyte multilayers. Additional literature can be found in reference [140].

Contact Angle

The wetting of a solid surface is described by the contact angle Θ, which is the angle between a droplet of fluid (usually water) and the surface. Using the Young equation the contact angle can be used to determine the surface energy of the solid.
Here contact angles were only measured as a check for the hydrophobization of the Si-Masters or the hydrophilization of the PDMS was successful.
More information can be found in [141,142].

Zeta Potential

The Zeta-potential is the apparent potential of a particle in a solution measured by micro-electrophoreses. Apparent because its most closely associated ions are influencing the effective surface charge and the particle mobility. The zeta potential is therefore a function of the surface charge of the particle, any adsorbed layers at the interface, and the nature and composition of the surrounding medium in which the particle is suspended. The measurement gives information on surface charge at the shear plane of the particle. This is of high relevance, because it reflects the stability of colloidal suspensions as well as their adhesion properties. More information can be found in reference [143].

Membrane Osmometry

Membrane osmometry is used to determine the molecular weight of a polymer. Osmotic pressure is a colligative property, which means it depends on the number of particles. If a certain amount of polymer is dissolved in a solution, it generates an osmotic pressure, which is related to the number of chains. Therefore, the number average of the molecular weight can be calculated from the generated pressure. Practically the pressure difference across a membrane, which is impermeable for the polymer but permeable for the solvent, is measured. It is noteworthy that molecular weights of polyelectrolytes can only be determined with a large excess of salt, because without added salt the osmotic pressure scales with the counterion pressure [144].

4 Experimental Section

4.1 Chemicals and Materials

Polyelectrolytes and Polymers

All the unlabeled polyelectrolytes (see Table 1) were obtained from Aldrich and used without further purification except for the PSS, which was dialyzed against water (molecular weight cutoff of the dialysis membrane 10 kg/mol) until the resistance of the outer solution was stable and around 0.1 MΩ/cm and lyophilized prior to use. The PLL-g-PEG was a gift from the group of Markus Textor, ETH Zürich but is also commercially available from Surface Solutions (Zürich, Switzerland)

Polymer	**Abbreviation**	**M_W [kg/mol]**
poly-(styrenesulfonate, sodium salt)	PSS	70
poly-(acrylic acid, sodium salt)	PAA	5.1
poly-(allylamine-hydrochloride)	PAH	15* and 70
branched poly-(ethyleneimine)	PEI	25
Poly(diallyldimethylammonium chloride)	PDADMAC	100 – 200** and 200-350
Rhodamine labeled poly-(allylamine-hydrochloride)	PAH-Rh	70
Fluorescein labeled poly-(allylamine-hydrochloride)	PAH-FITC	70
Alexa labeled poly-(allylamine-hydrochloride)	PAH-Al	15
Fluorescein labeled dextran	FITC-Dextran	500
Polylysine-grafted-Polylethyleneglycole, grafting ratio 3.5	PLL-g-PEG	20 (PLL), 2 (PEG)

*the PAH used for cell encapsulation was of lower molecular weight

* the PDADMAC for the printing was of lower molecular weight, while for the osmotic pressure experiments the one with higher molecular weight was used.

Table 1: Polyelectrolytes, labeled polyelectrolytes and labeled polymers used in this work

For visualization of the polyelectrolyte multilayers, fluorescently labeled polyelectrolytes were used (for molecular weight, and abbreviation see Table 1). Rhodamine-B-isothiocyanate (RBITC; λ_{exc} = 541 nm; Fluka, Germany) or Alexa (555) Fluor® (λ_{exc} = 555 nm; Molecular Probes, Eugene, OR, USA) were covalently bound to PAH as follows:

A solution of 11 mmol (0.1090 g) PAH in 4 ml sodium-hydrogen-carbonate buffer (pH≈9) was prepared and 0.1 mmol (0.0045 g) Rhodamine-B-isothiocyanat dissolved in 1 ml methanol was added. The degree of labeling therefore was maximal 1:100. This was chosen to be sure that the dye did not affect the behavior of the polymer. The obtained solution was stirred for 3 h at room temperature. Unbound dye was removed by performing a dialysis against Milli-Q-grade water for at least one week by means of a 3.5 kDa cut-off dialysis membrane (Spectrum Laboratory, Rancho Domiguez, CA, USA) until no fluorescence was detectable in the washing water. The coupling of Alexa 555 was performed similarly [145,146].

Rhodamine-B-labeled-PAH used for the labeling of freestanding membrane sheets was purchased from Capsulution Nanoscience AG (Berlin, Germany), degree of labeling: 1:500 Rho:PAH-Mon.), produced according to Richter et. al [145]. FITC-dextran was obtained from Sigma.

Bovine serum albumin (BSA-TRITC) was purchased from Sigma Aldrich and labeled as described for the PAH to visualize the passiviation of the PLL-g-PEG surfaces.

Milli-Q-grade water (Millipore Inc., Bedford, USA (experiments in Genova, Italy) or Purelab Plus UV/UF, Elga LabWater, Germany (experiments in Golm, Germany) with a resistance of 18.2 MΩ/cm was used for all solutions and cleaning steps. The total of organic content in the water was measured regularly and was between 2 and 12 ppb. Organic solvents (chloroform, isopropanol, hexane, ethanol) and the inorganic salts used were of analytical grade (p.A.).

The polydimethylsiloxane (PDMS) Base Silicon Elastomer Sylgard 184 and the curing agent were obtained from DowCorning (Midland, MI, USA).

Design and Surface Modification of Silicon Templates for PDMS Stamps

The silicon-masters used for producing microcontact-printing-stamps were obtained from GeSim (Großerkmannsdorf, Germany) and hydrophobized using Heptadecafluoro-1,1,2,2-tetrahydrodecyldimethylchlorsilan (ABCR Germany).

The silicon masters (and a silicon wafer for measuring the contact angle) were activated for 2 min in an air-plasma (Harrick PDC 32 G-2, high intensity, pressure

$<10^{-2}$ mbar), followed by a gas phase deposition of the fluorosilane, performed at 20 mbar in a desiccator. After 4 hours the surfaces where carefully rinsed with ethanol.

Silicon-masters purchased from the Fraunhofer Institut für Biomedizinische Technik (Berlin, Germany), were designed to fit our requirements. The masters were already hydrophobized when received. The hydrophobic coating is sensitive to organic solvents, thus cleaning may only be done using water or 1:1 water/i-propanol mixtures. The particular design of the master can be found in Appendix I.

4.2 Characterisation Methods

Optical Techniques

Fluorescence Microscopy

Fluorescence microscopy measurements were carried out on a Zeiss Axiovert 200 (Zeiss, Germany) using a LD A-Plan 20× objective, illuminating with an Hg-vapor lamp. For fluorescein the excitation and the emission were filtered between 450-490 nm and 515-565 nm, respectively. For rhodamine the excitation was filtered around 546 nm and for the emission a low pass filter of 590 nm was in use. The images were recorded with a Zeiss AxiocamHR monochromatic camera.

Confocal Laser Scanning Microscopy

The results for the coated yeast cells were obtained by a Nikon C1 (Nikon Instruments, Florence, Italy) confocal laser scanning microscope (CLSM). The C1 scanning head was mounted on a Nikon inverted optical microscope. An Ar-ion laser (488 nm, 514 nm) and a He-Ne laser (543 nm) source, enclosed in a common multi laser module, provided the excitation beams and a Nikon Plan Apochromat 40×, and a 100×/1.4 NA oil immersion objective were used for imaging.

The results from section 5.2 (freestanding membranes) were taken on a Leica TSC NT SP confocal system (Leica, Germany), equipped with a 100× and 40× oil immersion objective with a N.A. of 1.4 and 1.25, respectively. The sample was excited by Ar-ion laser (488 nm, 514 nm) and a He-Ne laser (543 nm) source. For imaging the filled microarrays, a step motor with an accuracy of 100 nm was taken for the z-scans.

For the osmotic pressure experiments, a galvanometer driven z-stage with an accuracy of 40 nm was used, to scan in the xz-direction.

Reflection Interference Contrast Microscopy

The reflection interference contrast microscopy was carried out on a Zeiss Axiovert 200 (Zeiss, Germany) using a Zeiss Antiflex 63× oil immersion objective with a N. A. of 1.25, illuminated with a Hg-vapor lamp. A monochromator with a wavelength of 546 nm was used. The images were recorded with a Zeiss AxiocamHR monochromatic camera.

Imaging AFM

The atomic force microscopy (AFM) images for determining capsule thicknesses and printed structure heights were taken using a Nanoscope IIIa AFM in Tapping Mode®. The AFM-tips used (PPP-NCH-W) were purchased from Nanosensors (Wetzlar, Germany). They had a typical resonance frequency of 302-354 kHz and a stiffness of 25-42 N/m.

The thicknesses of the freestanding films were measured by Ingo Dönch (MPI Kolloid und Grenzflächenforschung, Abt. Grenzflächen, AG Dr. Fery) on a NanoWizard® AFM (JPK Instruments, Berlin, Germany), using Ultrasharp CSC 12-AIBS-50 contact mode AFM tips with a typical spring constant 0,08 N/m and a resonance frequency of 20kHz from Micromash (Madrid, Spain) in water.

Others

Contact Angle

Contact angles were measured on a contact-angle-measuring-system G10 (Krüss, Hamburg, Germany), using the system software to extract the droplet shape and the contact angle.

Membrane Osmometry

The determination of the osmotic coefficient of the PDADMAC solutions was done with a Gonotec Osmomat 090 (Gonotec, Berlin, Germany) by Christoph Wieland (Fraunhofer Institut für Angewandte Polymerforschug, AG Prof. Dr. Thünemann). As membranes, cellulosetriacetate 20 kD and 10 kD were used.

4.3 Standard protocols for sample preparation

Production and Surface Modification of PDMS Stamps

PDMS Sylgard 184 and the respective curing agent were mixed in a 10:1 mass-ratio, degassed in vacuum and stored at -18°C for 1 month maximum. For obtaining flexible PDMS stamps, the pre-polymer was poured over a structured silicon wafer in a Teflon® bowl, degassed and cured for 24 h at 60°C. After curing, the stamps were carefully cut out. Then they were hydrophilized in an air plasma for 60 s (low intensity, corresponding to 40 W, pressure < $4 \cdot 10^{-3}$ mbar).

To produce thin PDMS structures on a cover slip as support, 500 µl of the pre-polymer were poured on the silicon structure, degassed, and pressed on a coverslip (Roth, Germany) and treated as explained above.

Polymer on Polymer Printing

Printing from water/ethanol mixtures

As stamping solutions polyelectrolyte solutions (PDADMAC, PSS) in water/ethanol mixtures of different concentrations were used (PDADMAC 0.125 M, 1:1 ethanol/ water, PSS 0.04 M, 2:3)

The ink was brushed on the PDMS stamp and blown dry in a stream of nitrogen after 3 min of waiting. The stamps were brought into contact with dried, coated silicon-wafers for 1 min, and then removed. The structured surfaces were carefully rinsed with water and stored under water until use and characterized using Tapping Mode® AFM.

Printing from water solution

A 1 mg/ml solution of PAH-Rh (or PLL-g-PEG) with an ionic strength of 0.5 M (NaCl) solution was spread on the stamp. The pH of the PAH-Rh solution was 8.7. After 15 min the stamps were rinsed with water and excess was removed in a stream of nitrogen. The inked stamps were brought into contact with dried, coated silicon-wafers or cover slips for 15 min, and then removed. The structured surfaces were carefully rinsed with water and stored under water until use and characterized using Tapping Mode® AFM and fluorescence microscopy

Production of Polyelectrolyte-Shells

The capsules were prepared according to Donath et. al. [109]. Weakly crosslinked melamine-formaldehyde-particles (MF-particles) with a diameter of 5.1 (±0.09) µm (monodisperse, 10 % in volume fraction) were purchased from Microparticles GmbH (Berlin, Germany) and coated by alternating adsorption of positively and negatively charged polyelectrolyte from aqueous solution (PSS/PAH; even number of layers; polyelectrolyte-concentration of 1mg/ml; ionic strength of 0.5 M NaCl). Subsequently, the MF particles were dissolved in 0.1 M HCl solution. Completeness of particle removal and thickness of the capsule walls were determined by AFM-imaging of capsules dried on mica. The dry thickness, measured by AFM after dissolving the core, was 2.8±0.3 nm per layer-pair. Capsules were prepared with 5 layer-pairs before dissolving the core. After dissolution, one layer PSS and one layer PAH-Rh were added.

Filled, strongly swollen capsules were purchased from Capsulution (Berlin, Germany). The capsules were made on a silica core, from PAH/PSS multilayers. This sample was polydisperse having a size distribution from 15 to 30 µm.

Encapsulation of Yeast Cells

For the encapsulation of living cells, two different strains of yeast were in use. In most of the experiments, common bakery yeast *Saccharomyces cerevisiae* was encapsulated. The coating follows the procedure for polyelectrolyte capsules and was described in detail in [147,148]. First the cells were stored for 2 h in YPD (10% yeast extract, 20 % peptone, 20% glucose) medium at 28°C for recovery, then the solution was exchanged to 0.5 M saline (NaCl). The resuspended cells were encapsulated by incubating them in PAH solution (2 mg/ml) containing 0.5 M NaCl[1], followed by 2 washing steps with 0.5 M (NaCl) saline solution. Then the next layer was deposited from 0.5 M saline PSS solution and so on, until the desired number of layers was reached. Usually we worked with 4 or 5 layers to have a negative or positive outermost layer. In one experiment, we encapsulated the cells with 7 layers due to a predicted higher charge density [1].

Because of the fluorescent dye Alexa (555) covalently bound to PAH, we were capable to detect the coating's homogeneity. The polyelectrolyte deposition gave

[1] The PAH used for yeast cell encapsulation had a M_w of 15 kg/mol in contrast to the PAH used in all other cases

also information about the cell viability. In case of membrane rupture, the labeled polyions entered the cells and stained them red. Only cells with intact membranes excluded the polyelectrolyte completely.

The yeast strain expressing the green fluorescent protein (GFP) under galactose promotion was a gift of Prof. C. Palleschi from the University La Sapienza in Rome, Italy. The encapsulation process for the GFP expressing yeast was the same.

Imaging in fluorescence and phase contrast mode of ordinary yeast cells was performed in 0.5 M NaCl solution. In contrast, the GFP expressing yeast was incubated in 15% galactose in water for two hours at a constant temperature of 28°C to induce the GFP production. Under this condition the green protein was kept inside and so co-localization of the capsule and the cell interior was possible.

Directed adhesion of capsules or encapsulated yeast cells

The results presented in for the directed adhesion of capsules and yeast cells were performed similarly. The patterned glass was dried in a nitrogen jet. A droplet of capsule dispersion was put on the structure. After an incubation time of app. 15 min the dispersion was agitated using an Eppendorf pipette. After a second incubation time the dispersion was diluted and characterized.

Coating Si-Wafers for Membrane Transfer

Silicon wafers (a gift from Silchem Handelsgesellschaft GmbH, Freiberg, Germany) were cleaned with the RCA method [149] before coating: ultrasonic cleaning of the wafers in an isopropanol/water mixture (1:1) and treatment with a 1:1:5 mixture of ammonia-solution, hydrogen peroxide, water for 10 min at 70°C to remove all organic material on the surface.

For the buildup of the films presented in the chapter dealing with filled microarrays, the wafers were dipped for 20 min in polyelectrolyte solutions and rinsed 3 times with pure water using a dipping robot (Dipping Robot DR-3, Riegler & Kirstein GmbH, Berlin, Germany; program see Appendix II). The film consisted of the following multilayer sequence:

PEI/(PSS/PAH$^{\blacklozenge}$)$_5$/(PAA/PAH$^{\#}$)$_5$/(PAH$^{\blacklozenge}$/PSS)$_n$/PAH-Rh$^{\blacklozenge}$/PSS/PAH$^{\blacklozenge}$/PSS (n= 5, 40).

The dipping solutions were prepared as follows:

PEI: 1 mg/ml, no salt;

PSS: 10^{-3} M, 0.5 M NaCl;

PAH, 10^{-3} M, *[$\blacklozenge$]*: 0.5 M NaCl; *[#]*:1 mM NaCl;

PAA 10^{-3} M, 1 mM NaCl, pH 3.5.

The membranes in for the mechano-sensing were built-up using the spraying technique. Household spraying bottles (Sidolin glascleaner, Henkel, Düsseldorf, Germany) were cleaned and filled with the solutions mentioned above. The cleaned silicon wafers were placed on a gel-pack. For each deposition process, the handle was pressed 4 times with 5 s pause after two times, for the washing solution this was doubled. The produced films, had the same multilayer sequence as mentioned above. However, the spraying was done for all layers except the PEI and the layers including and after the PAH-Rh.

Membrane transfer

For the filled microarrys the PDMS pieces were coated with PEI/$(PSS/PDADMAC)_3$, while for the pressure sensors a coating with only PEI was used (see for PDMS preparation and modification page 34). After drying the PDMS and the coated substrate carefully the PDMS was pressed gently onto the wafer and transferred to a Petri-dish containing HCl solution of pH 1 to dissolve the PAA/PAH layers. After 12 h incubation the HCl solution was removed and replaced by water, obtaining the freestanding film on top of the PDMS structures.

Permeability and filling of membrane structures

The permeability of the membrane structure was tested with 500 kg/mol FITC labeled dextan and FITC, respectively. A droplet of the solutions was given on a glass slide, mounted on a confocal microscope. The membrane covering the PDMS was placed on the droplet, with the membrane facing downwards in the direction of the objective. After an incubation time of approx. 15 min, a 3-D stack was imaged using confocal microscopy.

Osmotic pressure experiments

PDMS structures on a coverslip with a membrane were placed in a chamber sealed by vacuum grease and mounted on the confocal microscope, without drying the membrane. The chamber was filled with 2 ml of water. A set of cavities was imaged in the xy- and xz-directions (across the center of the hole). In the following step, the water was replaced by a salt free PDADMAC solution. The very same cavities were imaged again and the PDADMAC concentration was increased stepwise by exchanging the liquid completely.

5 Results and Discussion

The transfer and coupling of freestanding polyelectrolyte membranes to flat substrates in aqueous environment will be presented in this chapter. This was done in two different ways. Capsule arrays were built by directed adhesion of polyelectrolyte-capsules on micro-patterned surfaces. Polyelectrolyte-films were transferred to topographically structured substrates, to obtain freestanding membranes. These two approaches look quite different on the first view but have several aspects in common. In both cases, arrays of micron sized cavities are formed. They are separated from the surroundings by integration of a semipermeable polyelectrolyte membrane. In both cases, adhesion properties of the membranes are crucial for successful assembly. Another connecting element in the construction of both types of arrays is the stamping of the polyelectrolyte layers.

In this chapter, the results of the polymer on polymer stamping will be discussed first because the principle of stamping will remain important throughout the discussion. The directed adhesion of polyelectrolyte capsules and encapsulated yeast cells on the printed pattern will be the next topic. The construction and application of freestanding multilayer lids and examples of their application will be the subject of the last part of this chapter.

5.1 Capsule Arrays

Polymer on Polymer Stamping

Polymer on polymer stamping (POPS), which is a variation of microcontact-printing, was introduced 2002 [92] by Hammond et al. This technique creates patterns of different functionality on all kind of surfaces and is based on physisorption due to electrostatic interactions. The latter is the major difference form the first experiments done in the Whitesides-group 1994 [150]. They developed microcontact-printing with thiols or silanes, which is based on covalent bonding of the surface coating. As for the conventional microcontact-printing, the result is a patterned surface. The patterned functionality may be differences in surface charge [55,92,151] (which was used in this thesis predominantly), biological activity [152] (first results from a cooperation with Dr. José Toca Herrera and Verónica Saravia from the University of Tarragona, Spain are presented as well) chemical activity [153] or wetting properties [65] (both not a subject in this thesis). Here this patterning was used to

direct the adhesion of polyelectrolyte microcapsules. A flow diagram of the printing process is shown in Figure 5-1.

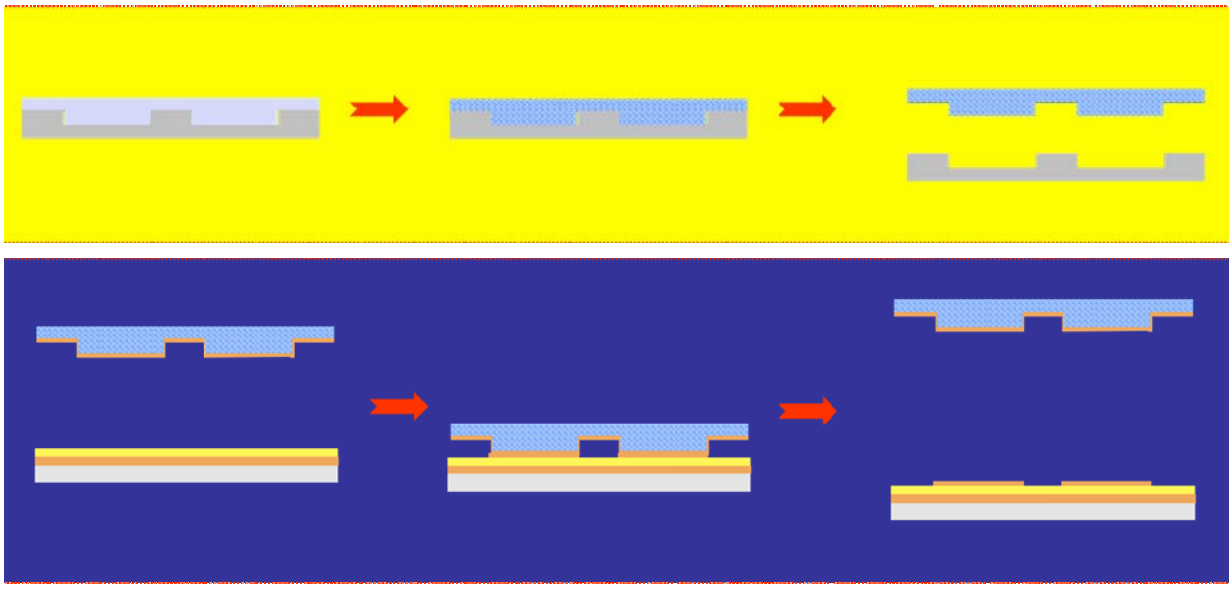

Figure 5-1 : Flow diagram of the printing process: For the production of the PDMS substrate (orange background) the prepolymer is given on a prestructured silicon (the Si-master) wafer, cured at elevated temperatures, peeled off the master, hydrophilized becoming the stamp. This stamp was used for printing polymer solution (blue background). Therefore the stamping solution was applied, and the stamp was washed carefully. After drying, it was pressed slightly to the homogeneously coated substrate. After peeling the stamp off, the substrate is patterned respectively to the structure on the stamp.

The silicon wafer, which is used as a master, is commercially available and usually prepared using photolithography. The structure is either etched into the master or sputtered onto the master after the photolithographic process [154]. The wafers used in this thesis were structured using standard photolithography and the structure was etched in the wafer. (See experimental sections for details.)

The Si-master is hydrophilic, which causes problems for curing PDMS on it. During the curing process, the PDMS reacts with the hydroxy groups of the silicon oxide. This causes a covalent connection between the stamp and the master, which destroys both. To avoid destroying stamp and master, the master is hydrophobized by gas-phase deposition of hydrophobic silanes (see experimental part). The hydrophobic layer inhibits the reaction of the master with the PDMS in the curing process. This and the low surface energy of the master's surface allow for an easy peal-off-process. After peeling off the cured PDMS, the native surface is hydrophobic and the water based stamping solution does not wet the stamp. This problem can be

overcome by plasma treating the PDMS. In Figure 5-2, the effect of plasma treatment on the wetting properties of PDMS is shown [155].

The crucial experimental details of the plasma treatment are given in the experimental section. Using air plasma for 60 s with a pressure of $<4 \cdot 10^{-3}$ mbar with an intensity of 40 W gave the reported effect without destroying the PDMS surface (Figure 5-2). Too intense plasma treatment will result in partial oxidation of the PDMS to glass and should therefore avoided [156,157].

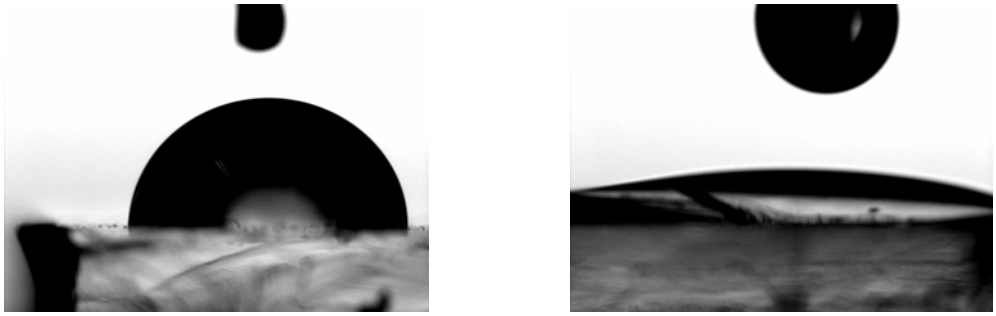

Figure 5-2 : A droplet of water is placed on a native PDMS surface (left, microscopy image from the side). The contact angle of around 90° was extracted from the drop profile. Upon plasma treatment (60s at 40 W, pressure $<4 \cdot 10^{-3}$ mbar), the PDMS surface becomes hydrophilic. A droplet of water wets the PDMS surface completely (right).

After the PDMS was hydrophilized, it was stored in water up to 48 hours or until it was used. For the stamping process, two approaches were used. Principally the stamping solution was brought to the stamp and the stamp was slightly pressed to the polyelectrolyte-coated surface. After the appropriate contact time, the stamp was removed and the surface was carefully rinsed with water.

Stamping ethanol/water polyelectrolyte solutions is related to the work of Jiang et al. [92]. In contrast to his work, we printed not on a polyelectrolyte multilayer but rather on a single or double layer of polyelectrolyte on the surface, which was sufficient to achieve patterning for our applications. The stamping solutions, which were used, were ethanol/water mixtures containing PDADMAC and PSS as described in the experimental part.

In agreement with Jiang et al. [92], the heights of the printed structures were several tens of nm before and five to 10 nm after rinsing, respectively (see Figure 5-3). The height of the transferred structure is a function of the water/ethanol ratio, the amount of material brushed on the stamp, the waiting time, and the concentration and type of

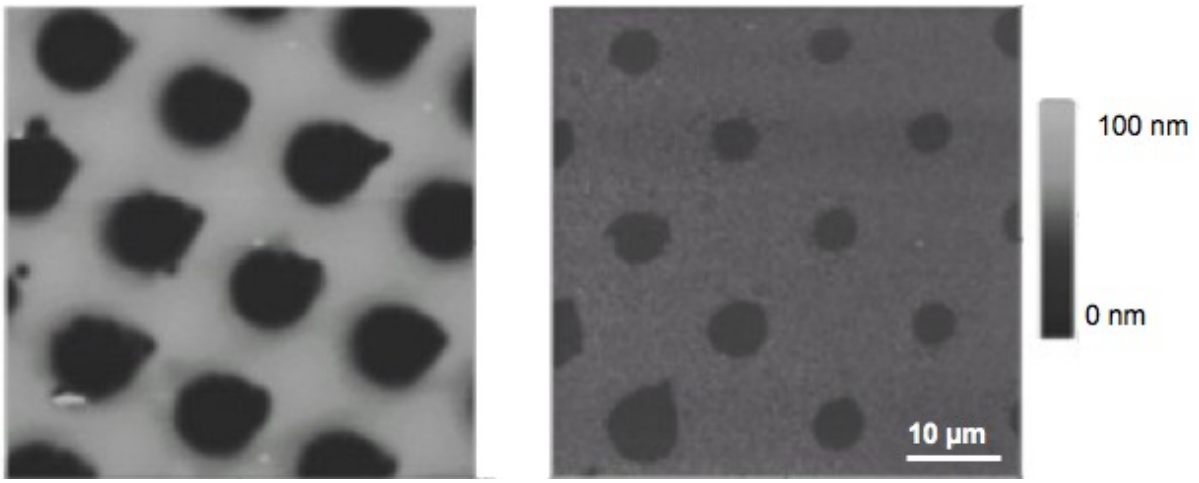

Figure 5-3 : The AFM image shows the effect of rinsing on the thickness of a printed structure (left before, right after rinsing). The excess of polymer (PDADMAC) can be washed away. The height of the stamped structures decreases from several tens to 5-10 nm after rinsing. The smaller size of the uncoated areas (dark) after rinsing may be due to polyelectrolyte diffusing from the already coated areas to the uncoated ones.

polyelectrolyte used. With increasing amount of ethanol, the mixture becomes a bad solvent for the polyelectrolyte, leading to a collapse of polyelectrolyte coils in solution and precipitation as extreme. The solvent quality affects the amount of polyelectrolyte on the hydrophilic PDMS surface. Therefore, the thickness of the initial print increases, with decreasing solvent quality (i.e. increasing ethanol concentration). After rinsing, the thickness was on the order of a monolayer. The best results for PDADMAC and PSS were obtained for the following polymer concentration and solvent ratios: 0.125 M, 1:1 water/ethanol (PDADMAC) and 0.04 M, 2:3 ethanol/water (PSS). The optimum contact time in both cases was 1 min.

As a first step, we tested the chemical contrast and the resulting selectivity of the stamped surfaces for polyelectrolyte adsorption. The interactions between the polyelectrolytes used here (PSS and PDADMAC or PAH) are mainly electrostatic, as it was shown in previous colloidal probe AFM experiments [87]. To be more accurate, the driving force in this case is the exchange of counterions by the polyion. This exchange is driven by an increase in the entropy of the system. PAH-Rh, a labeled probe, was adsorbed from solution to visualize the printed pattern. A droplet of the PAH-Rh solution was added to the sample, after ten minutes the sample was washed, and the result was observed with fluorescence microscopy (Figure 5-4). By printing the polymer of opposite charge the image can be inverted (not shown).

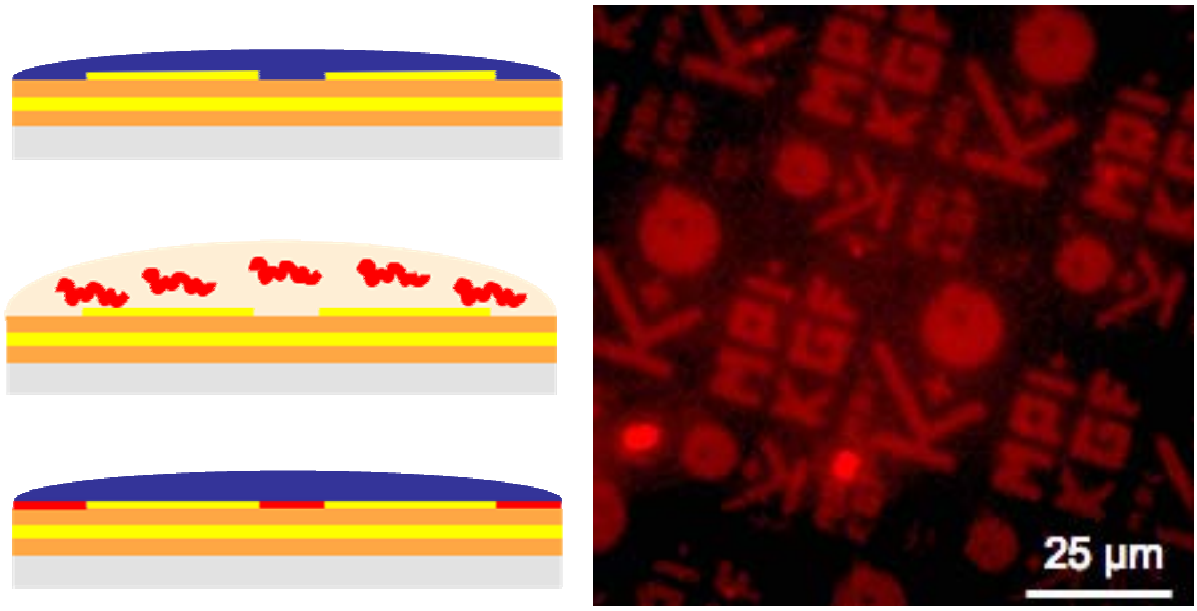

Figure 5-4 : The fluorescence micrograph shows (false colors) the selective adsorption of PAH-Rh as a fluorescent probe visualizes the printed pattern. The positively charged polymer only adsorbs on the negatively charged surface areas (right). The principle is sketched on the left. The positively charged labeled polymer (red) only adsorbs on the negative part of the structure (orange), while no adsorption can be found on the positive parts (yellow).

In a second approach, the stamping solution used was an aqueous polyelectrolyte solution, containing 0.5 M salt [158], and fluorescently labeled PAH was used as polyelectrolyte. Here the waiting time for incubation and contact were longer than the process described above. However, here less material was transferred and a better contrast and a sharper pattern resulted. For some cases, inverse prints (shown in Figure 5-5, right) were observed because the hydrophilic cavities in the PDMS keep the polymer solution by capillary forces and then release the polymer during the stamping process. This is usually called a “low print” because the ink is stored in the lower part of the structure. A “low print”, however, does not lead to the wanted contrast. Careful rinsing washes out the polymer from the cavities and leads to a situation referred to as a “high print”. In this situation the required contrast is achieved because the high part of the structure is transferring the ink.

The height of the printed structures was measured with tapping mode atomic force microscopy (AFM) in air. The heights that were obtained were 2.5±0.3 nm, which is on the order of the typical thicknesses of polyelectrolyte layers formed by adsorption. Figure 5-6 shows the distribution of heights obtained on different spots of different substrates by AFM and a typical AFM image including a cross section. The sharpness of the pattern’s edge is on the order of the accuracy of the AFM images.

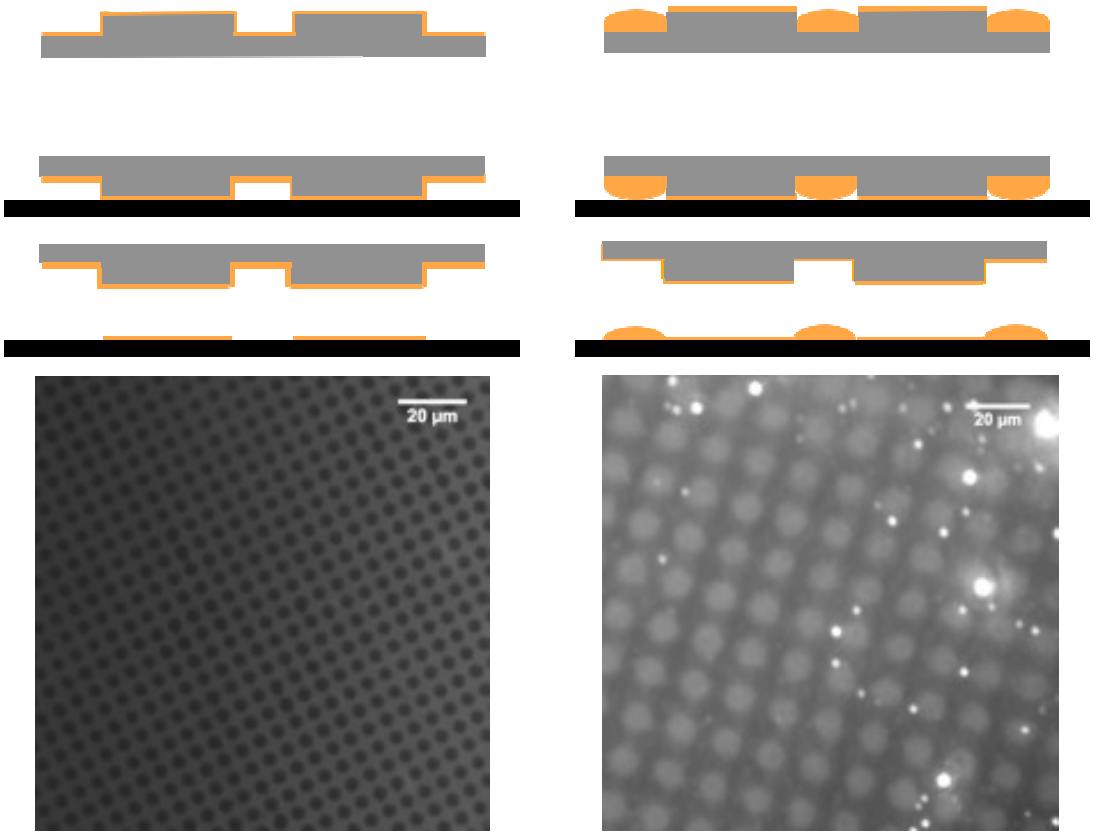

Figure 5-5 : "High print" (left) vs. "low print" (right). The scheme at the top shows the source of the inverse pattern (shown as fluorescence micrographs below, structures are not the same). In the "low print" case, the droplets inside the cavities give the fluorescent contrast and not the contact areas. However, for the “low print” case no functionality pattern exists.

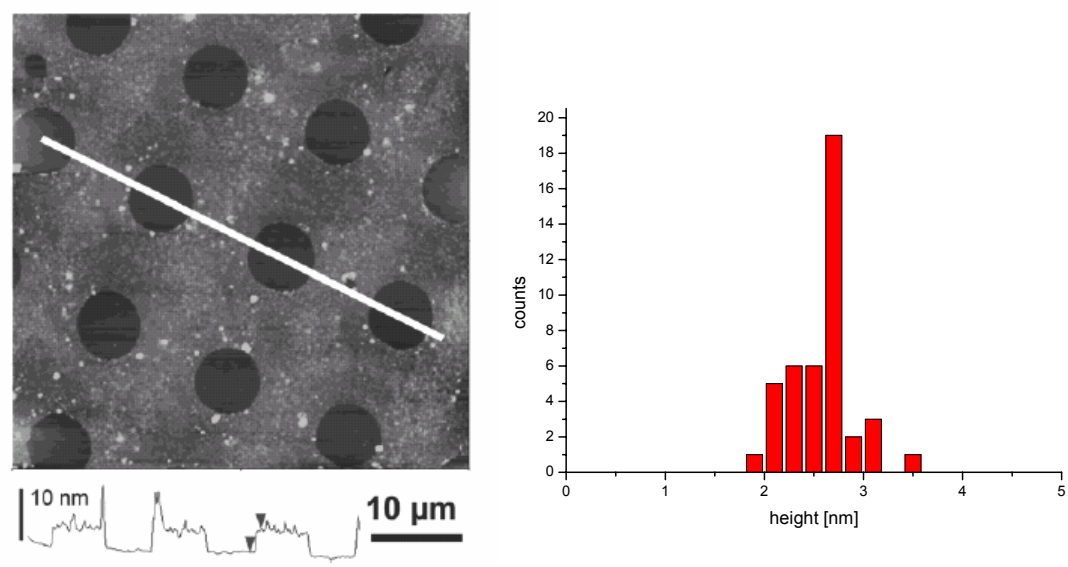

Figure 5-6: *Left:* AFM image of a printed pattern (circular non-printed areas exposing the PSS-terminated substrate surrounded by the printed PAH layer) and a corresponding cross section. *Right:* Distribution of heights for printing of PAH on a PEI/PSS layer pair.

Since fluorescently labeled polyelectrolyte was used for printing, the pattern could be recorded using fluorescence microscopy as shown in Figure 5-7. Thus the brightness of a fluorescence pattern could be related to a known pattern-height. Therefore we were able to estimate the pattern-height by the fluorescence intensity.

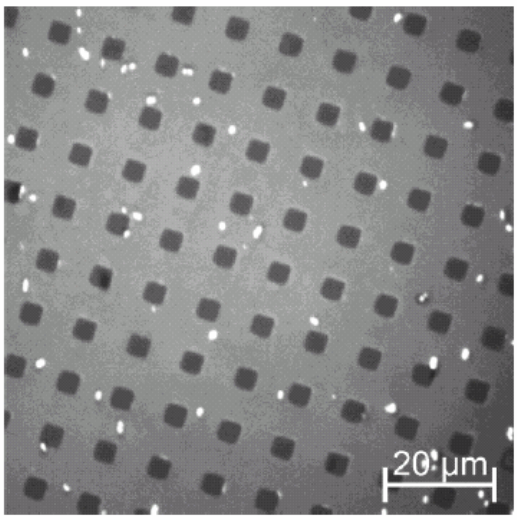

Figure 5-7 : Fluorescence micrograph of a printed rhodamine labeled PAH structure (quadratic non-printed areas surrounded by a printed PAH layer).

The fluorescence micrographs also allow for checking the homogeneity of the patterning over larger areas.

As in the approach reported above, incubating the pattern with a solution of PAH-FITC tested the contrast. Recording the pattern with a color camera, the selective adsorption of the PAH-FITC could be monitored (data not shown).

An important aspect for biological applications is the suppression of unspecific interactions of proteins with the surface. Surfaces that have a structure, which allows directing specific protein-receptor interactions on defined areas but inhibits unspecific interactions are of great interest. Polylysine side chain copolymers have proven to be very versatile in this respect and can be integrated into standard polyelectrolyte multilayer systems [159]. Polyethyleneglycol side chains (PLL-g-PEG) can efficiently block non-specific interactions while specific interactions can be introduced by terminating the PEG chain with biotin [59,160]. Huang et al. used this approach to report the sequential, selective adsorption of (strept)avidin and biotynilated goat anti-rabbit immunoglobulin monitored by waveguide spectroscopy. The approach does not only allow specific functionalization, but also control over the density and nature of the receptor [161].

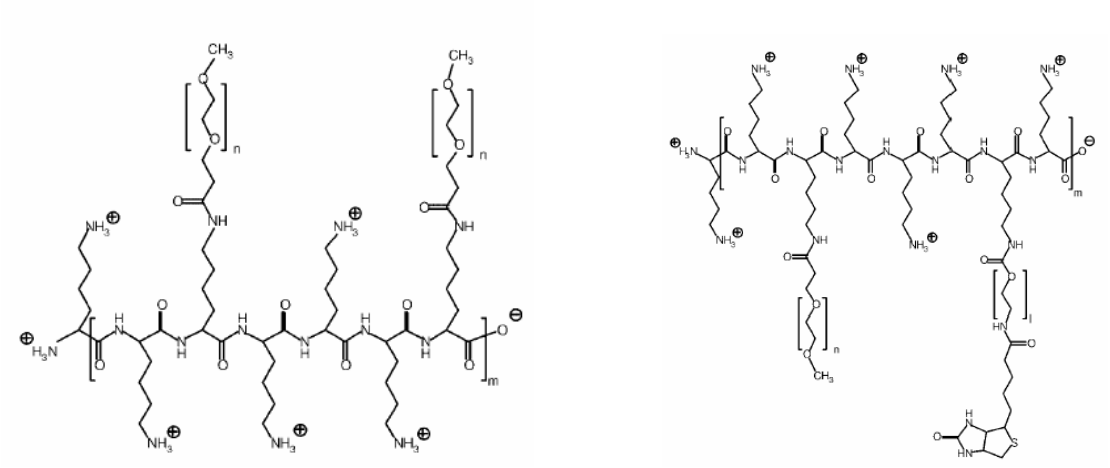

Figure 5-8 : Chemical Structure of PLL-g-PEG (left) and PLL-g-PEG-Biotin (right)

Using the water based printing process described above, PLL-g-PEG patterns on the surface can be generated. The PLL-g-PEG is unlabeled. Due to addition of a labeled protein (BSA-TRITC), the non-passivated areas will fluoresce. AFM measurements show that due to the protein adsorption the height difference decreases from 9,3±2,5 nm to 2,3±0,3 nm.

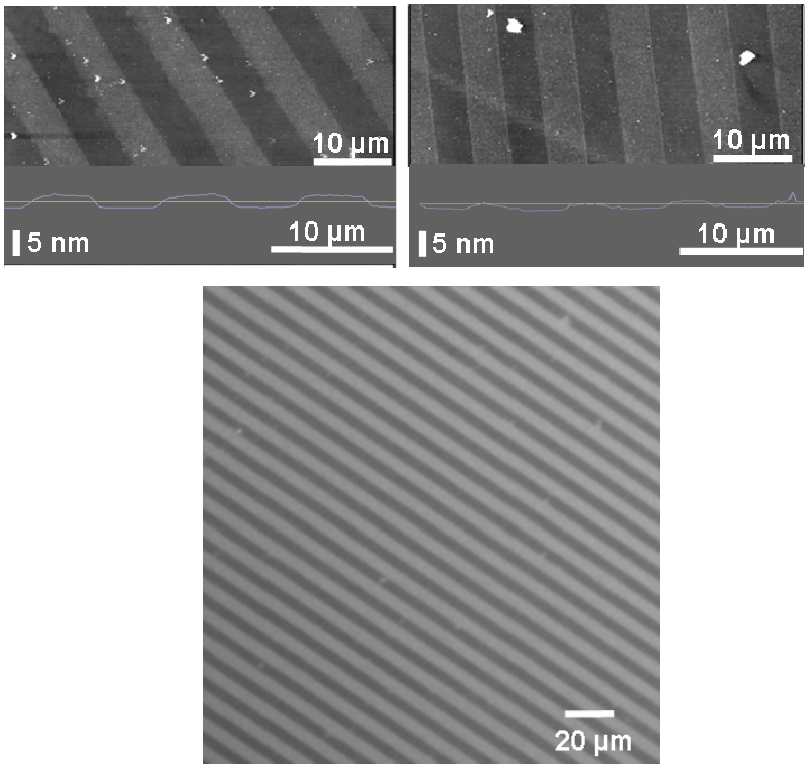

Figure 5-9: AFM image (top left) of a printed PLL-g-PEG pattern with cross section. Upon addition of labeled BSA-TRITC the printed structure with reduced height contrast (top right) emerges due to the selective adsorption of the protein Very bright spots in the AFM images are dust particles. The structure's homogeneity is presented in the fluorescent micrograph (bottom).

Because the PLL-g-PEG exposes the uncharged component to the water (shown by Zeta-potential measurements on particles [159]) the passivation is surly an effect of the PLL-g-PEG and not electrostatic repulsion [161,162]. As the BSA is charged, the adsorption process may be still governed by the charge of the underlying structure. To achieve complete specific adsorption electrostatics have to be eliminated.

Selective Adhesion of Polyelectrolyte Multilayer Capsules

In previous work on capsule adhesion on homogeneous surfaces, we have found that PSS-terminated polyelectrolyte capsules adhere to surfaces coated with PEI at pH 7, while no adhesion was found for the same capsules on bare glass or surfaces coated with PSS [89]. Zheng et al. showed that surfaces patterned by the polymer on polymer printing approach presented above can be used to direct adhesion of colloidal particles [163,164]. Little attention has been devoted so far to adhesion of hollow capsules on patterned substrates. The possibility of patterned capsule adhesion on substrates by electron beam irradiation was shown by Erokhin [165]. However, in this approach, processing steps in vacuum that usually lead to capsule collapse or fracture of the membrane are necessary. The coupling of intact micrometer sized hollow polyelectrolyte capsules to flat substrates shown here opens new perspectives for applications in combinatorial chemistry or biosensing [91,166]. The typical enclosed volume of an individual polyelectrolyte capsule is only of the order of femtoliters, and capsules can be filled with various agents [109,112,116,146,167]. If the capsules are immobilized on a flat substrate, the interior can be analyzed or influenced using surface sensitive methods. Applying a gradient along the substrate results in a different environment with respect to the particular parameter for each capsule. In this case, solution properties can be sensed with high lateral resolution or the influence of changing a parameter on the interior can be studied in a single step. By adjusting the dimensions of the pattern, all these experiments can be carried out on individual capsules. An interesting perspective is the application of this strategy for immobilizing living cells coated by polyelectrolytes which will be shown in the next chapter.

Patterns generated from both approaches mentioned above were used to obtain capsule arrays. As already shown by adsorption of labeled PAH, these patterns have areas of positive and negative charge. The experiment to check whether the selectivity, which was obtained for polyelectrolytes, can also be found for polyelectrolyte-capsules was carried out in the same way. A suspension containing

the capsules was added to the substrate. After 20 min of waiting, the substrates were rinsed without intermediate drying of the substrates. Samples were afterwards analyzed either in the wet state or they were dried. Selective adsorption was found in both cases.

In Figure 5-10, a typical picture of directed adhesion of microcapsules in the dried state on a pattern created by the ethanol/water approach is shown. The image shows that the structure can have the dimensions of a single capsule (right part of the micrograph) and that capsule adhesion can be eliminated almost completely (middle part).

For the technological concepts mentioned above, the coupling of the capsules to the surface must be strong enough to withstand the shear stresses used in microfluidics. In addition, the capsules must be immobilized in a regular 2D pattern. This was studied with capsules directed using stamping solutions without ethanol.

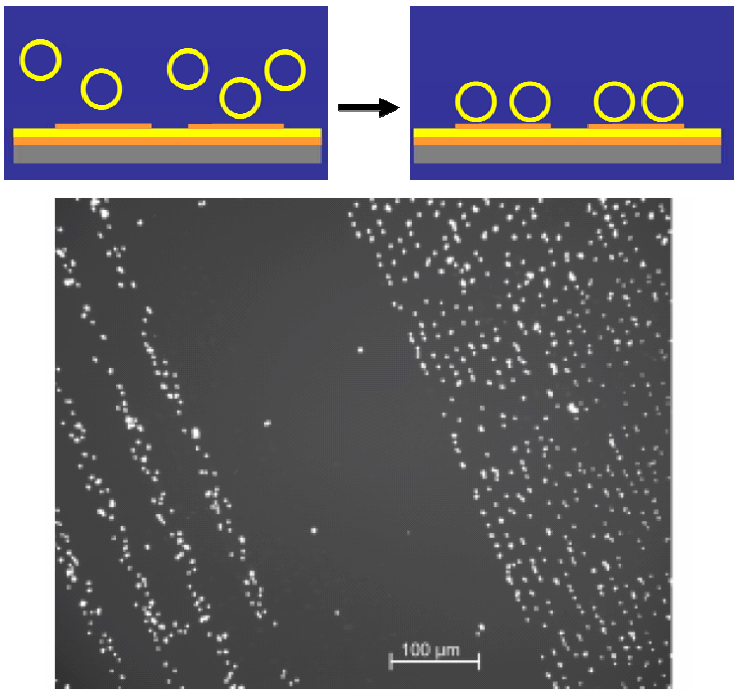

Figure 5-10: The scheme illustrates the process of directed adhesion, in this particular case the positively charged capsules (orange) adhere on the negatively charged printed pattern (yellow). The result is shown in the fluorescence micrograph of the printed structure (lines of two different width with wide area of like charge in the middle) Regions where the charge of the outermost layer of the capsules and substrate are opposite lead to adhesion of capsules and region with the same charge lead to passivation. The capsules are directed towards regions of opposite charge.

As shown above, capsule adhesion can also be directed as well to achieve 2D arrays. A droplet of a suspension of the capsules in pH neutral water was put on the

structured surfaces. After 20 min wait the surface was carefully rinsed and kept under water until observation using fluorescence microscopy. Figure 5-11 shows labeled shells adsorbed onto patterned substrates. It can clearly be seen, that shell adhesion can be directed and that shells can be immobilized in a way that isolates them individually. The result is a 2-D array.

The coverage in this experiment was not complete, although a high capsule density was observed on line patterns much bigger than the shell diameter. For an earlier set of experiments (not shown), a capsule density of around 40% was achieved. This corresponds to a capsule density of $5 \cdot 10^3 mm^{-2}$; full coverage would yield densities of $1.3 \bullet 10^4$ mm^{-2}. Using microcontact printing, patterns with a micron period can be created. Recently it was shown by Stamou and co-workers that even smaller periods can be created and vesicles can be immobilized on them with densities of 10^6 vesicles/mm^2. This would be the technological limit of our technique as well [152].

For a second set of experiments (Figure 5-11), domains with a high capsule density were found, and other parts of the sample were free of capsules. The lower density of capsules for small patterns may have several reasons. At first, it may be that the

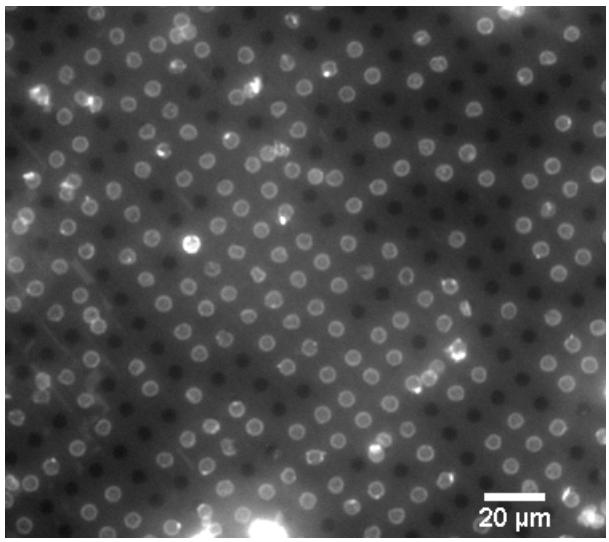

Figure 5-11: Selective deposition of polyelectrolyte shells on structured surfaces. The structure has the same size as the shell diameter. The structure was printed with labeled PAH, the shells were labeled as well; thus structure and shells are visible in the fluorescence image (very bright spots dust). The capsules are preferentially adsorbed to the non-printed areas that expose the oppositely charged PSS.

capsule density in the solutions or the waiting times were not long enough to achieve full coverage. Two arguments stand against this explanation. First the capsule

density on bigger structures, having the same incubation parameters, was very high (as it can be seen in Figure 5-10 and Figure 5-13). Secondly, the difference observed within two sets of experiments, where the only difference is the supplier of the Si-masters, suggests that quality differences between the Si-masters may be the cause of the incomplete coverage. However, the printing process could also lead to impurities on the adhesive areas, due to small amounts of polyelectrolyte left in the cavities even after rinsing. These impurities would make the adhesive areas less adhesive than expected, and result in a lower capsule density.

Since the fraction of adhesive spots is only around 25% while 75% of the surface is repulsive one could argue that the capsules only see the long range repulsive surface potential from far away, once the coverage is increasing. To rule out this argument, the distance where the sedimentation-force and the force of the surface long range repulsion of the surface are equal was calculated. This distance is around 150 nm, and is much smaller than the pattern size. For this calculation, the repulsion between two equally coated surfaces from colloidal probe AFM measurements were taken [88] and extrapolated. The sedimentation force was calculated for a hollow capsule with the known membrane thickness and density of 1.2 kg/l [24] and was around 50 fN. Therefore we believe that the quality of the Si-masters determines the density in our samples.

However, if the capsules adhere, then they adhere very strongly and are mechanically very stable in contrast to vesicles which rupture easily. In no case we observed desorption of capsules or detachment due to flow. In addition, a once formed pattern survives the drying process where large capillary forces are acting. Adhesion to oppositely charged surfaces such as those used here, results in circular adhesion areas with radii that depend on the wall thickness of the capsules [89]. The adhesion energy of PSS-terminated capsules on PEI was estimated using colloidal probe AFM to be in the range of 0.1 mJ/m^2 [88]. The interactions in this case are expected to be comparable to the ones investigated here, since one polyelectrolyte is the same (PSS) and the other has similar linear charge densities and amines as ionizable groups like PEI (PAH). For capsules with the same wall thickness as used here, adhesion disk radii on the order of 30-50% of the capsule radius are expected [89]. This would correspond to a total adhesion energy around 10^{-14} J/capsule. Thus, the adhesion energy is about seven orders of magnitude bigger than the thermal energy $k_B T$ at room temperature and spontaneous desorption

can be ruled out. It is not straightforward to estimate the peel-off force from the adhesion energy as in the case of massive spherical particles. However, independent measurements of Cordeiro using a flow chamber showed that PAH/PSS capsules of larger wall thickness (and thus lower adhesion area) on PEI surfaces could withstand surface shear stresses of 12 N/m^2, corresponding to peel off forces around 160 nN, [90]. We have found, using a micromanipulator, that capsules cannot be peeled off the surface but break away and leave the adhering part behind (data not shown [168]). Thus the anchoring is strong enough for applications in microfluidic systems where shear stresses and peel-off forces due to flow are orders of magnitude below these values.

If the size of the printed pattern is the order of or smaller than the adhesion area of the capsule, the repulsive interaction influence the shape of the adhesion area. This can be visualized by RICM. The adhesion area of a polyelectrolyte-capsule appears darker than the bare substrate. The first fringe of the fringe pattern appears if a water layer is between the capsule wall and the substrate. Due to the phase shift for the reflection at the interface of water/polyelectrolyte-membrane (lower to higher *n*) this fringe is dark, but still close to the surface, while the later fringes are a function of the distance to the surface (as explained in chapter 3.1 on page 23). For adhesion areas on the order of the pattern size, the shape of the area is deformed to optimize the adhesion of the shell (Figure 5-12, middle). If however the adhesion area is much bigger than the pattern size, non-adhesive areas will be found surrounded by adhesive ones due to the geometrical restrictions of the capsule's spherical shape (Figure 5-12, right). At the circumference of the adhesion area, non-adhesive spots are avoided and as discussed above the spherical shape of the adhesion area is deformed. These experiments visualize adhesion and repulsion of a single capsule in one image [118]. Topography effects do not play a role as the step size is only around 2 nm as already discussed.

The experiments shown above prove the principle of directed adhesion of polyelectrolyte capsules on patterned surfaces. An important issue in this context is the adhesion of filled capsules on patterned surfaces. Three methods are primarily utilized to load multilayer capsules as described in chapter 2.5: The precipitation on

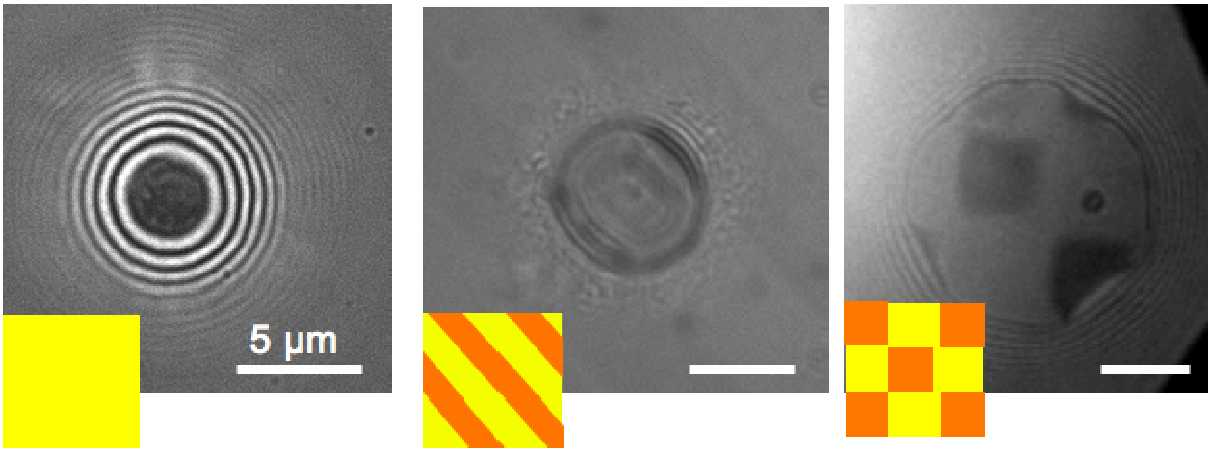

Figure 5-12: Adhesion of capsules on surface patterns on the order of the capsules adhesion area. Left: capsule on a homogeneous surface, having a circular adhesion area Middle: capsule on a surface with lines: The adhesion area is deformed to an ellipsoid by the structure being in the same size. Right: capsule with a large adhesion area on a checkerboard like structure. The adhesion is deformed at the border (not adhering in the dark areas). In the center of the adhering capsule a non adhering area can be found (square and dark dot).

or co-crystallization with the core, the polymerization in the capsule (ship in a bottle) or the switchable permeability of the wall [3,115]. The zeta potential does not alter in the filling process. In the first case, the encapsulation is part of the coating procedure and does not affect the outermost layer. For the other two cases this is only true when encapsulating neutral polymers or polyelectrolytes have the same charge as the outermost layer. Therefore it should be possible to direct the adhesion in same way for filled and empty capsules.

As one can see from Figure 5-13 for the adhesion on big structures the density of capsules loaded using the precipitation on the core is comparable to the density of empty ones. This comparison shows the applicability of the concept. Using capsules filled by the “ship in the bottle approach” [169], the result is similar (data not shown).

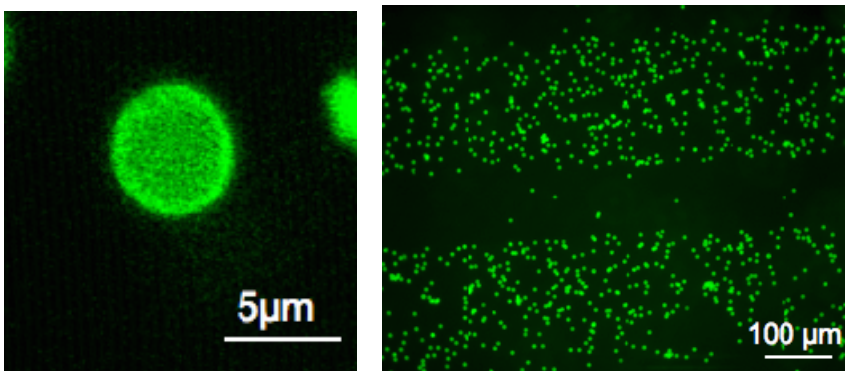

Figure 5-13: Left: Confocal micrograph of a FITC-Dextran filled polyelectrolyte capsule. Right: Directed adhesion of these capsules.

Selective Adhesion of Polyelectrolyte coated Yeast Cells

An interesting perspective is the application of the strategy just described for immobilizing cells coated by polyelectrolytes [170]. In previous work, it has been shown by our cooperation partner Dr. Silke Krol, Genoa, Italy, that cells survive coating with the polyelectrolytes used here and that the polyelectrolyte coating can serve as a protective coating [171]. (A general review on cell encapsulation can be found in reference [172]) The cell coating is an easy and elegant way to immobilize cells on glass or other charged surfaces structured by microcontact printing as described in before. In this study, the adhesion of cells is driven by the charge of the capsule, which is in contrast to a study of Zheng et al, who introduced the RGD peptide to trigger adhesion [173]. Furthermore, the polyelectrolyte on the cell surface protects the cells against shear stress or aggressive environments without altering the viability of the coated organisms, which is in accordance with former experiments [147,148]. The capsule walls are mechanically robust and can protect cells against external forces. In addition the capsules around the cells are strongly attached to surfaces so that high shear rates do not cause detachment. This feature is an important feature for applications [91,166,174]. In the current study, it was shown that the coating allows for a signal induction. Moreover, for capsules, a molecular weight cut-off between 20 and 40 kDa was stated, which is good enough for larger molecules but as mentioned in the introduction variations and fine-tuning of the cut-off is possible (see supporting information of reference [170]). Due to the extraordinary features inherent to the applied polyelectrolyte capsule, the opening and closing of the capsule wall is possible as well as tuning its permeability. Therefore the coating can even regulate the flux in and out of the cell [78,175].

Living yeast cells were coated with the same polyelectrolytes (PAH and PSS) used for the patterned substrates. The only exception was that in this case the PAH was of lower molecular weight and labeled with Alexa (555) which fluoresces brighter red than rhodamine and permits one to distinguish between the underlying layer and coated cells. The printed structure was checked like described in before by fluorescence microscopy. Next, we investigated the self-assembly of coated cells onto the patterned substrate. In the case of the coated cells having a surface charge opposite to that of the stamped regions of the glass slide, a clear ordered arrangement of the cells over large areas was observable after carefully rinsing with water (Figure 5-14 a). The low magnification of the image was chosen to show that

large areas are covered with the coated cells. These appear as small bright red spots and the fact that they bind only to printed regions of the template is clearly visible. In the phase contrast image (Figure 5-14 b), the cells are fixed along the stripes of opposite charge. Here, it is noteworthy that cells that are in the like charged region of the glass are still moving and thus appear blurred (arrows).

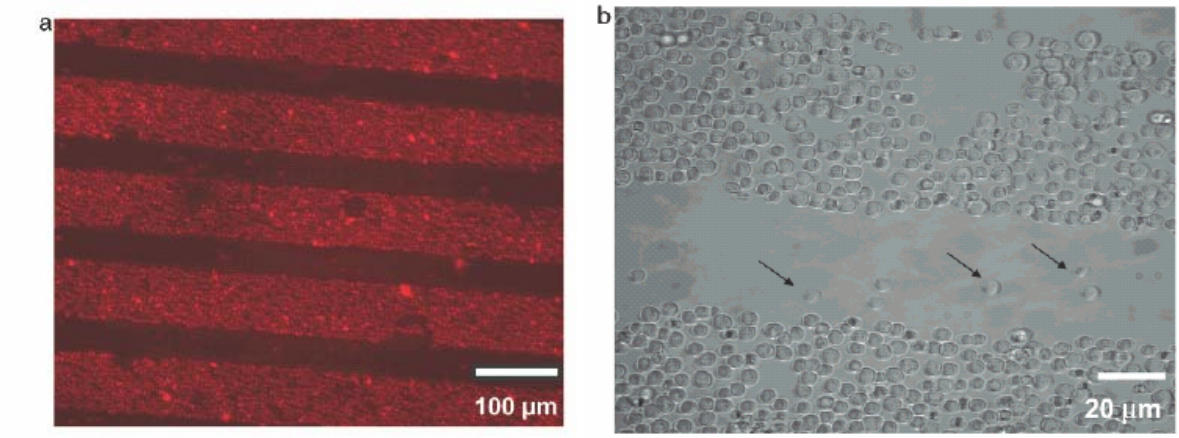

Figure 5-14: (a) Fluorescence micrograph showing the selectivity of coated (PAH/PSS/PAH-Al/PSS) cell adsorption on a patterned (PEI/PSS/PAH-Rh) substrate over a large area. (b) Phase contrast image of encapsulated yeast cells attached by electrostatic self-assembly to a 200 µm stripe structure. Unattached cells in the like-charged region of the glass are blurred due to movement (arrows).

In a time series performed after rinsing the template and attached cells with water, we were able to see that the free cells carried continued to drift until they reached an area of opposite charge (data not shown). Next, we investigated the influence of the stripe size, which in this set of experiments are the same size as the cells. For yeast, the cell size is 5 *µ*m. Figure 5-15 shows that self-assembly along the stripes 5 µm wide is observable.

Due to the higher magnification of the images with respect to the former ones, one can clearly see the red polyelectrolyte capsule of four layers, labeled with Alexa (555). These observations support the idea that the attachment is electrostatically driven. Furthermore, the present findings are in accordance with the results found in our previous work concerning the selective deposition of hollow capsules [91,166]. The coupling of the cells is strong [174] because the structure is still recognizable after rinsing and even after the substrate was removed from water and dried out, which is accompanied by large capillary forces acting on the cells

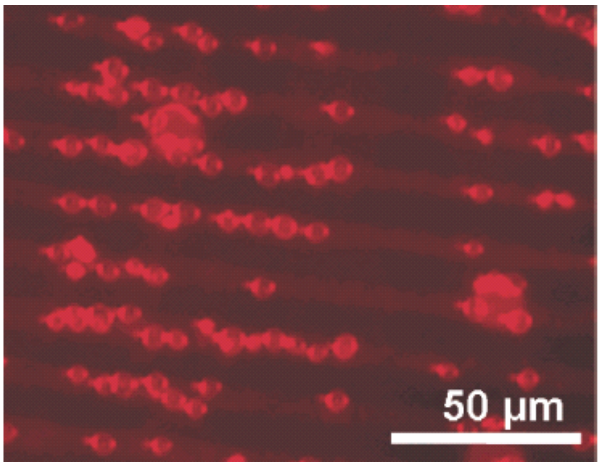

Figure 5-15: Fluorescence image of 5 µm wide stripes transferred by microcontact printing of RBITC-PAH onto a PEI/PSS covered glass slide. The attached yeast cells were coated with $(PAH/PSS)_2$ with the third layer labeled by Alexa (555). It is obvious that they adsorb preferentially to the small lines.

(data not shown). The strong adhesion for hollow capsules of the same size as the coated yeast cells supports the experimental findings presented here. The patterned adhesion shown above, which was observed for negatively terminated coatings, changed to a random distribution in experiments with positively terminated a coating. This effect does not depend on the number of layers that were assembled on the cells. The number of layers was varied between four and seven, which rules out the idea that there were defects in the coating [23]. Rather, preliminary time dependent Zeta-potential measurements give evidence that the living cells actively are able to change the surface charge of the attached polyelectrolyte layers. A detailed quantitative analysis of the surface charge density of the coated cells as a function of the outermost layer and its evolution with time is in progress but not presented here.

The viability as well as the addressability of the attached cells was investigated on a cell line that produces GFP upon galactose incubation. Encapsulated yeast was assembled on the pattern in a 0.5 M NaCl solution, which was exchanged to 15% galactose in water. The template was then stored for 2 h at 28 °C in an incubator. Under the fluorescence microscope, the GFP level was visualized as a detector for induced protein production and was therefore considered as a viability indicator. In the left image of Figure 5-16, a CLSM micrograph is depicted that shows the coated GFP-filled cells as small yellow spots due to co-localization of the green GFP and the red Alexa (555) fluorescence.

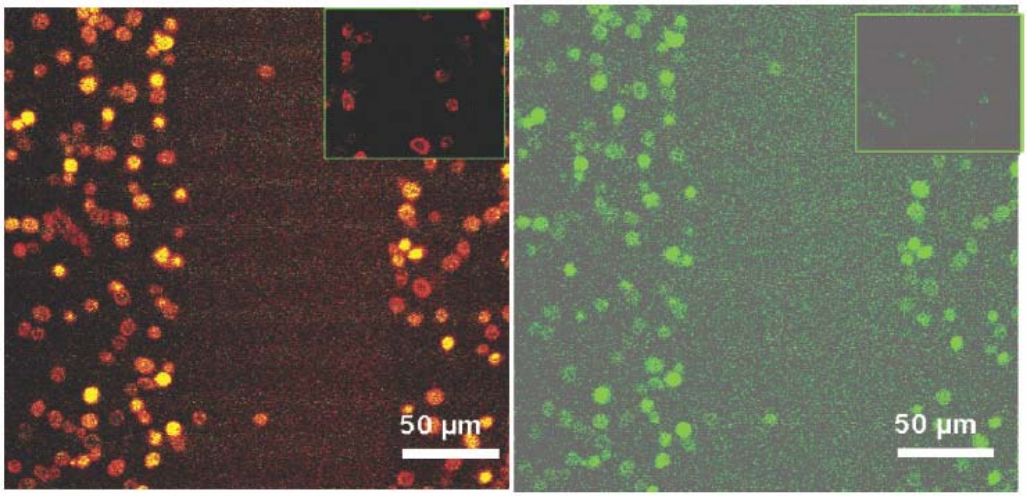

Figure 5-16: CLSM micrograph of GFP-filled, coated yeast self-assembled to a stripe structure induced by microcontact printing. The printed polyelectrolyte was PAH-Rh onto PEI/PSS coated glass, while the shell on the cells consisted of $(PAH/PSS)_2$, with the third layer labeled with Alexa (555). Fluorescence was excited with two laser lines, GFP (green) with I_{max} = 488 nm and the red dyes at I_{max}= 514 nm. The yellow appearance of the cells in the left image is due to co-localization of the green and red emission. The right image shows only the green channel of the same image. Both insets show the cells before incubation

The right image of Figure 5-16 shows only the green channel of the same picture to visualize the production of GFP more clearly. Both insets show the lack of GFP fluorescence before incubation with galactose. Also, in these experiments, a preferential deposition on the oppositely charged printed structure is evident. Higher magnification of the cells reveals in the focal plane a small red fluorescent rim, while the interior is completely occupied by GFP, which emits green fluorescence (Figure 5-17).

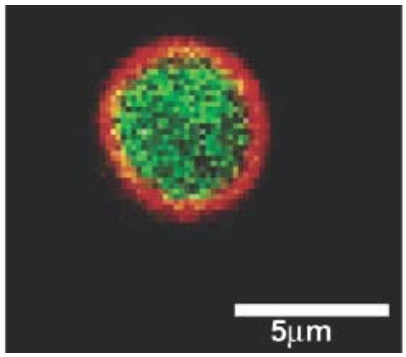

Figure 5-17: CLSM image of the focal plane of a single GFP expressing yeast cell with a polyelectrolyte capsule ((PAH/PSS)2, third PAH-Al) and green GFP signal inside. Excitation at λ_{max} = 488 nm and 514 nm at 100x magnification. The cells were imaged after 18 h of storage in 15% galactose and incubated at 28 °C.

Perspectives for the directed adhesion

The work presented in this thesis is the first approach for directed adhesion of polyelectrolyte microcapsules on interfaces. In the meantime, Feng and coworkers presented a similar approach [176]. The use of specific interactions like receptor/ligand, antigen/antibody or base pairing of two complimentary single stranded DNA would increase the variety of possible interplays. The passivation of unspecific interactions by using PLL-g-PEG presented in this work, represent some of the first experiments in this direction. Specific interactions can be introduced by coating both capsules and the attractive part of the surface pattern with biotinylated PLL-g-PEG. The interaction then can be induced by adding streptavidin. However, capsules coated with either biotinylated PLL-g-PEG and or PLL-g-PEG without biotin only settled on streptavidin-coated surfaces without detectable adhesion areas. Thus, for the degrees of biontinylation, tested specific interactions were not strong enough to achieve reasonable capsule adhesion [177]. This could be overcome by increasing the degree biotinylation or by softening the capsules.

Capsules and encapsulated cells may become important in “lab-on-a-chip” devices because the capsules can be used to transport their load to specific positions. After coupling the capsule interior can be analyzed using surface sensitive techniques, for which the coupling to the chip is important In this context, the reversible coupling on switchable patterns or release of the load by changing the interaction potential is exciting.

5.2 Flat Freestanding Films

Freestanding polyelectrolyte membranes with a thickness down to 50 nm were integrated in soft lithography structures. This forms a microarray of cavities that are sealed by the membrane. It will be shown that the polyelectrolyte membranes act as diffusion barriers for macromolecules, and are permeable to low molecular weight species [94].

Advantages from this can be taken in different directions. The enclosed volume can be used as a micron-sized reaction chamber or as sensor for solution properties with high lateral resolution. Therefore, they must be filled with a macromolecular sensor material such as the fluorescently labeled molecules used in the present study.

The impermeability of polyelectrolyte multilayers to high molecular weight species makes it possible to use them as osmotic pressure sensors when monitoring the

membrane's deflection due to pressure differences between the interior and exterior of the cavity.

It is advantageous for possible applications for that the arrays to be based on soft lithography which is also widely used in microfluidics and allows for multiple structure designs [7,8] that may be easily integrated in microfluidic systems. First promising experiments following this line were already performed; however they will not be presented here.

We used polyelectrolyte multilayer films as a membrane material. The material was chosen for reasons already mentioned in detail in chapter 2.4. Summarizing, polyelectrolyte multilayers have controllable thickness and can be tailored in terms of their mechanical and chemical properties. Most importantly for the present study the semi-permeability of freestanding polyelectrolyte membranes (as polyelectrolyte-shells) has been previously demonstrated [66,68-78].

Multilayer Membrane Transfer

For the purpose of using such ultrathin layers as separation membranes, the membrane must be transferred from the solid substrate where it is assembled and made partially free-standing. For floating layers the Langmuir-Blodget technique can be applied, but for polyelectrolyte multilayers no comparable method has yet been presented. Instead the films are usually picked up with grids or substrates in a rather undefined way. Rupture of the films, and particularly crumpling are therefore serious problems. That can be explained from fundamental considerations. The stretching elasticity of membranes scales proportionally to the membrane thickness h. Thus, the forces necessary to reach critical rupture tensions diminish accordingly with $1/h$. For crumpling, the situation is even more unfavorable: Here, the bending stiffness is proportional to the third power of h and a thin membrane will react to minute compressive forces by folding (see Figure 5-18).

Therefore, successful transfer has so far only been reported for thick films of several 100 nm or for materials that have been especially reinforced, such as inorganic organic composites [96,105,106] or composites including carbon nanotubes [41]. We

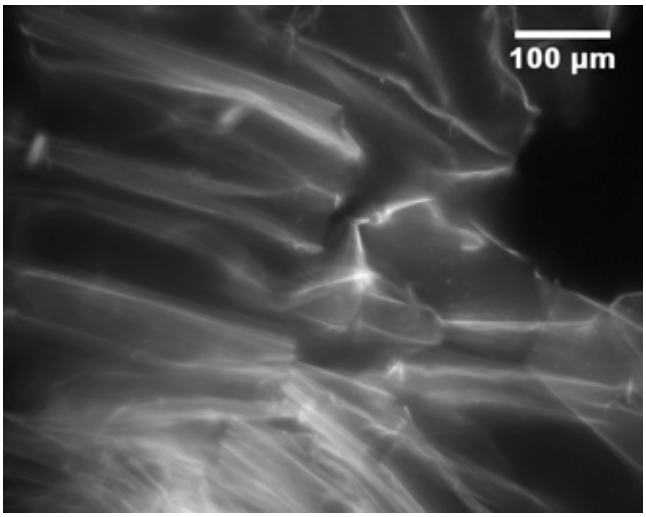

Figure 5-18: Fluorescent micrograph of a crumpled polyelectrolyte-film with a thickness of several tens of nm.

chose here an alternative strategy, in which forces act only normal to the membrane. The scheme in Figure 5-19 shows the general procedure.

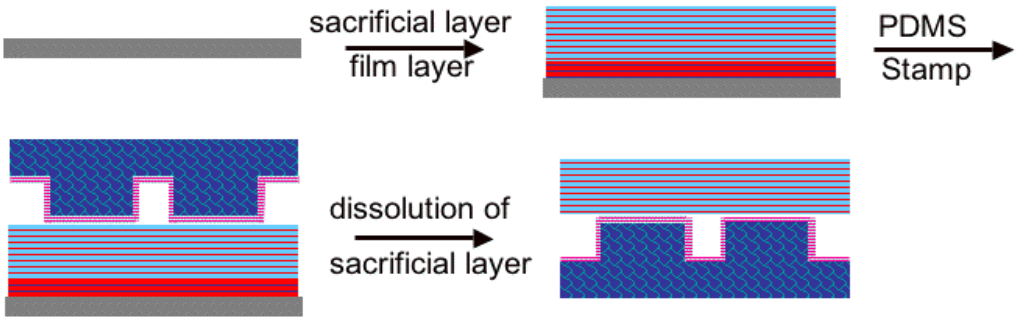

Figure 5-19*:* Scheme of the transfer process.

The film is first formed on a solid support and consists of a dissolvable (sacrificial) layer and a non-dissolvable layer. A polydimethylsiloxane (PDMS) structure that has been coated such that it adheres to the film it is brought in contact with. The sacrificial layer is subsequently dissolved. This step results in delamination of the film from the substrate, but does not affect its connection to the PDMS structure. During the whole process, only normal forces act on the film while any stretching and compressing forces parallel to the film are avoided due to the PDMS. The method is based on microcontact printing of multilayers, as demonstrated by Park and Hammond [93]. In contrast to the printing technique, where a multilayer is transferred from a structured PDMS to a homogeneous substrate, we transfer the multilayer from the homogeneous substrate to the structured PDMS. Therefore multilayer transfer to

substrates that have holes is possible. This transfer leads to freestanding membranes for the use in applications outlined in the introduction. In this way, we can routinely transfer defect free polymer films down to thicknesses of 50 nm over areas comparable to the sample size, as demonstrated in Figure 5-20 for a fluorescently-labeled film of PAH/PSS.

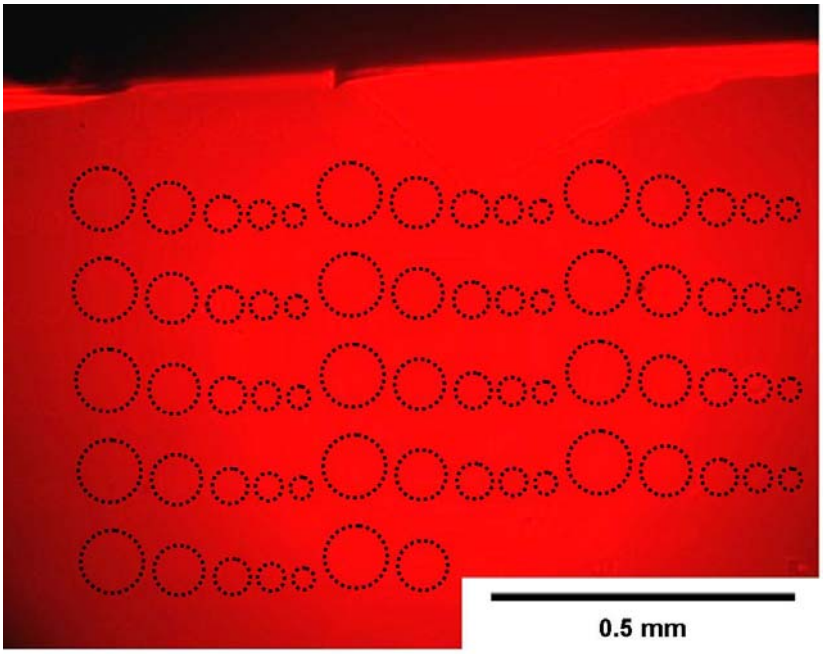

Figure 5-20: Fluorescence micrograph: The edge of a PDMS substrate with the polyelectrolyte film (light red) is shown. The film is free standing in the areas located over the circular holes (only slightly visible, marked with a dotted line) in the PDMS that have different sizes from 2-100 µm

The bright part in Figure 5-20 is the transferred film that is attached to the PDMS stamp. Note that crumpling, folding, or film rupture is avoided over large areas of mm^2 dimensions. The structure of the PDMS stamp (spherical holes of 10 microns depth) is indicated on the areas coated with the film. Although a part of the membrane is supported on the PDMS, the parts located over the holes are free standing.

The CLSM image (Figure 5-21) shows that these films are really free-standing and do not touch the bottom of the cylindrical holes. AFM imaging of the step height of the films edge are measured to have a thickness of 58 nm.

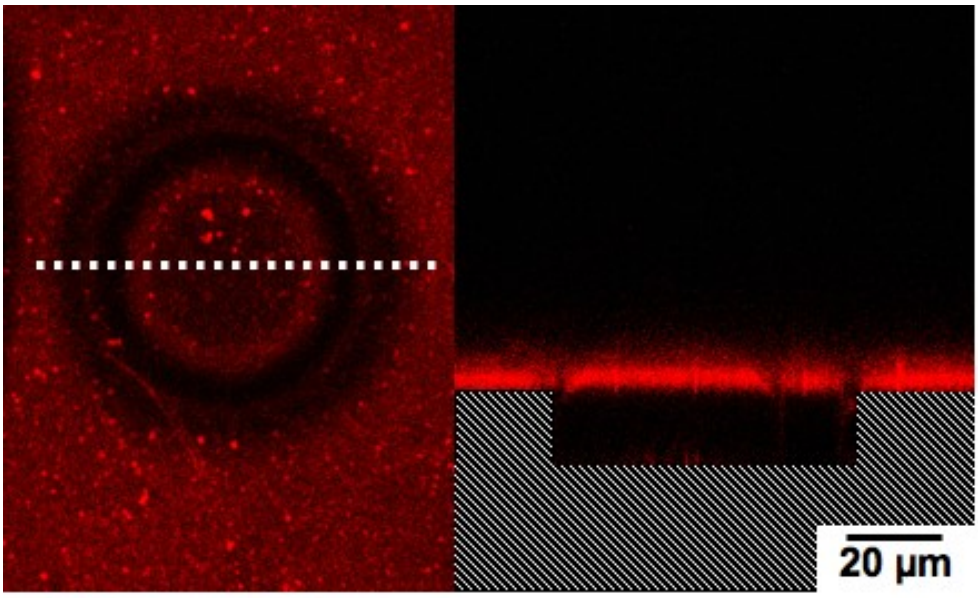

Figure 5-21: Confocal Laser Scanning fluorescence micrograph: The picture shows a xy-scan and vertical sections of a transferred film. The xy-scan is taken in the substrate plane, showing the film over the hole, the black ring is an artifact, which will be discussed later (see Figure 5-29). The corresponding xz-scan is taken along the dotted lines (the PDMS is invisible in the micrograph and indicated with white stripes in the image). The discontinuity in the xz-scan is the same artifact.

To assemble the freestanding membranes the adhesion of the membrane to the PDMS and complete dissolution of the sacrificial layer are crucial. Native PDMS is hydrophobic, as it was previously discussed (see Production and Surface Modification of PDMS Stamps on page 37) and can be used to stamp polyelectrolyte multilayers on solid supports [93]. A strong binding of the film is required for the application presented here, must be ensured. Electrostatics can induce strong interactions between polyelectrolyte multilayers. This means PDMS must be charged. The easiest way to charge the PDMS is to hydrophilize it as it was previously described and to coat it with polyelectrolyte. We used PEI as basis for polyelectrolyte multilayer assembly [87]. As already discussed for the printing, intensive washing after the coating is important. Polyelectrolytes inside the cavities produce an osmotic pressure, that bends the membrane outwards (see Figure 5-32 on page 71). This effect will be discussed in greater later in detail, (see Pressure Sensors on page 67.

As a sacrificial layer $(PAA/PAH)_5$ was used in this thesis. When assembled with 1 mM NaCl for both and a pH of 3.5 for the PAA solution, these layers dissolve at pH 1, as previously reported [95]. This however limits the film layers to compositions stable under these conditions such as the PAH/PSS layers used here. The

development of other sacrificial layers therefore is important. It has also been shown that the dissolution of the substrate will lead to the wanted result [9,41,96-99].

The most elegant way to remove sacrificial layers would be the digestion of these layers by a protein, which would be highly specific mechanism. Pronase is known to digest polyelectrolyte capsules made from BSA/PAH [178]. Therefore 5 bilayers of BSA/PAH were used as sacrificial layers and covered by 20 bilayers of PAH/PSS. The digestion was performed in a 1mg/ml pronase solution in TRIS-HCl buffer, with an ionic strength of 0.1 M CaCl. These were the same conditions used for the capsule digestion. However, no digestion was observed: The attack of the protein is likely hindered because the size of the protein is about the same as the sacrificial layer thickness.

Microcompartments as Model sensors and reaction chambers

To test the permeability properties of these membranes, they were incubated in solutions of both fluorescein and of FITC-dextran of molecular weight 500 kDa. CLSM shows if these substances have penetrated through the membranes directly as shown in Figure 5-22. The vertical sections of fluorescence intensity show that the high molecular weight molecules cannot penetrate into the cavities sealed by the membrane (Figure 5-22, right), but that the low molecular weight species are able to penetrate (Figure 5-22, left). This observation is compatible with other studies of the permeation properties of the same membranes forming capsules [66,69,70,78], where a molecular weight cutoff between 4000 and 70000 g/mol for uncharged molecules was found [70].

Because permeation of low molecular weight species was observed on the timescale of minutes, a lower estimate of the diffusion constant of the molecules through the membrane can be done. Assuming a diffusion controlled permeation mechanism, as expected for a defect free film, diffusion time *t*, diffusion coefficient *D* and film thickness *x* are related by :

5-1 $$t = \frac{< x^2 >}{2D}$$

Therefore, *D* for fluorescein must be smaller than 10^{-18} m^2/s, which is consistent with observations made by others [68-70]. This value of *D* also shows that to achieve permeation on timescales of minutes, the membranes must be of thicknesses on the scale of several tens of nm. In the present case, this is achieved.

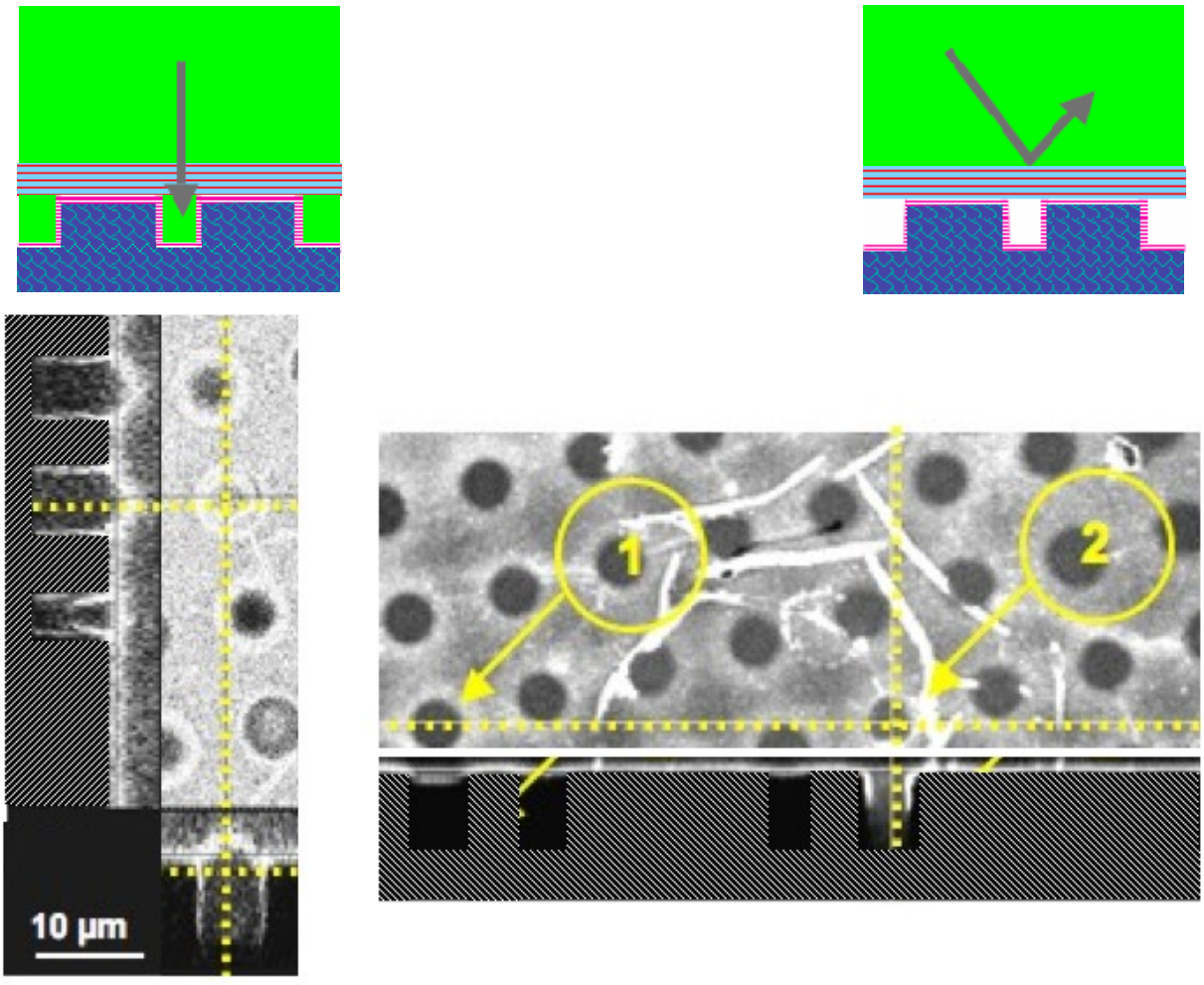

Figure 5-22: Schematic representation (top) of permeability and impermeability. 3-D plot of a CLSM image series: *Left:* Low molecular weight fluorescein can penetrate the membrane and fluorescence inside and outside the cavity is equal in all cases. *Right:* 500 kDa Dextran cannot pass the polyelectrolyte membrane if it is intact (1). If the membrane is ruptured (2), fluorescence can be recorded from inside the cavity. The PDMS is invisible in the CLSM images, the structure is indicated with white stripes.

The permeation properties can be used to trap large molecular weight molecules. To do this, the cavities were incubated with solution containing 500 kDa FITC-dextran prior to film transfer. After removing the excess solution, capillary forces keep the solution inside the cavities, by the same effect leading to the “low print” discussed before (see Figure 5-5). After the membrane is transferred, the loaded cavities are sealed (scheme Figure 5-23). The filling of the compartments was analyzed using CLSM and fluorescence microscopy (Figure 5-23, conf. micrograph). It was observed, that the cavities sealed by the film were filled completely but that the load

of the unprotected cavities was washed out with time, leaving only some adsorption to the cavity walls.

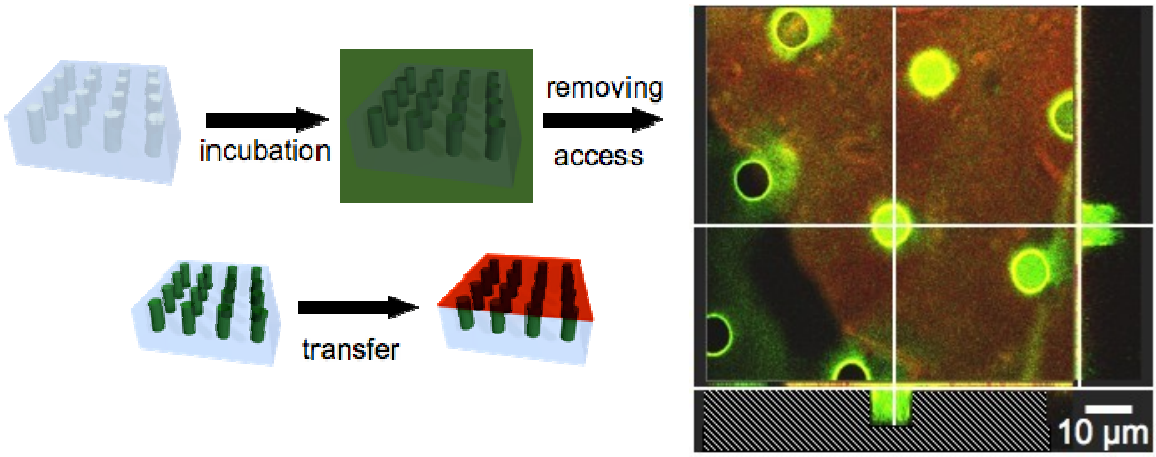

Figure 5-23: Filling of cavities: *Left*: scheme of the filling process. Due to capillary forces the solution stays inside the cavities. *Right*: The 3D-plot of the CLSM image series shows volume filling for the cavities (green) sealed by the membrane (red) and no filling without sealing (lower left), due to washing out of the solution. The PDMS is invisible in the CLSM image, but indicated with white stripes on the bottom z-section.

Two model experiments were performed. First, the possibility of accessing the cavities individually and avoiding crosstalk between two neighboring holes was tested. Secondly, the communication of the interior with the outer solution was checked. The first experiment was done by bleaching the entrapped dye by means of CLSM.

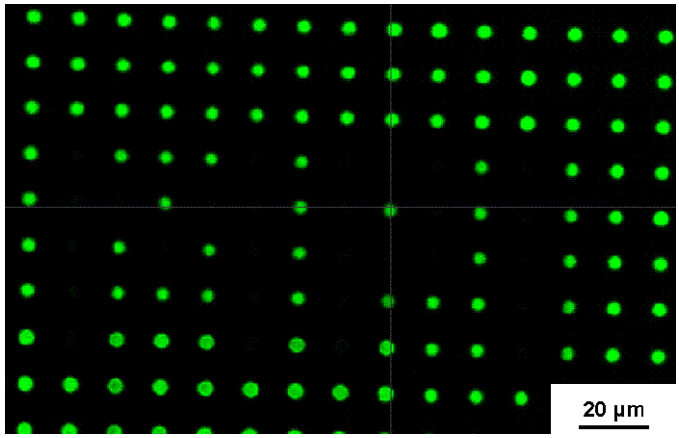

Figure 5-24: CLSM image with the focal plane through the center of the filled cavities. This bleached pattern was stable for at least a week.

The cavities could be manipulated individually and a pattern, bleached into the array, was stable at least a week (Figure 5-24). This is also a model for a photochemical reaction inside the cavity.

To test if the entrapped macromolecules can be influenced by changes in the solution outside the cavities, we have varied the pH and found that the fluorescence activity of the entrapped dye was affected, as expected for fluorescein. This dependency is shown in Figure 5-25. In the left hand picture the sample is in a pH 9 solution, showing strong fluorescence. When the sample is immersed into a pH 1 solution (middle), the pH changes also in the cavity interior due to the semipermeability of the membrane seal, and the fluorescence becomes weak. When returning to high pH, the fluorescence is recovered (right).

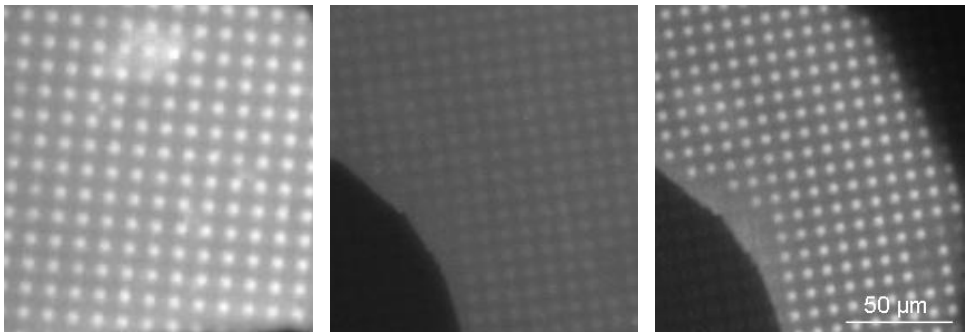

Figure 5-25: Fluorescence micrographs of FITC-dextran filled PDMS structures with polyelectrolyte membrane, When the pH of the outer solution is changed from pH 9 to pH1 the fluorescence decreases (left to middle), when going back to pH 9 (right) the intensity is recovered (all pictures with the same illumination intensity / gain settings and scale).

Pressure Sensors

An interesting perspective is the use of the freestanding membranes as force sensors as recently shown by Jiang and coworkers [9]. They used a common method to test the E-Modulus of thin metal films. This so called bulging test investigates the mechanical properties of polyelectrolyte membranes and polyelectrolyte membranes enforced with nanoparticles. These experiments, however, were done with dried membranes. Using our transfer process an array of pressure sensors can be built. In water, the E-Modulus of the polyelectrolyte membrane is lower, leading to a higher sensitivity and new possible applications.

The indentation pressure relation for a freestanding film, which is clamped at its edges, and suspended over a circular hole, can be derived analytically [179-181] and is given in equation 5-2.

5-2 $$P = \frac{16}{3a^4}\frac{Eh^3}{(1-\nu^2)}d + \frac{8}{3a^4}\frac{Eh}{(1-\nu)}d^3$$

The assumption of a clamped film holds because the film tightly adheres to the supporting structure. The clamping is achieved by choosing oppositely charged polyelectrolytes, at the film substrate interfaces.

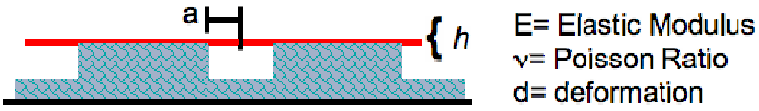

Figure 5-26: Parameters of a freestanding circular film, which is suspended over a circular hole and clamped at its edges.

The equation has two terms: a bending term, which dominates for small deformations (equation 5-2, first summand), and a stretching term, which dominates for big deformations (equation 5-2, second summand).
Plotting the pressure deformation function (Figure 5-27), it becomes visible that deformations on the order of a micrometer are clearly dominated by the stretching part of equation 5-2, that now simplifies to:

5-3 $$P = \frac{8}{3a^4}\frac{Eh}{(1-\nu)}d^3$$ [180].

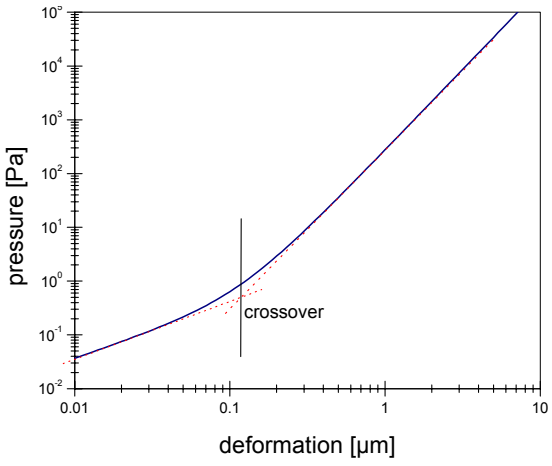

Figure 5-27: Plot of the pressure deformation function of a circular freestanding membrane. (Plot parameters: a = 25 µm, E = 200 MPa; h = 100 nm; ν = 0,5)

For the membrane system described, a polymer added to the bulk solution cannot pass through the semi-permeable membrane.

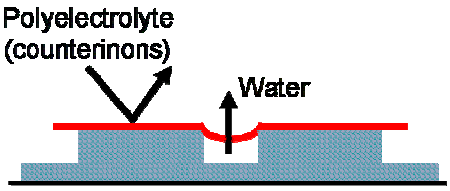

Figure 5-28: Scheme of the mechanism of membrane deformation by osmotic pressures.

This generates a difference in osmotic pressures across the membrane (Figure 5-28). To compensate the pressure, the membrane bends in the direction of the lower pressure. The osmotic pressure of polyelectrolyte solutions without added salt scales like the counterion concentration (equation 5-4). This scaling results because the counterions cannot pass through the membrane, if the polyion cannot pass through because of electroneutrality [12]. The osmotic coefficient is the proportionality constant. It depends on the counterion condensation to the polyelectrolyte chain. This condensation reduces the osmotic activity of the polyelectrolyte.

5-4 $$\frac{\Pi}{RT} \propto c \quad \text{proportionality constant } \phi, \text{osmotic coeffcient}$$

The proportionality constant can be determined by membrane osmometry.
The sample was arranged in a way that the bending of the freestanding membrane could be measured using confocal microscopy (see chapter 4.2). As already discussed, different indices of refraction lead to a distortion of the image in the z-direction. In this case, several light beams must be considered. The light traveling through the PDMS (refractive index 1.43 [182]) and illuminating the supported membrane, and the light traveling first through the PDMS, being reflected at the water PDMS interface and then illuminating the freestanding membrane. Due to the additional reflection at the water/PDMS interface, a discontinuity in the membrane is observed.
The distortion in the z-direction however can be neglected because it is smaller than the error in determining the deflection from the xz-confocal images. The distortion by the homogeneous part of the PDMS on the glass substrate, which is thick compared to the structure, only shifts the absolute position of the membrane relative to the

glass substrate, which is not of interest here. However, for very high concentrations of polyelectrolyte, the membrane bends down to the substrate (as shown in Figure 5-30). This provided an internal standard for the deflection measurements since the depth of the holes was known (L=10 µm, taken from the manufacturer).

To be able to recover the very same hole while scanning systematically different cavities having different diameters for one concentration, an image of a single cavity in the xy-direction was taken first. To measure the deflection, a scan in the

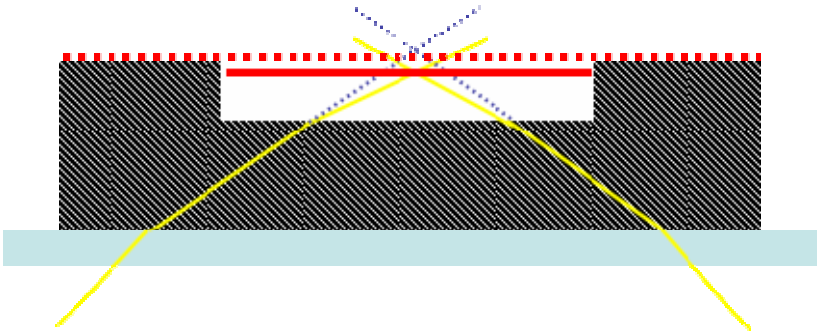

Figure 5-29: Effect of additional reflections in an xz-confocal microscope image. The light beam is reflected at the glass/PDMS (blue/white stripes) interface for the first time. The PDMS/water (white stripes/white) reflects the light imaging the membrane spanned across a hole (yellow beam, solid red membrane). This reflection does not take place for the membrane being supported by the PDMS (blue dotted beam, red dotted membrane). Therefore, a discontinuity of the membrane is observed: The dotted red line is imaged for the supported membrane. Without support, the solid line is imaged. This effect, however, is within the accuracy of the measurement. A confocal micrograph showing this effect is shown in Figure 5-32.

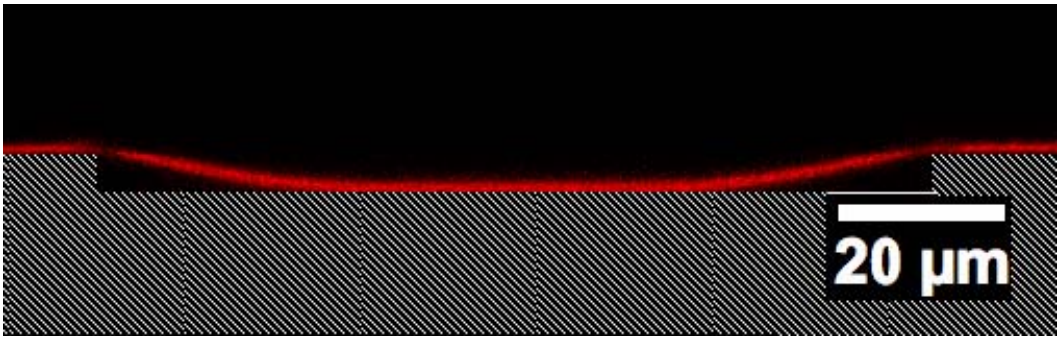

Figure 5-30: A confocal-micrograph, scanned in the xz-direction that shows the cross section of a freestanding membrane, touching the bottom of the cavity. The PDMS is invisible in the confocal micrograph but indicated with white stripes.

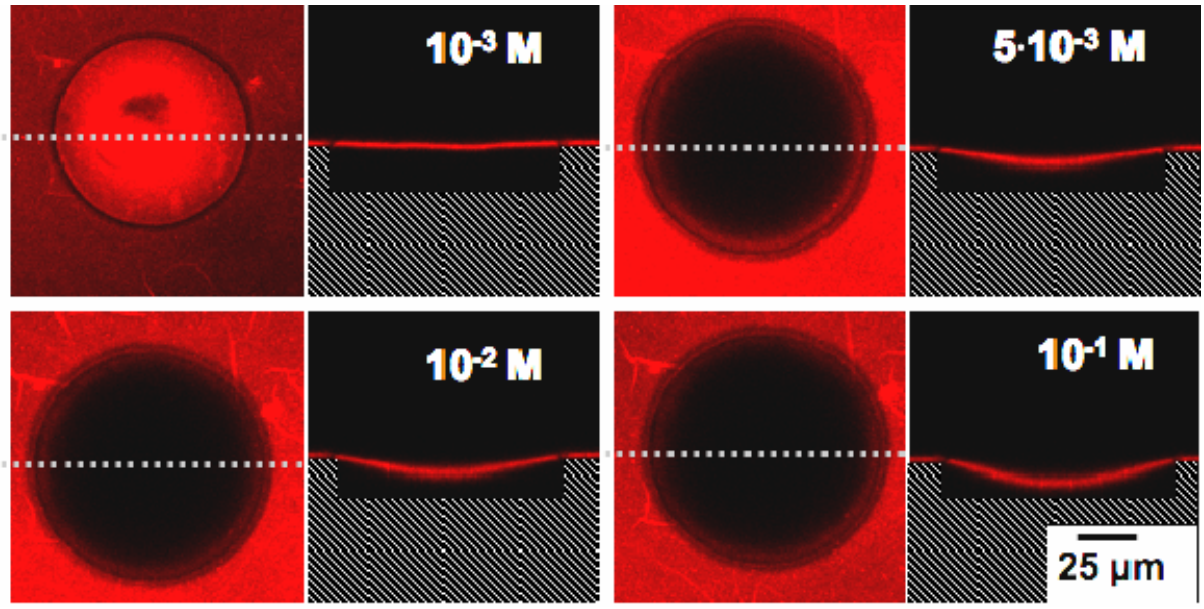

Figure 5-31: Confocal micrographs of a multilayer membrane free standing across a 37.5 µm hole. Images were taken in xy-direction (first of each set) and in xz-direction along the dotted line in the xy-image. The membrane bending increases gradually with increasing polyelectrolyte concentration in the bulk.

xz-direction was performed across the center of the hole. As it can be seen in Figure 5-31, with increasing polymer concentration the deflection of the membrane across the hole increases gradually [118].

For a quantitative analysis of this effect several holes of different diameters were measured. When no polyelectrolyte was added in some cases a bending to the outside was observed. Polyelectrolyte being trapped inside due to the preparation

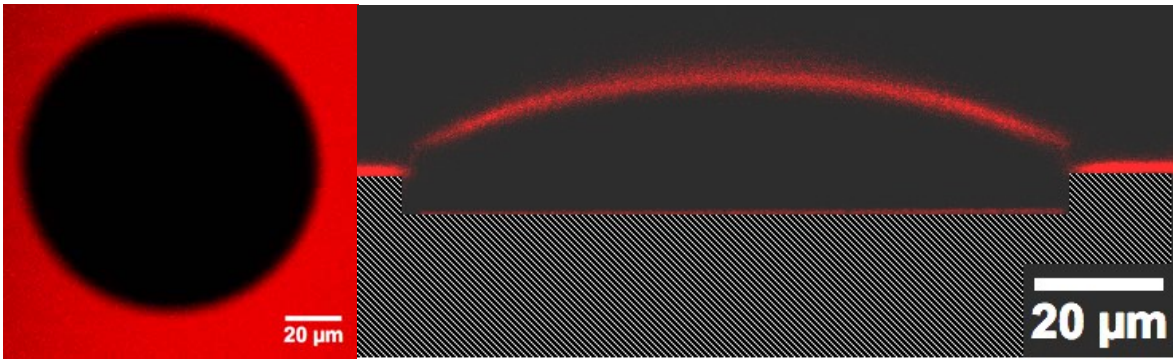

Figure 5-32: Confocal-micrographs (xy- and xz- scan) of a freestanding membrane bending outwards due to a negative osmotic pressure difference. This occurs if polyelectrolytes are entrapped inside the cavity. The structure is invisible in the micrograph but was indicated with white stripes. The discontinuity is due to the refractive index difference which was discussed before

process, will lead to a bending to the outside if the osmotic pressure on the outside is smaller than in the inside (Figure 5-32).

When the pressure on the outside increases, the membrane bending decreases. At the point where the osmotic pressures inside and outside are equal, the membrane bending should be zero. This is observed in most cases except for a high polymer concentration inside (i.e. a strong bending outwards) where plastic deformations as shown in Figure 5-33 were observed. This is in agreement with observations made with polyelectrolyte capsules under strong load [81].

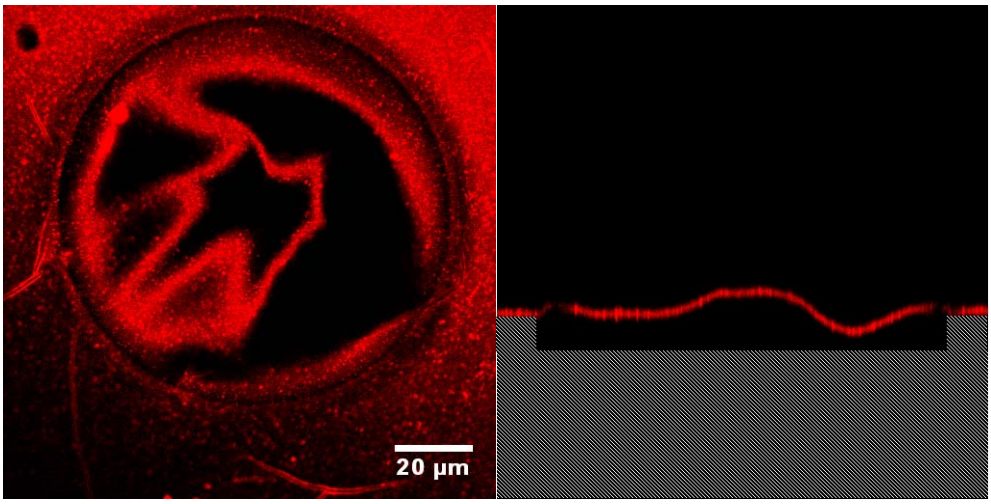

Figure 5-33: Confocal-micrograph (xy-scan and xz-scan) plastically deformed freestanding membrane at zero osmotic pressure difference, flipping from bulging out to bulging in.

For a quantitative analysis, the encapsulated polyelectrolyte has to be taken into account. Therefore equation 5-3 becomes:

5-5 $$\frac{\Delta\Pi(c_b,c_i)}{RT} = \phi[c_b - c_{i0}]$$

Plugging in equation 5-5 in the equation for the mechanics of a freestanding film (equation 5-3, taking care of the sign of the bulging), one gets:

5-6 $$c_b - c_{i0} = -\frac{8}{3a^4}\frac{Eh}{(1-\nu)}\frac{1}{\phi RT}d^3$$

As it can be seen from the fits in Figure 5-34 it is important to take the encapsulated polyelectrolyte into account. The red fit, neglecting the encapsulated polyelectrolyte does not fit the data as well as the other nor explain the bulging out.

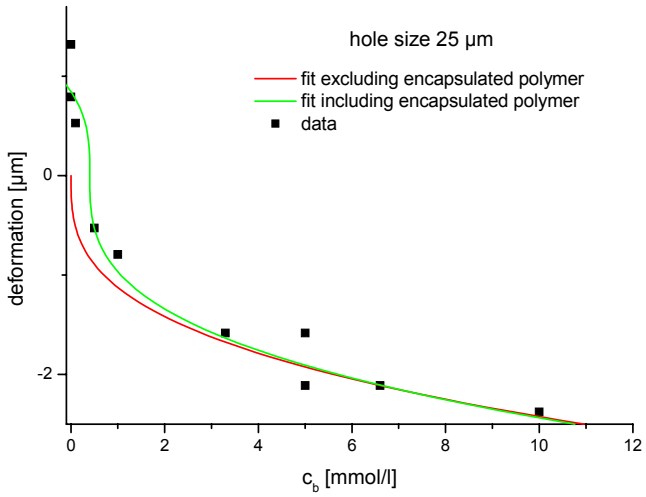

Figure 5-34: Deformation/concentration dataset fitted with equation 5-3 (red line) and equation 5-6 (green line). Ignoring or respecting encapsulated polymer, respectively. The fit including trapped polyelectrolyte agrees closer with the data, while the other does not and does not explain bulging out.

Another effect concerns the final volume of the cavity. Bending of the membrane changes the cavity volume and thus it couples to the osmotic pressure difference.

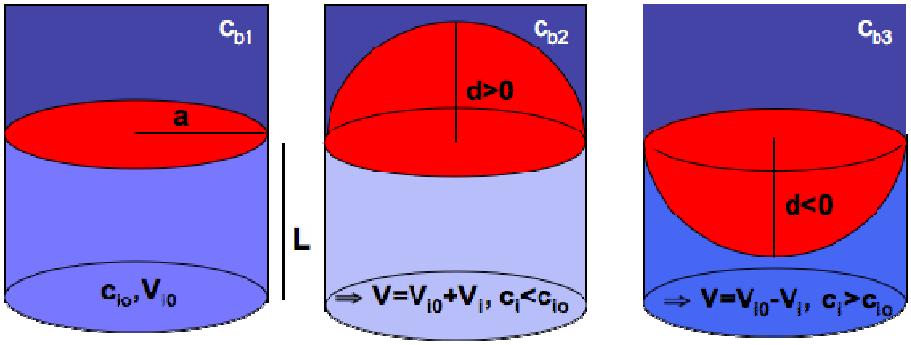

Figure 5-35: Scheme of the change of the encapsulated volume, V_i (i.e. concentration of encapsulated polymer, c_i) for different bulk concentration c_b

Assuming that the deformation of the membrane can be described as a spherical cap, the inner concentration c_i can be written as a function of c_{io}, d and L which are the concentration at zero deformation, the deformation of the membrane, and the depth of the hole respectively.

5-7 $$V_i = \frac{V_{io}}{V_{cap}} \Rightarrow c_i = c_{i0}\left(\frac{1}{1+\frac{d}{2L}}\right)$$

The pressure difference across the membrane is now a deformation dependent function. Taking equation 5-7 into account equation 5-6 becomes

5-8 $$c_b - c_{i0}\left(\frac{1}{1+\frac{d}{2L}}\right) = -\frac{8}{3a^4}\frac{Eh}{(1-\nu)}\frac{1}{\phi RT}d^3.$$

This can be rearranged to give equation 5-9, which analytically describes the concentration deformation relation.

5-9 $$c_b = Kd^3 + c_{i0}\left(\frac{1}{1+\frac{d}{2L}}\right) \quad K = -\frac{1}{\phi RT}\frac{8}{3a^4}\frac{Eh}{(1-\nu)}$$

However as it can be seen in Figure 5-36, the dependence of c_i on the deformation can be neglected. For small deformations, the change of the volume can be neglected, but for big deformations, the d^3 dependence of the mechanics term dominates the concentration change. The effect may become important if high pressures press the membrane against the bottom (like presented in Figure 5-30). However, a quantitative analysis is not possible with analytical approaches in these cases.

Therefore, equation 5-6 with E and c_{io} as free parameters was used to determine the concentration of the encapsulated polyelectrolyte (c_{i0}). To get a statistically more relevant fit, one can subtract c_{i0} from the bulk concentration c_b and combine several datasets, as the deformation dependence of the inner concentration can be neglected (as shown in Figure 5-37).

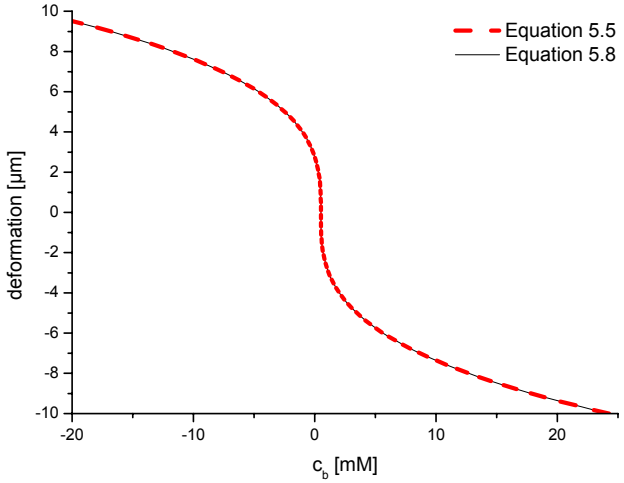

Figure 5-36: Comparison between equation 5-6 and equation 5-9, which ignores or respects the concentration change inside the cavity. The plot simulates a freestanding membrane with an E-Modulus of 500 MPa, a thickness of 70 nm, a Poisson ratio of 0.3 spanned over a 50 µm radius circular hole. The assumed encapsulated volume was 0.5 mM. The accuracy of equation 5-6 is sufficient.

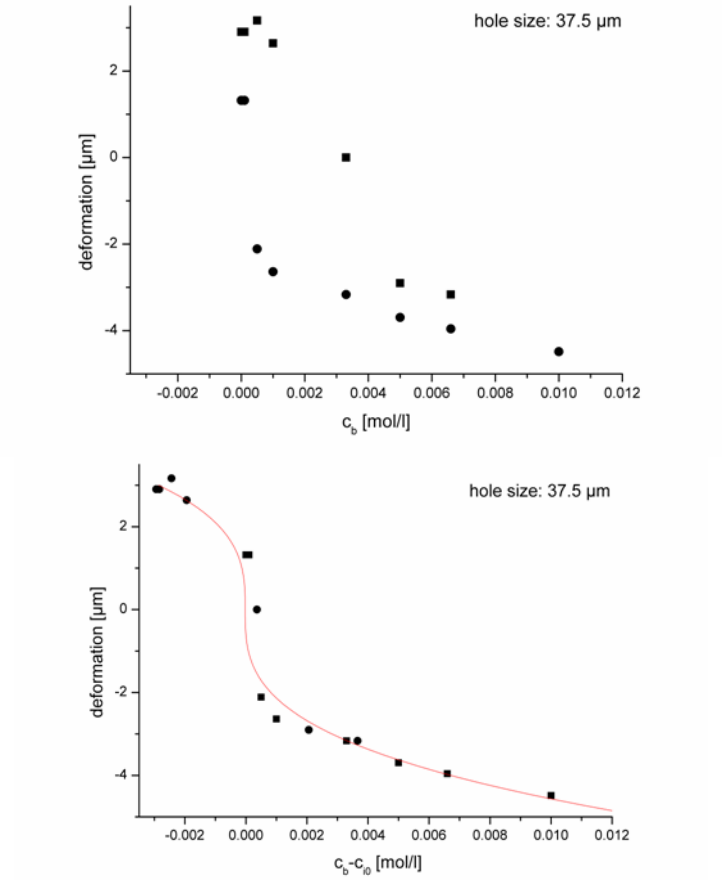

Figure 5-37: Two datasets having different inner concentrations c_{i0}, can be combined by subtracting c_{i0} obtained by fitting each dataset individually.

Encapsulating different defined concentrations in the cavities of an array offers an additional gain in sensitivity. The switch from bulging out to in is at the inner concentration c_{i0}. By this value the highest sensitivity range (i.e. the steepest slope) can be shifted. For simple pressure detection, it would only be necessary to detect at which inner concentration (pressure) the switch takes place.

After normalizing the datasets to c_{i0} and the diameter of the hole *a,* equation 5-6 was used to fit the datasets. *E* was the only adjustable parameter and the other parameters were measured independently, as shown in the master plot in Figure 5-38.

The proportionality constant was determined by membrane osmometry of solutions of different monomolar concentration at different temperatures and with different membrane cuttoffs. The slope of the obtained linear relation (the osmotic coefficient) was ϕ=0.04±0,002. Thus our value corresponds to a fraction of 4% of free counterions, which is around a factor of 8 lower than the expected value (found to be ϕ=0.3 for this system [183] and on the order of 0.4 for other polyelectrolytes [13,184]). A strong baseline drift indicates a presence of low molecular weight impurities. As we cannot assume the same permeability properties for our membrane system and the membranes used in the osmometry measurements, we used the literature value as for fitting the membrane's E-Modulus.

The Poisson ratio was assumed to be ν=0.3, and the membrane thickness was measured to be 70 nm. For an osmotic coefficient of ϕ=0.3, the fitted value of E is 599±52 MPa, the errors are statistical errors obtained from the fitting procedure. The estimates are in good agreement with the values reported in the literature [80,86] (as discussed in chapter 2.4).

The upper limit of pressure detection is related to the semipermeability of the membrane. When applying strong loads (polyelectrolyte concentration of 0.1 M), the membrane becomes permeable because strong forces are acting and the membrane is already quite stretched, even rupture of the membrane was observed (see e.g. black square being not on the fitting curve in Figure 5-38). When releasing the pressure by replacing the polymer solution by water, the membrane bulges outwards because of the encapsulated polymer. This method can also be used to fill the cavities with polymer.

The lower detection limit is mainly given by the concentration of the encapsulated polymer (c_{i0}) and the diameter of the hole. However, a much higher sensitivity in *d*

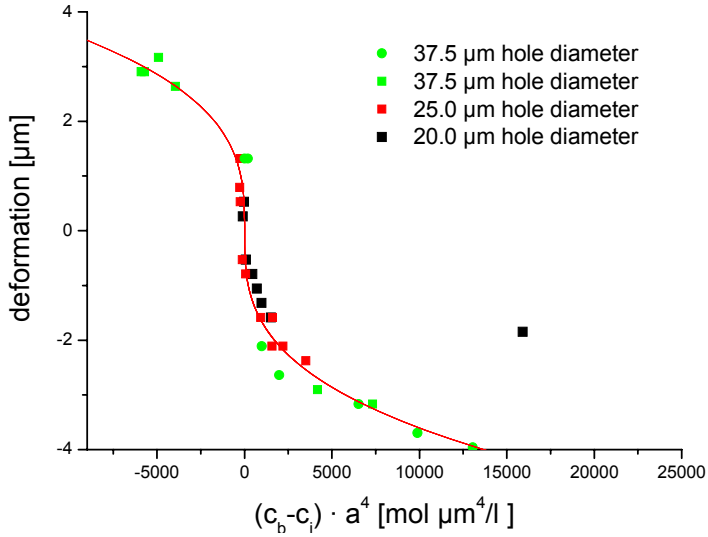

Figure 5-38: Master curve derived from concentration/deformation relation of different hole diameter cavities, normalized on the diameter and c_{io}, the latter obtained by fitting the respective datasets. The fit agrees with data of different hole diameters. Assuming the literature value for ϕ=0.3 the E-Modulus obtained from the fit is 599±52 MPa. The black square not on the fitting curve may have a smaller deformation due to leakage at high polyelectrolyte concentrations.

can be achieved by using interferometry methods. This is the way standard bulging tests are usually performed. As an interferometry method we used reflection-interference-contrast-microscopy (RICM).

In a simple approach, the number of minima and maxima (i_{max}) is a function of the indentation of the membrane, which is given below.

5-10 $$h = i_{\max} \frac{\lambda}{4\pi n_D}$$

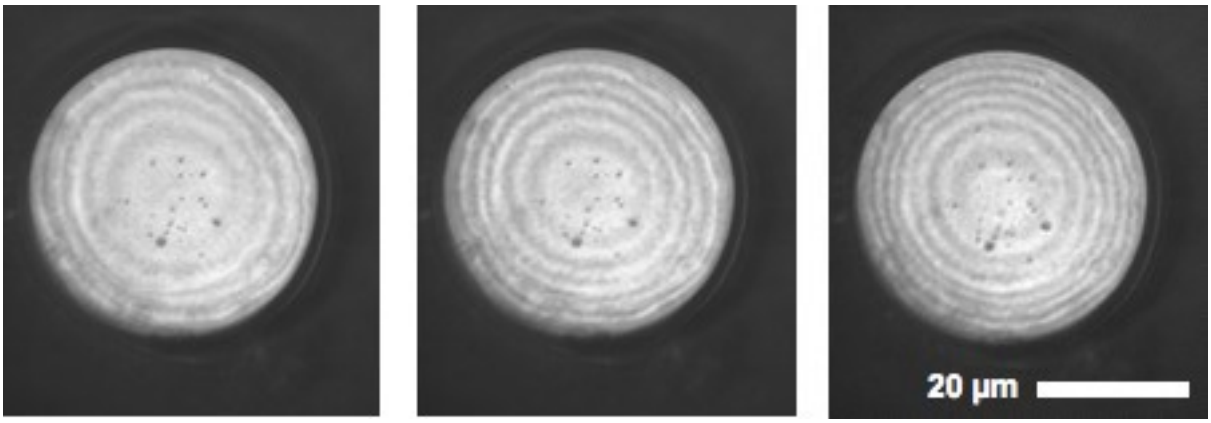

Figure 5-39: RIC-Micrographs of a freestanding film. The number of fringes increases with increasing polymer concentration. The respective indentations of the films determined by equation 5-10 are 264 nm, 330 nm and 429nm.

The accuracy of the simple method therefore is around 35 nm, which is already much more than the accuracy of the confocal measurements. As presented in Figure 5-39, the number of fringes increases with increasing polymer concentration and the respective indentations can be calculated as 264, 330, and 429 nm. This method, however must deal with the problem that the fringes close to the edge are hardly visible, even though it is there that the highest curvature can be found. This happens due to the limited coherence of the light. A detailed discussion of the accuracy of such tests can be found in reference [185].

Perspectives for flat freestanding films

The integration of flat freestanding films in larger scale structures that lead to microarrays is a new method, and opens the door to various new possibilities.

The most interesting aspect of further development is the incorporation of such arrays in microfluidic devices so to access single cavities. This allows for massive parallel analysis or reactions. First experiments in this direction were already performed.

The entrapment of smart polymers not only allows for probing solution properties chemically but also for inducing mechanical reactions of the membrane to chemical stimuli. The concentration of the entrapped molecule shifts the point of zero indentation. This can be used to move the most pressure sensitive part to higher bulk concentrations. The sensitivity of such sensors can be varied in general by the diameter of the hole, as the deformations scales proportionally to a^4.

If the bulk solution changes the osmotic pressure inside the cavity (e.g. by charging a polyelectrolyte by shifting the pH), both the design of intelligent valves, opening and closing with respect to the outer solution, and the sensing of solution properties are possible.

The membrane itself can also be the focus of interest because membrane array allows for fundamental studies on its mechanical properties. In this case, not only an E-Modulus can be derived but the entire stress strain relation can be recorded.

The membrane deflection can be used to determine osmotic pressure (as it previously presented), and thus the molecular weights of macromolecules can be determined, with the advantage, that only small sample volumes are needed. The membrane stiffness itself may be a function of the solution properties and could be probed using empty to the cavities.

6 Summary

In this thesis, it was shown through two different approaches that freestanding polyelectrolyte films can be integrated in larger scale structures. In the first approach, capsule adhesion was directed by patterned substrates, and in the second approach, flat freestanding membranes were transferred to topographically structured surfaces.

Polyelectrolyte multilayer capsules have been already intensively studied in the bulk. By directing their adhesion, new applications arise. In this work, substrates were patterned by means of polymer on polymer printing [92]. The printing is possible on various surfaces. The pattern generated this way was characterized by means of AFM imaging and fluorescence microscopy and was mainly a pattern of different surface charge. This pattern directed the adhesion of polyelectrolyte capsules [157,166]. First experiments with loaded capsules showed that filling the capsules has no effect on the outer charge of the capsule and therefore no effect on the adhesion properties. The isolation and defined position of the capsules offer possible applications in combinatorial chemistry, including using the capsules as semipermeable containers with an enclosed volume on the order of femtoliters. Patterns produced for the directed adhesion of capsules similarly directed the adhesion of encapsulated living yeast cells, which survived their coating and the coupling to the surface. Ordered, encapsulated living cells offer the possibility to build biosensors with a versatile, easy and less costly approach [170].

In the second part of this thesis, a method for the transfer of freestanding membranes was developed. This method eliminates defects induced by in-plane stresses, the main source for defects. Membranes with a thickness around 50 nm were transferred defect free over large areas. Investigations on this system were performed in two directions. First, the separation of the cavity interior from the bulk by the membrane was studied. The freestanding membrane was found to be semipermeable using confocal microscopy. High molecular weight molecules were trapped in the cavities by capillary forces. It was shown that bulk properties can be sensed in the cavities and no crosstalk was observed between neighboring cavities, This is an important aspect for integration of these membranes in “lab-on-a-chip” devices [94]. Second, a pressure sensor based on the membranes deflection due to osmotic pressures was built. Osmotic pressure, generated by adding a polyelectrolyte to the outside solution, was probed by detecting the deflection of the membrane using xz-confocal microscopy or interferometry (RICM). Osmotic pressure

measurements were also used for quantitative analysis of the membrane's E-Modulus.

In conclusion, two approaches of integrating ultrathin freestanding membranes in larger scale structures were successfully established. The presented principle for directing adhesion of capsules can be used as well to direct the adhesion of encapsulated living cells. Flat freestanding membranes can be transferred defect free to topographically structured surfaces. The arrays of sealed cavities created this way can be used as sensors for solution properties by probing them with trapped macromolecules or by measuring the deflection of the freestanding membrane.

7 Bibliography

[1] G. Decher, J. B. Schlenoff, *Multilayer Thin Films*, Wiley-VCH, Heidelberg, **2003**.

[2] A. Antipov, G. Sukhorukov, *Adv. Colloid. Interfac.* **2004**, *111*, 49.

[3] C. S. Peyratout, L. Dähne, *Angew. Chem. Int. Ed.* **2004**, *43*, 3762 – 3783.

[4] G. Decher, in *Multilayer Thin Films*: Polyelectrolyte Multilayers, an overview, (Ed.: J. B. Schlenoff), Wiley-VCH, Heidelberg, **2003**, pp. 1.

[5] L. Bousse, *Sensor Acuat. B-Chem.* **1996**, *34*, 270.

[6] W. Yicong, W. Ping, Y. Xuesong, Z. Qingtao, L. Rong, Y. Weimin, Z. Xiaoxiang, *Biosens. Bioelectron.* **2001**, *16*, 277.

[7] M. A. Unger, H. P. Chou, T. Thorsen, A. Scherer, S. R. Quake, *Science* **2000**, *288*, 113.

[8] G. M. Whitesides, A. D. Stroock, *Phys. Today* **2001**, *54*, 42.

[9] C. Y. Jiang, S. Markutsya, Y. Pikus, V. V. Tsukruk, *Nat. Mater.* **2004**, *3*, 721.

[10] R. R. Netz, D. Andelman, *Phys. Rep.* **2003**, *380*, 1.

[11] S. Förster, M. Schmidt, *Adv. Polym. Sci.* **1995**, *120*, 51.

[12] L. X. Wang, V. A. Bloomfield, *Macromolecules* **1990**, *23*, 804.

[13] M. Deserno, C. Holm, J. Blaul, M. Ballauff, M. Rehahn, *Eur. Phys. J. E* **2001**, *5*, 97.

[14] P. M. Biesheuvel, M. van der Veen, W. Norde, *J. Phys. Chem. B* **2005**, *109*, 4172.

[15] H. Dautzenberg, *Macromolecules* **1997**, *30*, 7810.

[16] D. Kovacevic, S. van der Burgh, A. de Keizer, M. A. C. Stuart, *Langmuir* **2002**, *18*, 5607.

[17] P. M. Biesheuvel, M. A. C. Stuart, *Langmiur* **2004**, *20*, 2785.

[18] H. Dautzenberg, *Macromol. Sym.* **2000**, *162*, 1.

[19] V. Kabanov, in *Multilayer Thin Films*: Fundamentals of Polyelectrolyte Complexes in Solution and the Bulk, (Eds.: G. Decher, J. B. Schlenoff), Viley-VCH, Heidelberg, **2003**, pp. 47.

[20] H. Dautzenberg, W. Jaeger, J. Kötz, B. Phillipp, C. Seidel, D. Stscherbina, *Polyelectrolytes: formation, characterization and application*, Hanser Verlag, München, **1994**.

[21] A. Thünemann, M. Muller, H. Dautzenberg, J. Joanny, H. Lowne, *Adv. Polym. Sci.* **2004**, *166*, 113.

[22] G. Decher, J. D. Hong, J. Schmitt, *Thin Solid Films* **1992**, *210*, 831.

[23] G. Decher, J. B. Schlenoff, in *Multilayer Thin Films*: Sequential Assembly of Nanocomposite Materials, Wiley-VCH, Heidelberg, **2003**, p. 524.

[24] F. Caruso, K. Niikura, D. N. Furlong, Y. Okahata, *Langmiur* **1997**, *13*, 3422.

[25] A. Tronin, Y. Lvov, C. Nicolini, *Colloid Polym. Sci.* **1994**, *272*, 1317.

[26] M. Lösche, J. Schmitt, G. Decher, W. G. Bouwman, K. Kjaer, *Macromolecules* **1998**, *31*, 8893.

[27] M. Schönhoff, *Curr. Opin. Colloid Interface Sci* **2003**, *8*, 86.

[28] J. B. Schlenoff, S. T. Dubas, T. Farhat, *Langmiur* **2000**, *16*, 9968.

[29] A. Izquierdo, S. S. Ono, J. C. Voegel, P. Schaaff, G. Decher, *Langmuir* **2005**, *21*, 7558.

[30] T. R. Farhat, J. B. Schlenoff, *Elechtrochem. Solid St.* **2002**, *5*, B13.

[31] P. A. Chiarelli, M. S. Johal, D. J. Holmes, J. L. Casson, J. M. Robinson, H. L. Wang, *Langmuir* **2002**, *18*, 168.

[32] P. Bertrand, A. Jonas, A. Laschewsky, R. Legras, *Macromol. Rapid Comm.* **2000**, *21*, 319.

[33] X. Arys, A. M. Jonas, A. Laschewsky, R. Legras, P. Figures, in *Supramolecular Polymers*: Supramolecular polyelectrolyte assemblies, (Ed.: C. A), Marcel Dekker, New York, **2000**, pp. 505.

[34] C. Picart, P. Lavalle, P. Hubert, F. J. G. Cuisinier, G. Decher, P. Schaaf, J. C. Voegel, *Langmiur* **2001**, *17*, 7414.

[35] T. Serizawa, M. Yamaguchi, M. Akashi, *Biomacromolecules* **2002**, *3*, 724.

[36] T. Serizawa, M. Yamaguchi, T. Matsuyama, M. Akashi, *Biomacromolecules* **2000**, *1*, 306.

[37] G. Berth, A. Voigt, H. Dautzenberg, E. Donath, H. Möhwald, *Biomacromolecules* **2002**, *3*, 579.

[38] Y. Lvov, K. Ariga, I. Ichinose, T. Kunitake, *J. Am. Chem. Soc.* **1995**, *117*, 6117.

[39] F. Caruso, H. Möhwald, *J. Am. Chem. Soc.* **1999**, *121*, 6039.

[40] G. B. Sukhorukov, M. M. Montrel, A. I. Petrov, L. I. Shabarchina, B. I. Sukhorukov, *Biosens. Bioelectron.* **1996**, *11*, 913.

[41] A. A. Mamedov, N. A. Kotov, M. Prato, D. M. Guldi, J. P. Wicksted, A. Hirsch, *Nat. Mater.* **2002**, *1*, 190.

[42] D. G. Kurth, M. Schutte, J. Wen, *Coll. Surf. A* **2002**, *198-200*, 633.

[43] R. v. Klitzing, J. E. Wong, W. Jaeger, R. Steitz, *Curr. Op. Coll. Interf. Sci.* **2004**, *9*, 158.

[44] K. Glinel, A. M. Jonas, A. Laschewsky, P. Y. Vuilaume, in *Multilayer Thin Films*: Internally Structured Polyelectrolyte Multilayers, (Ed.: J. B. Schlenoff), Wiley-VCH, Heidelberg, **2003**.

[45] G. Decher, *Science* **1997**, *277*, 1232.

[46] C. Picart, P. Lavalle, L. Richert, P. Schaff, J. C. Voegel, **2003**, *84*, 297A.

[47] P. Nazaran, Master Thesis, TU Berlin (Berlin), **2005**.

[48] H. Jomaa, J. Schlenoff, *Macromolecules* **2005**, *38*, 8473.

[49] R. V. Klitzing, R. Steitz, in *Handbook of Polyelectrolytes and Their Applications*: Internal structure of polyelectrolyte multilayers, (Eds.: S. K. Tripathy, J. Kumar, H. S. Nalwa), American Scientific Publishers, North Lewis Way, **2002**, pp. 313.

[50] R. v. Klitzing, H. Möhwald, *Macromolecules* **1996**, *29*, 6901.

[51] S. T. Dubas, J. B. Schlenoff, *Macromolecules* **1999**, *32*, 8153.

[52] E. Hübsch, V. Ball, B. Senger, G. Decher, J. C. Voegel, P. Schaaf, *Langmiur* **2004**, *20*, 1980.

[53] B. Schoeler, G. Kumaraswamy, F. Caruso, *Macromolecules* **2002**, *35*, 889.

[54] S. L. Clark, P. T. Hammond, *Langmuir* **2000**, *16*, 10206.

[55] P. T. Hammond, in *Multilayer Thin Films*: Chemistry Directed Deposition via Electrostatic and Secondary Interactionis: A Nonlithographic Approach to Patterned Polyelectrolyte Multilayer Systems, (Eds.: G. Decher, b. Schlenoff), Wiley VCH, Heidelberg, **2003**, pp. 271.

[56] B. Schoeler, E. Poptoschev, F. Caruso, *Macromolecules* **2003**, *36*, 5258.

[57] C. Picart, J. Mutterer, Y. Arntz, J. C. Voegel, P. Schaaf, B. Senger, *Microsc. Res. Techniq.* **2005**, *66*, 43.

[58] C. A. Constantine, K. M. Gattas-Asfura, S. V. Mello, G. Crespo, V. Rastogi, T. C. Cheng, J. J. DeFrank, R. M. Leblanc, *Langmuir* **2003**, *19*, 9863.

[59] J. Chluba, J. C. Voegel, G. Decher, P. Erbacher, P. Schaaf, J. Ogier, *Biomacromolecules* **2001**, *2*, 800.

[60] J. D. Mendelsohn, S. Y. Yang, J. Hiller, A. I. Hochbaum, M. F. Rubner, *Biomacromolecules* **2003**, *4*, 96.

[61] L. Richert, F. Boulmedais, P. Lavalle, J. Mutterer, E. Ferreux, G. Decher, P. Schaaf, J. C. Voegel, C. Picart, *Biomacromolecules* **2004**, *5*, 284.

[62] D. S. Salloum, S. G. Olenych, T. C. S. Keller, J. B. Schlenoff, *Biomacromolecules* **2005**, *6*, 161.

[63] C. Picart, R. Elkaim, L. Richert, T. Audoin, Y. Arntz, M. D. Cardoso, P. Schaaf, J. C. Voegel, B. Frisch, *Adv. Funct. Mater.* **2005**, *15*, 83.

[64] C. Boura, S. Muller, D. Vautier, D. Dumas, P. Schaaf, J. C. Voegel, J. F. Stoltz, P. Menu, *Biomaterials* **2005**, *26*, 4568.

[65] L. Zhai, F. C. Cebeci, R. E. Cohen, M. F. Rubner, *Nano Lett.* **2004**, *4*, 1349.

[66] H. Ibarz, Ph.D. Thesis, University of Potsdam (Potsdam), **2003**.

[67] G. Ibarz, L. Dähne, E. Donath, H. Möhwald, *Chem. Mater.* **2002**, *14*, 4059.

[68] R. Georgieva, S. Moya, E. Donath, H. Baumler, *Langmuir* **2004**, *20*, 1895.

[69] A. A. Antipov, G. B. Sukhorukov, E. Donath, H. Möhwald, *J. Phys. Chem. B* **2001**, *105*, 2281.

[70] G. Ibarz, L. Dähne, E. Donath, H. Möhwald, *Macr. Rap. Com.* **2002**, *23*, 474.

[71] T. R. Farhat, J. B. Schlenoff, *Langmiur* **2001**, *17*, 1184.

[72] T. R. Farhat, J. B. Schlenoff, *J. Am. Chem. Soc.* **2003**, *125*, 4627.

[73] J. J. Harris, J. L. Stair, M. L. Bruening, *Chem. Mater.* **2000**, *12*, 1941.

[74] L. Krasemann, B. Tieke, *Mat. Sci. Eng. C-Bio S* **1999**, *8-9*, 513.

[75] L. Krasemann, B. Tieke, *Langmuir* **2000**, *16*, 287.

[76] D. M. Sullivan, M. L. Bruening, *J. Am. Chem. Soc.* **2001**, *123*, 11805.

[77] J. Lukas, H. H. Schwarz, K. Richau, *Macromol. Symp.* **2002**, *188*, 155.

[78] A. A. Antipov, G. B. Sukhorukov, H. Möhwald, *Langmiur* **2003**, *19*, 2444.

[79] R. Müller, K. Köhler, G. Sukhorukov, A. Fery, *Macromolecules* **2005**, *38*, 9766.

[80] J. Heuvingh, M. Zappa, A. Fery, *Langmiur* **2005**, *21*, 3165.

[81] C. Gao, E. Donath, S. Moya, V. Dudnik, H. Möhwald, *Eur. Phy. J. A* **2001**, *5*, 21.

[82] F. Dubreuil, N. Elsner, A. Fery, *Eur. Phys. J. E* **2003**, *12*, 215.

[83] A. Fery, F. Dubreuil, H. Möhwald, *New J. Phys.* **2004**, *6*.

[84] N. Elsner, Ph.D. Thesis, Universtät Potsdam (Potsdam), **2005**.

[85] K. Efimenko, M. Rackaitis, E. Manias, A. Vaziri, L. Mahadevan, J. Genzer, *Nat. Mater.* **2005**, *4*, 293.

[86] A. J. Nolte, M. F. Rubner, R. E. Cohen, *Macromolecules* **2005**, *38*, 5367.

[87] V. Bosio, F. Dubreuil, G. Bogdanovic, A. Fery, *Coll. Surf. A* **2004**, *243*, 147.

[88] V. Bosio, Ph.D. Thesis, Universität Potsdam (Potsdam), **2003**.

[89] N. Elsner, F. Dubreuil, A. Fery, *Phys. Rev. E* **2004**, *69*, 031802/1.

[90] A. L. Cordeiro, Ph.D. Thesis, Universidade do Porto (Porto), **2003**.

[91] M. Nolte, A. Fery, *Langmuir* **2004**, *20*, 2995.

[92] X. P. Jiang, H. P. Zheng, S. Gourdin, P. T. Hammond, *Langmuir* **2002**, *18*, 2607.

[93] J. Park, P. T. Hammond, *Adv. Mater.* **2004**, *16*.

[94] M. Nolte, B. Schoeler, C. S. Peyratout, D. G. Kurth, A. Fery, *Adv. Mater.* **2005**, *17*, 1665.

[95] S. T. Dubas, T. R. Farhat, J. B. Schlenoff, *J. Am. Chem. Soc.* **2001**, *123*, 5368.

[96] C. Y. Jiang, S. Markutsya, V. V. Tsukruk, *Adv. Mater.* **2004**, *16*, 157.

[97] P. Lavalle, F. Boulmedais, V. Ball, J. Mutterer, P. Schaaf, J. C. Voegel, *J. Membrane. Sci.* **2005**, *253*, 49.

[98] A. A. Mamedov, N. A. Kotov, *Langmiur* **2000**, *16*, 5530.

[99] Z. Y. Tang, N. A. Kotov, S. Magonov, B. Ozturk, *Nat. Mater.* **2003**, *2*, 413.

[100] F. Mallwitz, A. Laschewsky, *Adv. Mater.* **2005**, *17*, 1296.

[101] A. D. Stroock, R. S. Kane, M. Weck, S. J. Metallo, G. M. Whitesides, *Langmuir* **2003**, *19*, 2466.

[102] F. Shi, Z. Q. Wang, N. Zhao, X. Zhang, *Langmuir* **2005**, *21*, 1599.

[103] C. Jiang, B. Rybak, S. Markutsya, P. Kladitis, V. Tsukruk, *Appl. Phys. Lett.* **2005**, *86*.

[104] S. Markutsya, C. Jiang, Y. Pikus, V. Tsukruk, *Adv. Funct. Mater.* **2005**, *15*, 771.

[105] C. Jiang, V. Tsukruk, *Soft Matter* **2005**, *1*, 334.

[106] C. Jiang, S. Markutsya, H. Shulha, V. Tsukruk, *Adv. Mater.* **2005**, *17*, 1669.

[107] C. Jiang, H. Ko, V. Tsukruk, *Adv. Mater.* **2005**, *17*, 2127.

[108] C. Jiang, W. Lio, V. Tsukruk, *Phys. Rev. Lett.* **2005**, *95*.

[109] E. Donath, G. B. Sukhorukov, F. Caruso, S. A. Davis, H. Möhwald, *Angew. Chem. Int. Ed.* **1998**, *37*, 2202.

[110] G. Schneider, G. Decher, *Nano Lett.* **2004**, *4*, 1833.

[111] A. A. Antipov, G. B. Sukhorukov, S. Leporatti, I. L. Radtchenko, E. Donath, H. Möhwald, *Coll. Surfaces A* **2002**, *198*, 535.

[112] O. P. Tiourina, A. A. Antipov, G. B. Sukhorukov, N. L. Larionova, Y. Lvov, H. Möhwald, *Macromol. Biosci.* **2001**, *1*, 209.

[113] G. B. Sukhorukov, A. Fery, M. Brumen, H. Möhwald, *PCCP* **2004**, *6*, 4078.

[114] L. Dähne, S. Leporatti, E. Donath, H. Möhwald, *J. Am. Chem. Soc.* **2001**, *123*, 5431.

[115] H. Möhwald, E. Donath, G. Sukhorukov, in *Multilayer Thin Films*: Smart Capsules, (Eds.: G. Decher, b. Schlenoff), Wiley VCH, Heidelberg, **2003**, pp. 271.

[116] Y. Lvov, A. A. Antipov, A. Mamedov, H. Möhwald, G. B. Sukhorukov, *Nano Lett.* **2001**, *1*, 125.

[117] N. G. Balabushevitch, G. B. Sukhorukov, N. A. Moroz, D. V. Volodkin, N. I. Larionova, E. Donath, H. Möhwald, *Biotechnol. Bioeng.* **2001**, *76*, 207.

[118] M. Nolte, A. Fery, *IEE Proc. Nanobiotec.* **2006**, *accepted*.

[119] S. Inoue, S. Inoui, K. R. Spring, *Video Microscopy*, 2 ed., Plenum Press, New York, **1997**.

[120] H.-J. Eichler, A. Fleischer, J. Kross, M. Krystek, H. Lang, H. Niedrig, H. Rauch, G. Schmal, H. Schoenbeck, E. Sedlmayr, H. Weber, K. Weber, *Bergmann Schäfer - Optik, Vol. 3*, 9 ed., Walter de Gruyter, Berlin, New York, **1993**.

[121] F. Pedrotti, L. Pedrotti, W. Bausch, H. Schmidt, *Optik: Eine Einführung*, 1 ed., Prentice Hall Inc., München, **1996**.

[122] J. Rädler, E. Sackmann, in *Journal De Physique II, Vol. 3*, **1993**, pp. 727.

[123] G. Wiegand, T. Jaworek, G. Wegner, E. Sackmann, *J. Coll. Interf. Sci.* **1997**, *196*, 299.

[124] J. Schilling, K. Sengupta, S. Goennenwein, A. R. Bausch, E. Sackmann, *Phys. Rev. E* **2004**, *69*, 021901/1.

[125] A. Diaspro, *Confocal and Two-Photon Exciation Microscopy*, Summerschool on Nanocapsules with functionalised surfaces and walls, International University Bremen, **2003**.

[126] Olympus FluoView Resource Center: Theory of Confocal Microscopy, **2004-2005**, Retrieved on 05/10/18, from the world wide web, http://www.olympusconfocal.com/theory/index.html.

[127] K. R. Spring, T. J. Fellers, M. W. Davidson, Olympus FluoView Resource Center: Confocal Microscope Scanning Systems, **2004-2005**, Retrieved on 05/10/18, from the world wide web, http://www.olympusconfocal.com/theory/confocalscanningsystems.html.

[128] S. Hell, G. Reiner, C. Cremer, E. Stelzer, *J. Microsc. Oxford* **1993**, *169*, 391.

[129] R. H. Webb, *Rep. Prog. Phys.* **1996**, *59*, 427.

[130] P. Shaw, *Histochem. J.* **1994**, *26*, 687.

[131] J. R. Sheppard, D. M. Shotton, *Confocal Laser Scanning Microscopy*, Bios Scientic Publishers, **1997**.

[132] T. R. Corle, *Confocal Scanning Optical Microscopy and Related Imaging Systems*, Academic Press, **1996**.

[133] G. Binning, C. F. quate, C. Gerber, *Phys. Rev. Lett.* **1986**, *56*, 930.

[134] G. Binning, H. Rohrer, C. Gerber, E. Weibel, *Phys. Rev. Lett.* **1982**, *49*, 57.

[135] Y. Martin, C. C. Williams, H. K. Wickramasinghe, *J. Appl. Phys.* **1987**, *61*, 4723.

[136] J. Tamayo, R. Garcia, *Langmuir* **1996**, *12*, 4430.

[137] R. Garcia, R. Perez, *Surf. Sci. Rep.* **2002**, *47*, 197.

[138] S. N. Magonov, M.-H. Whangbo, *Surface analysis with STM and AFM: experimental and theoretical aspects of image analysis*, VCH, Weinheim, **1996**.

[139] H. Bubert, H. Jenett, *Surface and Thin Film Analysis*, Wiley-VCH, Weinheim, **2002**.

[140] H. Motschmann, R. Teppner, *Stud. Int. Sci.* **2001**, *11*, 1.

[141] G. Brezesinski, *Grenzflächen und Kolloide: physikalisch-chemische Grundlage*, Spektrum Akad. Verlag, Heidelberg, **1993**.

[142] N. A. Patankar, *Langmuir* **2003**, *19*, 1249.

[143] R. H. Müller, *Zetapotential und Partikelladung in der Laborpraxis*, Wissenschaftliche Verlagsgesellschaft mbH, Stuttgart, **1996**.

[144] P. W. Atkins, J. DePaula, *Physical chemistry*, 7. ed., W. H. Freeman, New York, **2002**.

[145] B. Richter, S. Kirstein, *J. Chem. Phys.* **1999**, *111*, 5191.

[146] G. Ibarz, L. Dähne, E. Donath, H. Möhwald, *Adv. Mater.* **2001**, *13*, 1324.

[147] A. Diaspro, D. Silvano, S. Krol, O. Cavalleri, A. Gliozzi, *Langmuir* **2002**, *18*, 5047.

[148] S. Krol, A. Diaspro, R. Magrassi, P. Ballario, B. Grimaldi, P. Filetici, P. Ornaghi, P. Ramoino, A. Gliozzi, *IEEE Trans. Nanobiosci.* **2004**, *3*, 32.

[149] W. Kern, D. A. Puotinen, *RCA Rev.* **1970**, *31*, 187.

[150] A. Kumar, H. A. Biebuyck, G. M. Whitesides, *Langmuir* **1994**, *10*, 1498.

[151] I. Lee, H. P. Zheng, M. F. Rubner, P. T. Hammond, *Adv. Mater.* **2002**, *14*, 572.

[152] D. Stamou, C. Duschl, E. Delamarche, H. Vogel, *Angew. Chem. Int. Ed.* **2003**, *42*, 5580.

[153] T. C. Wang, B. Chen, M. F. Rubner, R. E. Cohen, *Langmiur* **2001**, *17*, 6610.

[154] L. F. Thompson, C. G. Willson, M. J. Bowden, *Introduction to Microlithography, Vol. 219*, American Cemical Society, Seattle, Washington, **1983**.

[155] H. Hillborg, J. F. Ankner, U. W. Gedde, G. D. Smith, H. K. Yasuda, K. Wikstrom, *Polymer* **2000**, *41*, 6851.

[156] M. Ouyang, C. Yuan, R. J. Muisener, A. Boulares, J. T. Koberstein, *Chem. Mater.* **2000**, *12*, 1591.

[157] M. Nolte, Diploma Thesis, Universität Heidelberg (Heidelberg), **2002**.

[158] M. C. Berg, J. Choi, P. T. Hammond, M. F. Rubner, *Langmuir* **2003**, *19*, 2231.

[159] R. Heuberger, G. Sukhorukov, J. Voros, M. Textor, H. Möhwald, *Adv. Funct. Mater.* **2005**, *15*, 357.

[160] N. P. Huang, R. Michel, J. Voros, M. Textor, R. Hofer, A. Rossi, D. L. Elbert, J. A. Hubbell, N. D. Spencer, *Langmuir* **2001**, *17*, 489.

[161] N. P. Huang, J. Vörös, S. M. De Paul, M. Textor, N. D. Spencer, *Langmuir* **2002**, *18*, 220.

[162] M. Müller, J. Vörös, G. Csucs, E. Walter, G. Danuser, H. P. Merkle, N. D. Spencer, M. Textor, *J. Biomed. Mater. Res* **2003**, *66A*, 55.

[163] H. P. Zheng, M. F. Rubner, P. T. Hammond, *Langmiur* **2002**, *18*, 4505.

[164] H. P. Zheng, I. Lee, M. F. Rubner, P. T. Hammond, *Adv. Mater.* **2002**, *14*, 569.

[165] T. Berzina, S. Erokhina, D. Shchukin, G. Sukhorukov, V. Erokhin, *Macromolecules* **2003**, *36*, 6493.

[166] M. Nolte, A. Fery, *IEEE Trans. Nanobiosci.* **2004**, *3*, 22.

[167] I. L. Radtchenko, G. B. Sukhorukov, H. Möhwald, *Coll Surfaces A* **2002**, *202*, 127.

[168] F. Dubreuil, personal communication, **2004**

[169] M. Prevot, C. Dejugnat, G. Shukorukov, H. Möhwald, **2005**, *submitted*.

[170] S. Krol, M. Nolte, A. Diaspro, D. Mazza, R. Magrassi, A. Gliozzi, A. Fery, *Langmuir* **2005**, *21*, 705.

[171] S. Krol, O. Cavalleri, P. Ramoino, A. Gliozzi, A. Diaspro, *J. Microsc. Oxford* **2003**, *212*, 239.

[172] S. Bhatia, S. Khattak, S. Roberts, *Curr. Op. Coll. Interf. Sci.* **2005**, *10*, 45.

[173] H. P. Zheng, M. C. Berg, M. F. Rubner, P. T. Hammond, *Langmuir* **2004**, *20*, 7215.

[174] A. L. Cordeiro, M. Coelho, G. B. Sukhorukov, F. Dubreuil, H. Möhwald, *J. Colloid Interf. Sci.* **2004**, *280*, 68.

[175] R. Georgieva, S. Moya, M. Hin, R. Mitlöhner, E. Donath, H. Kiesewetter, H. Möhwald, H. Bäumler, *Biomacromolecules* **2002**, *3*, 517.

[176] J. Feng, B. Wang, C. Y. Gao, J. C. Shen, *Adv. Mater.* **2004**, *16*, 1940.

[177] A. Raichur, personal communication, **2005**

[178] A. Günther, personal communication, **2005**

[179] A. C. Ugural, *Stresses in plates and shells*, 2. ed., McGraw-Hill, New York; London, **1999**.

[180] W. A. Goedel, R. Heger, *Langmuir* **1998**, *14*, 3470.

[181] L. D. c. Landau, E. M. c. Lifschitz, H.-G. Schöpf, *Elastizitätstheorie*, 7., unveränderte Aufl. ed., Akademie-Verlag, Berlin, **1991**.

[182] R. Horvath, L. R. Lindvold, N. B. Larsen, *J. Micromech. Microeng.* **2003**, *13*, 419.

[183] C. Wandrey, D. Hunkeler, in *Handbook of Polyelectrolytes and Their Applications*: Study of Polyion Conterion Interaction by Electrochemical Methods, (Eds.: S. K. Tripathy, J. Kumar, H. S. Nalwa), American Scientific Publishers, North Lewis Way, **2002**, pp. 147.

[184] C. Wandrey, D. Hunkeler, U. Wendler, W. Jaeger, *Macromolecules* **2000**, *33*, 7136.

[185] M. K. Small, W. D. Nix, *J. Mater. Res.* **1992**, *7*, 1553.

8 Acknowledgement / Danksagung

First I would like to thank *Prof. Helmut Möhwald* for giving me the possibility to prepare my Ph.D. Thesis in his department, for enlightening discussions and his supervision. I would like to say thank you as well to *Andreas Fery* for giving me the topic to work on. He was a committed supervisor and always open for fruitful discussion.

The work would not have been so easy without my co-workers in the group. Therefore I would like to acknowledge those I worked with: In the freestanding film project *Ingo Dönch, Björn Schöler and Goran Bogdanovic* for a nice and effective working atmosphere and sharing work and knowledge. In other projects I would like to thank *Ashok Raichur* for helpful discussions concerning specific interactions, *Philippe Carl* for software development and last but not least *Anne Heilig* for performing AFM measurements.

The cooperation with people within and outside the institute was always very helpful to me. Without them a lot of results would not exist. For that reason thanks to: *Verónica Saravia* and *José Toca Herrera* from the University of Tarragona, Spain (patterning and specific interactions); *Silke Krol* from the University of Genoa, Italy (directed adhesion of encapsulated yeast cells); *Richard Weinkammer* (Dep. Biomaterials), *Dirk Kurth*, and *Claire Peyratout* (both at that time Dep. Interfaces) in the institute for stimulating discussion in the freestanding membrane project; *Andreas Thünemann* and *Christoph Wieland* (Fraunhofer Institut für Angewandte Polymerforschung, Deutschland) for the calibration measurements in the osmotic sensing project and *Regine von Klitzing* now at Universität Kiel Deutschland, for stimulating discussions in several projects.

For the supply of materials I would like to acknowledge *Markus Textor* and his group from the ETH, Zürich, Switzerland (PLL-g-PEG) and *Prof. Palleschi* from the University La Sapienza, Rome, Italy (GFP producing yeast cells).

I'd like to thank *Annabel Edwards* for carefully correcting the manuscript.

Finally I would like to acknowledge the *SFB 448*, for financial support.

Unabhängig von der formalen Danksagung, gibt es auch Menschen, denen ich persönlich zu Dank verpflichtet bin. Zunächst *Isolde Winter*, die viel Verständnis für dringende Arbeiten aufgebracht hat und mir immer zur Seite stand wenn gerade „Holland in Not" war.

Meinen Bürokollegen *Annika Vergin* und *Ralf Köhler* möchte ich für die diskussionsfreundliche Atmosphäre danken, die sich nicht nur auf wissenschaftliche Diskussionen und auch nicht auf die Arbeitszeit beschränkt hat.

Den Mitgliedern der *„Kaffeecke"*, die ich leider nicht alle aufzählen kann, die aber den Arbeitsalltag aufgehellt haben.

Meinem Vater dafür, der immer für mich da war, wenn ich ihn brauchte.

Zuletzt aber deshalb nicht weniger herzlich möchte ich meiner *Mutter* für die Energie danken die sie aufgebracht hat um mich zu bestärken, zu unterstützen und zu fördern.

9 Appendix I: Design of the Masters

9.1 Circles

Circles prominent

2 µm diameter, distance 10 µm

3 µm diameter, distance 10 µm

5 µm diameter, distance 10 µm

10 µm diameter, distance 15 µm

Circles low lying

2 µm diameter, distance 10 µm

3 µm diameter, distance 10 µm

5 µm diameter, distance 10 µm

10 µm diameter, distance 15 µm

9.2 Lines

2 µm line width, distance 10 µm

3 µm line width, distance 10 µm

5 µm line width, distance 10 µm

10 µm line width, distance 15 µm

9.3 Triangles

Triangles prominent

2 µm side length, equilateral, distance 10 µm

3 µm side length, equilateral, 10 µm

Triangles low lying

2 µm side length, equilateral, distance 10 µm

3 µm side length, equilateral, 10 µm

9.4 Squares

Squares prominent

2 µm side length, distance 10 µm

3 µm side length, distance10 µm

Squares low lying

2 µm side length, distance 10 µm

3 µm side length, distance10 µm

9.5 Checker board

5 µm side length

10 µm side length

9.6 Graphic

Graphic prominent, like drawn; Graphic low lying, like drawn

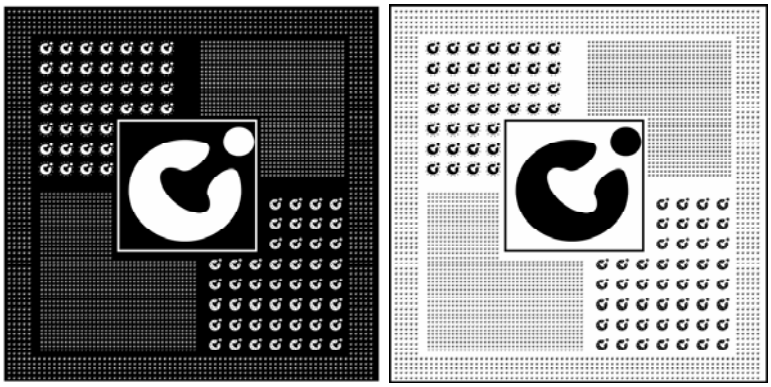

9.7 Holes with different diameters

prominent and low lying like drawn. The numbers represent the respective diameters and are not part of the structures.

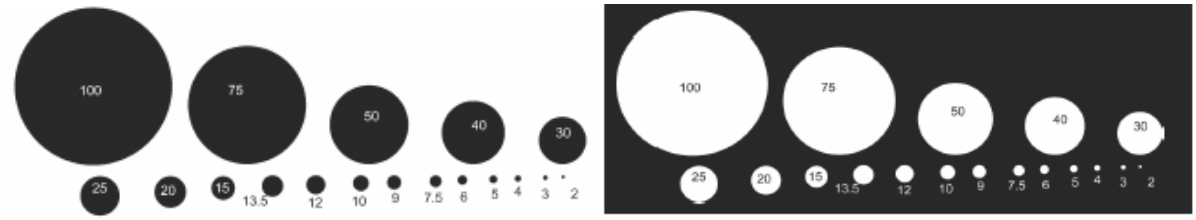

10 Appendix II Program of the dipping robot

The comments written in this type starting with "//" must be removed before usage.

//Header

```
Dipp3D, Version: 2.0
 6.4000000000E+01    4.5000000000E+01    2.5000000000E+01
Number Of Rows: 10
```

// gives the number and the coordinates of the position. These coordinates correspond to the labels on the ground plate.

```
Pot Number And Positions:
20
 4.6846733471E-02    3.0025953743E-01   1
 4.6846733471E-02    6.7934495510E-01   1
 4.6846733471E-02    8.1974781231E-01   1
 1.3525460523E-01    8.1947219734E-01   2
 2.3070993723E-01    8.1947219734E-01   3
 3.2772263210E-01    8.1947219734E-01   4
 4.3367049977E-01    8.1947219734E-01   5
 5.3054161620E-01    8.1947219734E-01   6
 6.3128254338E-01    8.1947219734E-01   7
 7.3232235838E-01    8.1947219734E-01   8
 8.2914628199E-01    8.1947219734E-01   9
 1.3569507150E-01    6.7815062358E-01   2
 2.3133917475E-01    6.7815062358E-01   3
 3.2662146644E-01    6.7815062358E-01   4
 4.3233337004E-01    6.7815062358E-01   5
 5.3106073715E-01    6.7815062358E-01   6
 6.3096792462E-01    6.7815062358E-01   7
 7.3273136277E-01    6.7815062358E-01   8
 8.2990136702E-01    6.7815062358E-01   9
 4.6893926285E-02    1.5207055743E-01   1
Dipp3D, Version: 2.0
```

//The number of processes

```
19
```

//The names of the processes, the position used for the process, SpeedD and SpeedU are the speeds to go to PosT and to continue to PosB, while the Robot stops for the time [s] BreakT and BreakB, at the respective positions.

```
        Name Pos  SpeedD  SpeedU  PosT  PosB  BreakT  BreakB  Dipp  F-No -Mode
        pahr 20      3.0     3.0  12.0  18.0     1.0     1200.0     1     0     0
        pahs  8      3.0     3.0  12.0  18.0     1.0     1200.0     1     0     0
         pei  1      3.0     3.0  12.0  18.0     1.0     1200.0     1     0     0
    wash_a1 12      3.0     3.0  12.0  18.0     1.0     60.0       1     0     0
```

paa	16	3.0	3.0	12.0	18.0	1.0	1200.0	1	0	0
wash_a2	13	3.0	3.0	12.0	18.0	1.0	60.0	1	0	0
wash_a3	14	3.0	3.0	12.0	18.0	1.0	60.0	1	0	0
wash_sa1	17	3.0	3.0	12.0	18.0	1.0	60.0	1	0	0
wash_sa2	18	3.0	3.0	12.0	18.0	1.0	60.0	1	0	0
wash_c1	4	3.0	3.0	12.0	18.0	1.0	60.0	1	0	0
wash_sa3	19	3.0	3.0	12.0	18.0	1.0	60.0	1	0	0
wash_sc1	9	3.0	3.0	12.0	18.0	1.0	60.0	1	0	0
wash_sc2	10	3.0	3.0	12.0	18.0	1.0	60.0	1	0	0
wash_sc3	11	3.0	3.0	12.0	18.0	1.0	60.0	1	0	0
wash_c2	5	3.0	3.0	12.0	18.0	1.0	60.0	1	0	0
wash_c3	6	3.0	3.0	12.0	18.0	1.0	60.0	1	0	0
pss	2	3.0	3.0	12.0	18.0	1.0	1200.0	1	0	0
pah	3	3.0	3.0	12.0	18.0	1.0	1200.0	1	0	0
wait_a3	14	3.0	3.0	12.0	18.0	1.0	36000.0	1	0	0

//The call of the respective processes resulting in the entire dipping programm

```
pei+wash_c1+wash_c2+wash_c3+(pss+wash_a1+wash_a2+wash_a3+pah+wash_c1+wash_c2+wash_c
3)*5+(paa+wash_sa1+wash_sa2+wash_sa3+pahs+wash_sc1+wash_sc2+wash_sc3)*5+(pss+wash_a
1+wash_a2+wash_a3+pah+wash_c1+wash_c2+wash_c3)*40+pss+wash_a1+wash_a2+wait_a3
```